FRACTAL MRI AND BRAIN CONNECTIVITY IN ALZHEIMER'S DISEASE

THE FRACTAL NATURE AND FUNCTIONAL CONNECTIVITY OF BRAIN FUNCTION AS MEASURED BY BOLD MRI IN ALZHEIMER'S DISEASE

By

MOHAMMED ALI WARSI, (Hon) B.Sc., M.Sc., M.D.

A Thesis

Submitted to the School of Graduate Studies

in Partial Fulfillment of the Requirements for the Degree

Doctor of Philosophy

McMaster University

Doctor of Philosophy (2012)

McMaster University, School of Biomedical Engineering, Hamilton, Ontario

TITLE: The Fractal Nature and Functional Connectivity of Brain Function as Measured by BOLD MRI in Alzheimer's Disease

AUTHOR: Mohammed Ali Warsi (Hon) B.Sc., M.Sc., M.D., (University of Toronto), FRCP(C) (McMaster University)

SUPERVISOR: M. D. Noseworthy

NUMBER OF PAGES: xiii, 152

ABSTRACT

Alzheimer's disease (AD) is a degenerative disease with progressive deterioration of neural networks in the brain. Fractal dimension analysis (FD) of resting state blood oxygen level dependent (BOLD) signals acquired using functional magnetic resonance imaging (fMRI) allows us to quantify complex signalling in the brain and may offer a window into the network erosion. This novel approach can provide a sensitive tool to examine early stages of AD. As AD progresses, we expect to see a reduction in brain connectivity and signal complexity concurrent with biochemical changes (e.g. altered levels of N-acetyl aspartate (NAA), myoinositol (mI) and glutamate as measured using magnetic resonance spectroscopy, MRS), volumetric changes and abnormally high levels of brain iron.

Over a series of 4 studies we examined the relationship of BOLD signal complexity and functional connectivity with documented MRI markers of pathology in AD (n=38) as compared to normal controls (NC) (n=16). AD subjects were in early stage of illness (mild to moderate impairment on the mini mental state exam, MMSE). We validated the temporal (short term (within minutes) and longer term (over a number of months)) consistency of FD measurement and choice of BOLD acquisition method (spiral vs. EPI), provided MRI sequence repeat time (TR) was kept constant. FD reduction (decrease in signal complexity) correlated with worsening pathological values on MRS (↓NAA and ↑mI) and with a decrease in functional connectivity. This demonstrates that FD (signal complexity) reduces in proportion to AD severity. FD reduction is connected

to functional connectivity measured through resting state network (RSN) analysis suggesting the reduction in FD relates to neuronal loss rather than altered vascularity. The narrow range of cognitive impairment (such as scores on the MMSE or the clinical dementia rating scale, CDR) likely precluded correlation between these measures and FD or RSN. Functional connectivity (RSN) was also reduced when brain iron levels were increased within certain network nodes (posterior cingulate cortex and lateral parietal cortex). Therefore iron deposition may play a role in network disruption of AD brains.

The overall conclusion of this thesis is that signal complexity of BOLD fMRI signals, as measured with FD, may detect early pathology in the progression of AD. FD can detect neuronal changes in deep brain structures before volume loss in these structures and before significant changes in MRS markers were detectable between the AD and NC groups. An FD change mirrors disruptions in functional connectivity but detection is not limited to RSN nodes in the brain. This novel approach could further our understanding of AD and may be applied to other pathologies of the brain.

ACKNOWLEDGEMENTS

I wish to thank my supervisors, Dr. Michael Noseworthy and Dr. William Molloy. Dr. Noseworthy's vast knowledge of MRI (and beyond!), sleep resistance, mentorship and friendship have made the last four years endlessly fruitful and fun. Dr. Molloy's mentorship and friendship have extended well beyond my PhD and provided valuable life lessons. Dr. Gary Hasey, my committee advisor, clinical mentor and friend has been like a parent, always willing to sacrifice to ensure my progression as a student, clinician and academic. Dr. Mark Haacke, also my committee advisor, brought his vast expertise and supervisory experience to help better my PhD.

Dr. Dinesh Kumbhare, Dr. Adrian Crawley and Dr. Russell Bell generously donated their time and knowledge to help me through my PhD comprehensive examination and thesis defence, for which I am grateful.

I would like to acknowledge the members of the IRC for their mentorship (Aravinthan Jegatheesan, Andrew Davis, Graham Wardlaw, Ali Fatemi, Norm Konyer, Sergei Obruchkov and Peter Shefield) and companionship (Steve Madison, Evan McNabb, Gavin Jones, Brendon Boyd, Alex Weber, Raghda Hasswa, Alyaa Elzibak, Alireza Akbari, Ben Geraghty, Conrad Rockel, Oilei Wong, Peter Bevan, Jeff Thompson, Saurabh Shaw, Paul Polak, Marla Shaver and Saman Sarraf). The comradery and companionship will always be remembered.

Without the technologists and clinical assistants, my PhD would not have been possible. I would like to thank Cheryl Contant, Julie Lecomte, Janet Burr and Toni Cormier for their remarkable skills as MRI technologists; Tim Standish, Paula DiLoreto and Elizabeth Almeida for recruiting and retaining subjects and Eleanor Pullenayegum for her assistance in statistical analysis and project design.

Dr. Clive Kearon and Sharon Ciraolo have shown great dedication to the Clinician Investigator Program and towards each and every student, including myself, for which I am thankful.

Zeid Founouni and Top Gear provided the necessary subjects of procrastination while writing my thesis and studying for my defence.

Finally, I would like to thank the most important people in my life who have endured 17 years of full-time post secondary education and supported me all the way. My parents, Ghulam and Parveen, as well as my brother Mustafa Kamal have been with me through every examination and presentation. I could not have done it without them. My beautiful wife Majedeh has endured many a late night with me at the lab and supported me endlessly. Cyrus has patiently waited for me night after night and our new baby has patiently waited to be born. =)

"Beyond the horizon of the place we lived when we were young
In a world of magnets and miracles
Our thoughts strayed constantly and without boundary …"

Roger Waters, Pink Floyd, High Hopes

"We must ask ourselves crucial questions.
Where are we? How did we get here? Why did we come? Where do we want to go? How do we want to get to where we want to go? How far do we have to go before we get to where we want to be? How would we know where we were when we got there? Why did we leave places to get to where we are? Where were we before we had to leave to get to where we were before we knew we're going to go to where we want to be?
But surely you can see my point."

Sir Marcus Browning MP, Rowan Atkinson

TABLE OF CONTENTS

LISTS OF FIGURES AND TABLES

LIST OF ABBREVIATIONS

AD	Alzheimer's Disease
Ala	Alanine
ASL	Arterial Spin Labeling
BOLD	Blood Oxygen Level Dependant
CBF	Cerebral Blood Flow
Cho	Choline
CNR	Contrast to Noise Ratio
Cr	Creatine
CSF	Cerebral Spinal Fluid
DBS	Deep Brain Stimulation
DCE	Dynamic Contrast Enhanced
dHb	Deoxygenated Hemoglobin
DMN	Default Mode Network
DTI	Diffusion Tensor Imaging
EEG	Electroencephalography
EPI	Echo-Planer Imaging
fBm	Fractional Brownian Motion
FD	Fractal Dimension
FDG	Fluorodeoxyglucose
Fe	Iron
FFT	Fourier Transformation
fGn	Fractional Gaussian Noise
fMRI	Functional Magnetic Resonance Imaging
FWHM	Full-with-half-max
GABA	Gamma-Aminobutyric Acid
gc	Glucose
GLM	General Linear Model
gln	Glutamine
glu	Glutamate
GM	Grey Matter
H	Hurst Exponent
HF	Hippocampal Formation
ICA	Independent Component Analysis
jMRUI	Java Magnetic Resonance User Interface
lac	Lactate
LPC	Lateral Parietal Cortex
LS	Length of Scan
MCI	Mild Cognitive Impairment
MEG	Magnetoencephalography
mI	Myoinositol

MMSE	Mini Mental State Exam
MPC	Medial Prefrontal Cortex
MRS	Magnetic Resonance Spectroscopy
MS	Multiple Sclerosis
MTL	Medial Temporal Lobe
NAA	N-Acetylaspartate
NC	Healthy (Normal) Controls
NFT	Neurofibrillary Tangles
NMR	Nuclear Magnetic Resonance
OCD	Obsessive Compulsive Disorder
oHb	Oxygenated Hemoglobin
PCA	Principal Component Analysis
PCC	Posterior Cingulate Cortex
PET	Positron Emission Tomography
PIB	Pittsburgh Compound B
PS	Power Spectral Density
RD	Relative Dispersion
ROI	Region of Interest
rsBOLD	Resting State BOLD
RSN	Resting State Network
SD	Standard Deviation
SEM	Standard Error of the Mean
SNR	Signal to Noise Ratio
SP	Senile Plaques
STEAM	Stimulated Echo Acquisition Mode
SWI	Susceptibility Weighted Imaging
SWV	Scaled Windowed Variance
TARQUIN	Totally Automatic Robust Quantitation In NMR
TBI	Traumatic Brain Injury
TMS	Transcranial Magnetic Stimulation
TP	Number of Temporal Points
TR	Repetition Time
WM	White Matter

CHAPTER 1

BRAIN FUNCTION AND MRI

1.1 BRAIN FUNCTION AT REST

The knowledge that cognitive tasks can produce regional brain changes dates as far back as 1881 when Angelo Mosso studied pulsations of the human cortex (Mosso 1881). In recent decades, imaging has been used to examine the resting brain. Positron Emission Tomography (PET) provided some of the earlier examinations of brain function and revealed that the brain is quite metabolically demanding, even at rest (Wintermark 2005). Although earlier PET studies focused on regional blood flow, glucose utilization soon became the benchmark for brain function (Raichle 1998). While accounting for 5% of body weight, the brain utilizes 20% of the body's energy (as measured by oxygen metabolism) (Clark 1999). Most of this energy is spent on neuronal signaling, while a smaller proportion is spent on maintaining resting potentials for neurons and glia (Attwell 2001). Brain activation produces a very small increase in energy use (Raichle 2002) although more recent work suggests brain activity is primarily affected by changes in excitation–inhibition balance (Logothetis 2008). This suggests that brain task related activations are merely a shift in brain metabolic functions that are already occurring at rest. Thus, much of the brain's complex signaling occurs at rest, and therefore lends itself to signal characterization.

There are various states of rest, each with it's own signal characteristics. Electroencephalography (EEG) reveals differences between stages of sleep, when eyes are open or closed, and between being attentive to an object or not. Despite the

differences between these states, the characteristics of EEG signals are quite predictable within any given state. For example, the ranges of frequencies for each stage of sleep are consistent between subjects without pathology and EEG power can be used to identify stages of sleep (De Weerd 1999). This marks the importance of differentiation state vs. trait findings when studying the brain at rest. Some features are consistent despite changes in the internal or external environment (e.g. brain volume) while other's change with changes in condition (e.g. EEG coherence during eyes open vs. closed). Trait features are generally more helpful when comparing features across subjects.

1.2 RESTING BRAIN MRI

Initially, clinical MRI scanning focused on structure, providing an alternative to CT scans but with superior soft tissue contrast. Not long after, the versatility of MRI was used for functional assessment of the brain. Although traditional "fMRI" or functional MRI refers to BOLD (blood oxygen level dependant) MRI, various other MRI techniques can also assess function. For example, repeated magnetic resonance spectroscopy (MRS) MRI scans have been used to assess changes in brain biochemistry (such as lactate levels) as a measure of brain function (Frahm 1996; Richards 1997). Arterial spin labeling (ASL) or dynamic contrast enhanced (DCE) MRI can be used to look at functional blood flow. Even repeated structural imaging can provide functional information by observing the brain pulsations and CSF flow (using phase contrast) (Wagshul 2011).

1.3 BOLD FMRI

By far, BOLD fMRI is the most common MRI method of measuring brain function. This is because BOLD fMRI can provide a good balance between spatial and temporal resolution. Thus function can be assessed at the millimeter and decisecond scales. BOLD fMRI is usually task based where the subjects perform a task (such as observing light or reacting to sad images) and the resultant brain areas activated are deduced from regional blood oxygenation changes. The variety of tasks presented is unlimited and can be fashioned to specific pathologies (such as memory tasks to study mild cognitive impairment). Because the MR signal within activation regions are only a few percent over noise, the task has to be repeated multiple times to increase the contrast to noise ratio (CNR).

A newer method of measuring brain function is to observe the brain using BOLD MRI at rest. In the early 1990's, it was discovered that brain "noise", what was minimized in task based BOLD studies, actually has important information about brain function. Although there are many ways of analyzing this signal, two major methods have dominated the literature. The first is based on resting state functional connectivity and the other is based on resting state signal complexity. These methods and the detailed mechanism by which BOLD MRI provides a signal are discussed in more detail in chapter 2. Unlike task-driven methods, resting state does not require a paradigm, which reduces some *a priori* assumptions about how the paradigm models the illness. For example, seeing sad faces during a depression paradigm may or may not activate the

same areas of the brain that are activated due to intrinsic sadness from a depressive state. Task based fMRI studies often have low inter-subject reliability as well as intra-subject variability (Fleisher 2009). Results can vary based on task performance, and exposure to the same stimulus can frequently provide different activation patterns (Ances 2008). This often results in the need for a large number of subjects and many task repetitions resulting in long scan times. A head-to-head comparison of tasked based fMRI and resting state network fMRI (RSN) showed that resting state analysis can provide a greater effect size for identifying subjects at risk of Alzheimer's disease (AD) (Fleisher 2009).

1.4 RESTING STATE NETWORK FMRI

Resting state network fMRI (RSN) is a widely used functional imaging method for analyzing brain connectivity at rest. When analyzing fMRI at rest, it was noted that spatially separated areas of the brain have synchronous BOLD signal, suggesting functional connectivity (Biswal 1995). Multiple such networks have been discovered, and the number increases as analysis methods become more sensitive and MRIs provide better signal to noise ratio (SNR). One of the strongest (and earliest discovered) networks is the default mode network (DMN) (Raichle 2001). The DMN is a network connecting the posterior cingulate cortex (PCC) to the medial prefrontal cortex (MPC), left and right lateral parietal cortex (l-LPC and r-LPC) and the left and right hippocampal formation (l-HF and r-HF) (Van Dijk 2010). This network exhibits intra and inter-subject consistency

and is also altered in certain pathologies such as schizophrenia, Alzheimer's disease and multiple sclerosis (Rosazza 2011).

There are two methods of detecting RSNs. One involves seed placement in a predetermined area (such as the PCC) and all other BOLD voxel time courses are compared to that seed. A correlation map then reveals areas showing functional connectivity to the seed region. This approach requires an *a priori* determination for seed placement, and is therefore useful for studying already well established networks such as the DMN, where the nodes are predictably located within the brain. Seed based analysis can also be done using a 'brute force' approach by placing seeds one voxel at a time, each obtaining a correlation map. This method can identify novel networks and does not make *a priori* assumptions regarding seed placement. However, it is very data intense and requires large computing power to amalgamate the information for multiple correlation maps.

The second method of identifying networks in the brain uses independent component analysis (ICA). ICA is a technique that assumes recorded signals are a mixture of a pre-specified number of independent signals. ICA then uses an iterative method to locate a linear transformation that maximally demonstrates independence. ICA can identify a variable number of networks depending on how many components are assumed. But generally 8 major networks can be reliably identified (Cole 2010). One difficulty with ICA is the identified networks sometimes overlap introducing the need to subjectively identify specific networks such as the DMN. Initially, it was difficult to do group analysis with ICA but newer mathematical techniques (and software packages)

allow for group analysis (Calhoun 2001). Comparing strength of functional connectivity with other measures (such as brain volume) is harder to standardize relative to seed based methods (Van Dijk 2010).

1.5 BRAIN SIGNAL COMPLEXITY ANALYSIS

The resting state analysis described above is all based on linear models. However, it is well known from the EEG literature that the brain is best assessed using non-linear dynamic models (Kannathal 2004). In essence, the brain is best modeled as a complex system. Resting BOLD fMRI can also be assessed for brain signal complexity. Rather than correlating connectivity between brain areas, the signal within any given voxel can reveal complexity of the resting state. Fractal analysis is the most common method of analyzing complexity of physiological signals, since these signals often demonstrate scalar self similarity (exhibit similar patterns at different scales of measurement). Scalar self similar patterns can be quantified into a fractal dimension (FD) or other similar units such as the Hurst exponent (H). Each voxel can be assessed for it's FD or H value to determine how complex the signal is. In the brain, BOLD signal complexity can be influenced by the microvascular environment (Wardlaw 2008) or neuronal interconnectivity (Warsi 2012). Thus, FD analysis of resting state BOLD fMRI can reveal information about brain function. FD of fMRI has already been applied to the study of AD (Maxim 2005; Warsi 2012) and more recently autism (Lai 2010), but is still in its infancy with regards to it application to brain pathology.

CHAPTER 2

BOLD fMRI AND FRACTAL ANALYSIS

2.1 BOLD FMRI

2.1.1 Physiological Basis of Blood Oxygen Level Dependent (BOLD) Signal

The coupling of cerebral blood flow (CBF) to neuronal activity was shown as early as 1890 in dogs (Roy 1890). In the 1970's, optical imaging was developed for measuring blood oxygenation (Jobsis 1977) and has become a significant adjunct (in some cases a replacement) for modern blood oxygen measurement techniques (Hillman 2007). Based on the principle that hemoglobin changes magnetic properties between the deoxygenated and oxygenated forms (Pauling 1936), Thulborn discovered a nuclear magnetic resonance (NMR) method of measuring *ex vivo* blood oxygenation using the transverse relaxation of water (T2 effect) (Thulborn 1982). This pioneering work correlated the fraction of deoxyhemoglobin with T_2 relaxation times and showed that this change was a direct result of changes in magnetic susceptibilities (Thulborn 1982). It wasn't until 1990 that MRI field strength was sufficient such that blood oxygen level dependent (BOLD) signal was described *in vivo* (Ogawa 1990). BOLD fMRI is a technique of indirect detection of neuronal activation. An increase in blood flow during neuronal activation changes the relative concentration ratio of oxygenated hemoglobin (oHb) to deoxygenated hemoglobin (dHb). The oHb molecule is diamagnetic (has negative magnetic susceptibility) and dHb is paramagnetic (positive magnetic susceptibility) (Pauling 1936). Different susceptibilities cause distortions in the magnetic field which can be detected by MRI. The changes in susceptibility from changes in Hb

creates the contrast for BOLD fMR imaging (Ogawa 1990). When neurons in a region are activated, there is an initial reduction in the oHb/dHb ratio. Afterwards, there is a relatively large increase in this ratio as vasodilatation brings in fresh oxygenated blood (Figure 2.1).

The initial reduction in oHb/dHb is not reliably detectable, but is more evident at higher field strengths (Nair 2005). It's origin remains under debate but is most likely due to an initial utilization of oxygen before oxygenated blood perfuses the tissue (Ernst 1994; Yacoub 1999). Most fMRI studies use the subsequent increase in the oHb/dHb ratio (the hemodynamic response) to measure BOLD contrast. The exact mechanism of how neuronal activity causes the BOLD response is still being studied, but the general steps are agreed upon (Nair 2005). Specifically, neuronal signaling uses glutamate in the synapse as a neurotransmitter. Glutamate is taken up by astrocytes. This causes a calcium signal cascade leading to release of various vasodilators including nitric oxide (NO) (Nair 2005; Raichle 2006; Jakovcevic 2007). Vasodilatation results in an increase in oxygenated blood, with a concurrent reduction in local magnetic susceptibility, χ.

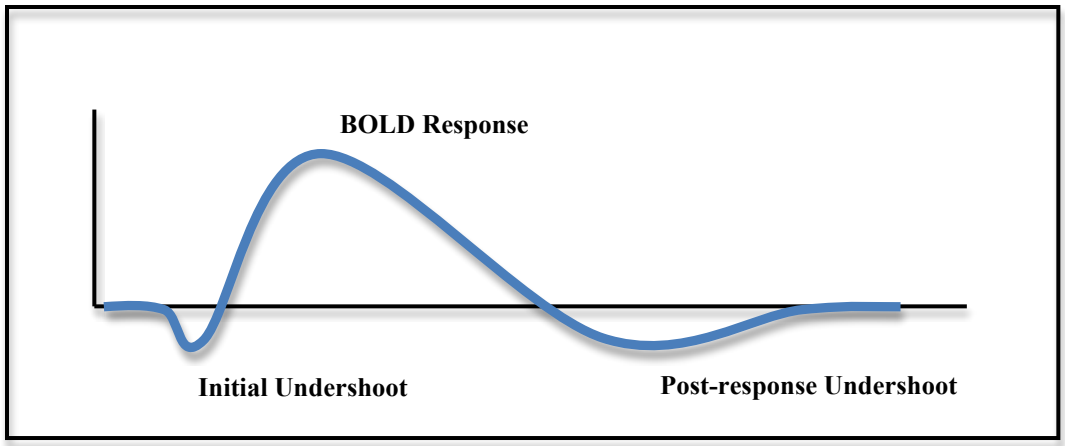

Figure 2.1: Signal vs. Time plot of BOLD signal showing initial reduction in oHb/dHb ratio followed by a large increase

2.1.2 BOLD fMRI acquisition

The hemodynamic response induces susceptibility changes by altering the oHb/dHb ratio thus altering the ratio of diamagnetic and paramagnetic substrate. BOLD fMRI uses parameters sensitive to changes in T2*. Echo-Planer Imaging (EPI) (Mansfield 1977) and spiral acquisitions (Glover 2012) are the most common type of functional MRI imaging strategies. Each can acquire a single slice of data in roughly 70ms, depending on required resolution, readout bandwidth, and gradient performance. The difference between EPI and spiral is the approach to k-space (i.e. raw data) navigation and filling: EPI rasterizes k-space while spiral follows one of a number of different possible trajectories (Euclidian, Archimedean, etc.) from the centre to the periphery of k-space, or vice-versa. EPI raw data can be 2D Fourier transformed to images following some phase corrections accounting for left-right sampling directions. The spiral data, however, requires regridding to a Cartesian framework prior to 2D Fourier transformation. The high temporal resolution of either approach comes at the

expense of spatial resolution. fMRI data are typically lower resolution also due to SNR requirements: the BOLD signal is only a few percent of the signal, necessitating larger voxels to improve SNR. If higher resolution BOLD data were to be acquired imaging would take much longer (due to the longer readout time) and the increased gradient slew rates required would result in more geometric distortion due to eddy currents and concomitant field effects.

2.1.3 Task-based fMRI

Typical task-based fMRI experiments involve collection of MRI volumes while inducing various (often 2) neurocognitive states from sensory or cognitive stimuli (Glover 2011). Two states often represent a task "on" state and a task "off" or baseline state. These two states are induced in blocks of about 10-30 seconds, usually alternating between the two states. This induces a BOLD response in areas activated by the task (Figure 2.2). This task type is called a "block design" as paradigms are presented in blocks. Other more complex designs are event related and may have many stimuli within one run.

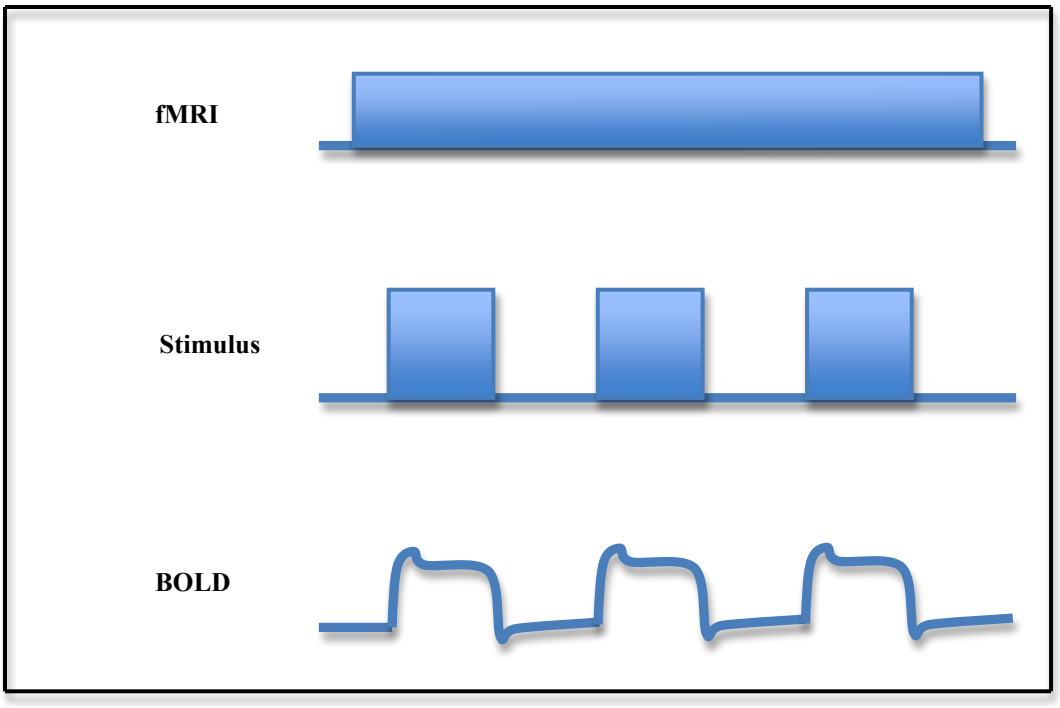

Figure 2.2: Schematic of a task-based fMRI acquisition and resultant BOLD signal

Acquired images are processed to correct for slice timing, B_0 imperfections, eddy currents, motion, spatial smoothing (to boost SNR) and sometimes low/high pass filtering to eliminate physiological noise such as cardio-respiratory signals (Glover 2011). The BOLD response (or voxel-by-voxel signal intensity) is statistically compared to the stimulus model usually using a general linear model (GLM) (Worsley 2002) to produce a statistical correlation map between each voxel and the stimulus model. This map can them be overlaid onto an anatomical map to identify areas of high correlation (thus activation) (Figure 2.3).

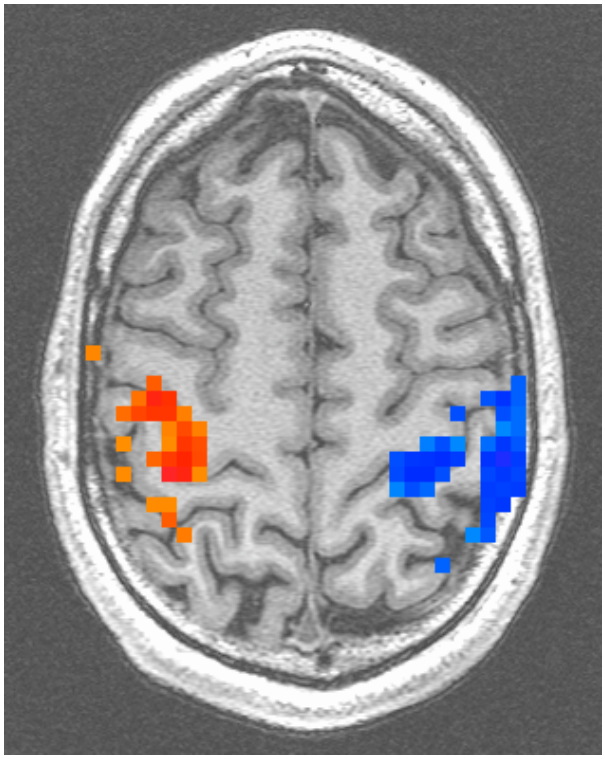

Figure 2.3: Activation map superimposed on an anatomical scan for a task-based fMRI paradigm, alternating hand (left and right) finger tapping. Areas in orange represent positive correlation while areas in blue represent negative correlation with the stimulus model.

2.2 FRACTAL ANALYSIS

2.2.1 Fractal Dimension

Many physiological signals appear random. However, it is now well understood that these are better described as complex systems (Bassingthwaighte 1994). Elements of chaos theory have been able to unravel complex systems leading to the discovery of patterns never before apparent. Fractals have been used to describe some elements of these complex systems. These are curious geometric structures that are self-similar at

multiple measurement scales and are seen extensively in the structural and temporal complexity of nature. Self-similarity is seen in the geography of coastlines, branching patterns of trees and in many physiological signals. It was in 1975 that Benoit Mandelbrot coined the term "fractal" (Mandelbrot 1977) and in 1982 published "The Fractal Geometry of Nature" (Mandelbrot 1982) which brought fractals into 'mainstream consciousness'. Synthesized fractal patterns such as Koch's Snowflake and Sierpinski's triangle demonstrate the concept of scalar self similarity (Figure 2.4)

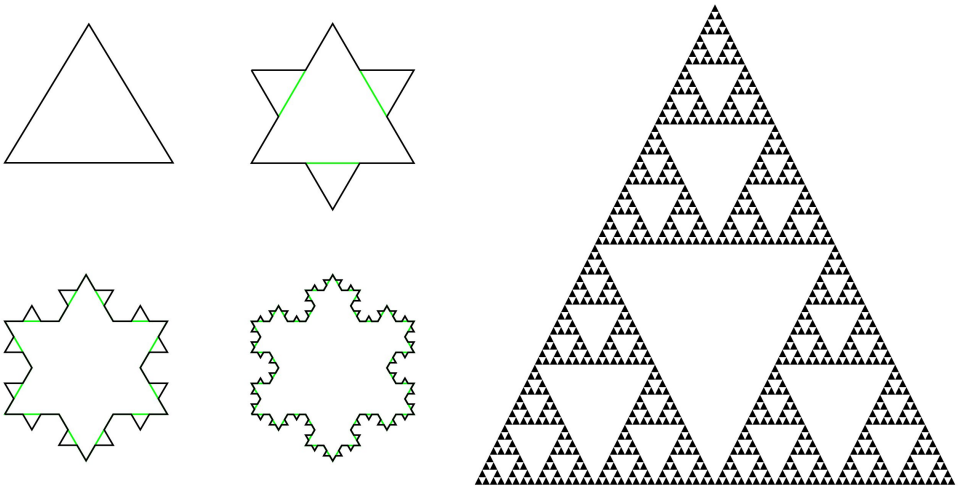

Figure 2.4: Schematics of the Koch's Snowflake and Sierpinski's triangle depicting recursive pattern repetition or a spatial fractal.

Biological systems that exhibit fractal patterns include the Romanesco broccoli (Figure 2.5) which has a general conical shape made of subunits (and sub-subunits) which themselves are conical. Spatial fractals are also exhibited by the branching pattern of guinea pig Purkinje cells (Tank 1988) (Figure 2.5).

Figure 2.5: Romanesco broccoli and guinea pig Purkinje cells (Tank 1988).

In addition to the spatial domain, fractal patterns can also be exhibited in the temporal domain. Figure 2.6 demonstrates a simulated time course where temporal patterns are repeated at smaller and smaller time scales. The resultant pattern seems random but has intrinsic order to it (i.e. is chaotic).

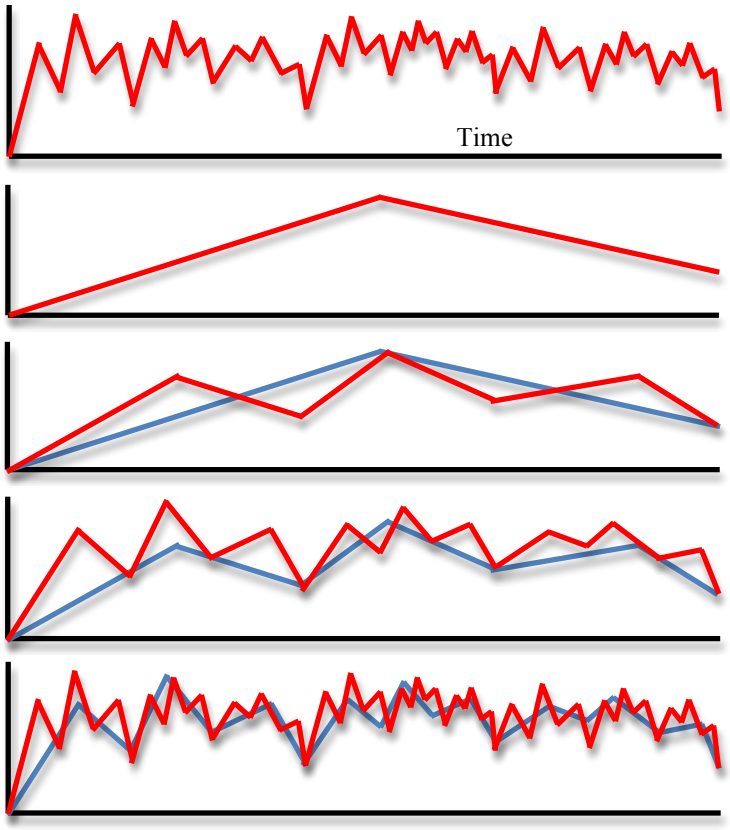

Figure 2.6: Simulated time course where a random seeming time course (top) can be generated by recursive repetition of a simple time course pattern.

Any time course can be examined for a deterministic pattern (one where the value of variables depends on the previous value) and subsequently reconstructed with nonlinear-dynamic mathematics to reveal potential fractal nature (Bassingthwaighte 1994).

2.2.2 Measuring Fractals

There are a variety of methods to calculate the fractal dimension (FD) of a complex system. Fractals by their nature exhibit a power law scaling relationship i.e. follow a $1/f^{\beta}$ relationship (equation 2.1):

$$q = ps^{\beta} \qquad \text{(eqn. 2.1)}$$

where $\boldsymbol{q}$ is the measured parameter (such as MRI signal intensity), dependant on scale parameter $\boldsymbol{s}$. Here, $\boldsymbol{p}$ is a proportionality factor and $\boldsymbol{\beta}$ the scaling exponent (a negative number by some definitions of fractals) (Eke 2002). Fractals not only show self-similarity, they also exhibit scale invariance. For this reason, any method of calculating fractals incorporates equation 2.1 to data pairs (log feature versus log scale) and uses the regression slope for finding the scaling exponent, $\boldsymbol{\beta}$ (Eke 2002). Sometimes, FD is represented by a similar scaled equivalent, the Hurst coefficient. Hurst's observational studies of storage capacities for reservoirs along the Nile identified a pattern of autocorrelation and long-range dependence in 1951 (Hurst 1951). The relation between FD and Hurst is simply;

$$FD = 2 - H \qquad \text{(eqn. 2.2)}$$

Two main categories of fractal analysis employ time-domain analysis (analyses done on signals without any prior transformation) and frequency-domain analysis

(Weitkunat 1991). Relative dispersion analysis (RD) is a basic method for time-domain analysis while power spectral density (PS) is applied to the frequency domain (Bassingthwaighte 1994; Wardlaw 2008). Signal RD is a measure of variance derived from the standard deviation (SD) and the mean of the signal (μ) (equation 2.3):

$$RD = \frac{SD}{\mu} \qquad \text{(eqn. 2.3)}$$

Bassingthwaighte observed a linear relationship between the log of the relative dispersion (RD) and log of measurement scale (Bassingthwaighte 1988; Bassingthwaighte 1989). This reproducible observation has been observed for many fractal patterns and mathematically can be described as:

$$FD = 1 - \frac{\log[RD(m)/RD(m_0)]}{\log(m/m_0)} \qquad \text{(eqn. 2.4)}$$

where ***FD*** is the fractal dimension, ***m*** is the scale of measurement used to calculated ***RD***, and $\boldsymbol{m_0}$ is an assigned reference value. For mathematical simplicity, $\boldsymbol{m_0}$ is often assigned to a value of 1. This equation is bounded by limits such that an FD can range from 1 to 2. A FD of 1.5 describes random uncorrelated noise (white noise) and FD of 1.0 represents completely ordered signal (or uniformity over measurement scale). FD between 1.5 and 2.0 are rarely found in physiological signals and represents negative autocorrelation (i.e. a change in one direction predicts future change in the other direction). Practically, FD can

be calculated from RD using the slope of a log-log plot of RD versus measurement scale. This plot is produced by calculating the RD of the whole signal, then averaging adjacent values (to effectively half the number of observations) and finding the RD of this new series. This can be done for multiple iterations to produce a set of data pairs (RD and series size) (Bassingthwaighte 1994).

FD calculated from power spectral density (PS) uses a fast Fourier transformation (FFT) for analysis in the frequency domain. The log of frequency plotted against log of signal power produces a linear relationship (equation 2.5):

$$|A|^2 = \frac{1}{f^{\beta}} \qquad \text{(eqn. 2.5)}$$

where A is amplitude of the signal Fourier transform, f is frequency and β is a constant used to calculate FD (equation 2.6):

$$FD = 2 - \frac{(\beta + 1)}{2} \qquad \text{(eqn. 2.6)}$$

Most physiological signals exhibit a noise pattern called fractional Gaussian noise (they are stationary signals) (Bassingthwaighte 1994; Maxim 2005; Wardlaw 2008).

2.2.3 Fractal Characterization

Fractal signals can exhibit patterns described either as fractional Gaussian noise (fGn) or fractional Brownian motion (fBm). fBm signals are described as non-stationary and can have a slow drift within the time course. There are more low frequency components and therefore β equation 2.5 represents a steep negative slope in the log-log plot for PS. fBm can occur from either non-physiological noise (e.g. MRI system noise) or represent some physiological signals such as MRI signal from brain CSF (Maxim 2005). fGn is the corollary of fBm and represents stable signals. Although most physiological signals have characteristics of fractional Gaussian noise (fGn), it is important to distinguish fGn from fBm since the FD calculations for each is different (Eke 2000; Eke 2002). The RD method is more accurate for fGn signals while PS can be biased for high FD values (Eke 2000).

With simple signal characterization into fGn or fBm, $\beta > 1$ represents fBm while $\beta < 1$ represents fGn. However, empirical evidence suggests that classification of β around 1.0 is inaccurate with about 40% uncertainty, specifically in the range of $0.38<\beta<1.04$ (Eke 2000). Therefore Eke *et al.* proposed a careful approach for FD signal classification. Signal with β close to 1 can be converted, through signal summation conversion (SSC), so that both fGn and fBm signals become fBm signals. β is then calculated via scaled windowed variance (SWV) analyses to reclassify the signal as either fGn or fBm. SWV is similar to RD but where RD is applicable only to fGn, SWV is for

fBm. SWV divides the series into non-overlapping windows of size τ, for which SD can be calculated. FD can be derived from the following equation;

$$SD(\tau) = SD(\tau_0)\left(\frac{\tau}{\tau_0}\right)^{(2-FD)} \qquad \text{(eqn 2.7)}$$

where τ_0 is a reference value for window size (similar to m_0 for RD in equation 2.4) (Eke 2000). This method can provide a better estimate of FD when there is a possibility of fBm contamination of a physiological signal. Once identified, fBm signal can either be filtered out or calculated separate from fGn.

2.2.4 Fractals and Physiology

When physiological systems were examined for chaotic patterns, many were found to contain fractal patterns (Bassingthwaighte 1994) exhibiting self-similar, $1/f^{\beta}$ relationship. Although this relationship exists both in the spatial and temporal domain, this discussion exclusively describes temporal fractals (no spatial fractal evaluation was done in this work). The 1/f relationship has been observed in brain electroencephalography (EEG) (Xu 1988), cardiac ECG (Bär 2007), respiratory volumes (Hoop 1993), voltage across cell membranes (Churilla 1996) and in perfusion of tumors (Craciunescu 1999). It is not clear why nature exhibits fractal patterning although one possible reason is fractals offer an efficient way for systems to store information and thus

exhibit "memory". This allows for adaptability and learning from previous experiences (Sharma 2009). Fractals in nature can occur due to interactions at small scale such as from closest neighbors (seen in many cellular interactions) or may be the result of large-scale processes (Bassingthwaighte 1994).

Fractal or chaotic behavior has been linked to health in physiological systems. One belief is that chaotic behavior represents enhanced ability for adaptability. Stationary, non-complex signals represent non-adaptive signals. For example, lack of fractal beat-to-beat variability has been related to mortality in myocardial infarction (Tapanainen 2002). This has also been seen in populations at high risk for heart disease such as patients with schizophrenia (Bär 2007) and those with stroke (D'Addio 2009). A recent review highlighted the importance of fractal scaling on health, including aging and mortality, sleep, growth, circulatory systems, and drug doses (West 2012).

In the brain, fractal analysis has long been used to understand brain electrophysiology. As early as 1988, fractal patterns within EEG traces was documented (Xu 1988). In 1992, researchers described details of 1/f scaling in EEG acquired in resting states with eyes-closed and eyes-open EEG (Pritchard 1992; Schepers 1992). Fractal patterns in EEG have been studied in normal subjects (Song 2005; Kiviniemi 2008) and in pathology, such as during epileptic seizures (Bullmore 1994; Kannathal 2004) (Song 2005). EEG fractal analysis can even identify seizures pre-ictally (Li 2005), an important factor in the behavioral and pharmacological treatment of epilepsy. Generally, seizure activity reduces EEG FD (Kannathal 2004), which is in keeping with neuronal synchrony decreasing signal complexity. Beyond EEG, there have been various

other brain electrophysiological signals that show a fractal pattern. This has included laser Doppler flowmetry from the brain cortex, laser speckle imaging (allowing for 2D perfusion analysis) and near infrared spectroscopy (Herman 2009). Early SPECT studies showed a fractal pattern to cerebral blood flow in vascular dementia (Yoshikawa 2003) and magnetoencephalography (MEG) demonstrated fractal patterns in normal subjects (Kitzbichler 2009) as well as in patients with AD (Gómez 2009).

2.2.5 Fractal fMRI of the Brain

Once MRI technology allowed for fMRI at high temporal frequency, it became a valuable tool for non-invasive investigation of fractal-type patterns of the brain at rest (Bullmore 1996; Zarahn 1997; Bullmore 2001). Notably, this occurred not long after invention of fMRI (Ogawa 1990). Similar to EEG, 1/f properties of BOLD time series were discovered, opening up a new window into the brain at rest. One major advantage of MRI over EEG, however, is the superior spatial resolution for fractal analysis. Earlier studies focused on identification and characterization of fractals in fMRI (Zarahn 1997) (Fadili 2002) then clinical applications began to emerge (Maxim 2005; Wink 2006; Lai 2010). Consistent with pre-fMRI findings, there is a correlation between the power spectrum of fMRI and EEG (Kiviniemi 2008) as well as MEG (Kitzbichler 2009).

Like resting state fMRI, fractal analysis of resting state BOLD bypasses the complexity and biases associated with task-based fMRI studies. The scans are relatively

simple to perform. Post imaging data processing can be time intensive, but commercially available software may reduce this bottleneck (e.g. fraclab, http://fraclab.saclay.inria.fr/). Despite the early identification of fractals in fMRI, there have been very few reports of it's clinical utility. The few clinical applications that do exist mostly revolve around aging and dementia (Maxim 2005; Wink 2006; Warsi 2012). This is likely due to difficulty finding overlapping expertise in clinical science and mathematics and may require more multidisciplinary and trans-disciplinary approaches (West 2012). The work herein bridges this gap.

CHAPTER 3

AD AS A MODEL OF BRAIN CONNECTIVITY

3.1 AD PATHOLOGY

Dementia is a prevalent and serious illness that affects an increasing proportion of our population. In addition to the debilitating morbidity and mortality to the individual, dementia causes significant burden on family, caregivers and health care systems. Estimates predict that in less than 30 years, prevalence rates of dementias will double in Canada and healthcare costs will increase 10 fold in this time period (MedicalNews 2010).

AD accounts for the vast majority of dementia in Canada (Prince 2009). Symptoms usually start in the 6th decade of life and involve a progressive degeneration of cognitive function. Histopathology through autopsy or biopsy is the only definitive way of diagnosing AD. The core histological features of AD are neurofibrillary tangles (NFT) and senile plaques (SP).

Abnormal NFT are found in the cell body of neurons and are a consequence of phosphorylation of the protein Tau rendering it insoluble. Formation of NFT disrupts cellular transportation, which can eventually lead to cell death. In this case, NFT skeletons are left behind. Plaques are formed from extracellular amyloid surrounded by dystrophic axons as well as inflammatory cell precursors (astrocytes and microglia). Furthermore, their formation is related to abnormalities in expression of the amyloid

precursor gene. This is worsened (but not caused) by a homozygous expression of ApoE4 (a genetic marker for elevated risk of AD) (Kandel 2000).

As neuronal cells progressively die, there is a slow reduction in brain volume and function (Dubois 2007). Volumetric changes have been studied *in vivo* since the advent of CT scanning and later with MRI. Due to the long history of structural imaging in AD (de Leon 1989), volumetric changes have been a significant part of the evaluation of AD (Dubois 2007).

3.2 STRUCTURAL CHANGES IN AD

CT is used extensively in the clinical assessment of dementia (Patterson 1999). The ability to rapidly acquire high resolution images, wide spread access to CT scanners and relatively low cost has contributed to its popularity. The primary purpose of CT scanning is to eliminate secondary causes of dementia (such as stroke, hydrocephalus, atrophy, or space-occupying lesions). A few characteristics of CT images can help differentiate and stage the severity of dementias such as volume changes in the medial temporal lobe (MTL) (Keyserling 2005). Unfortunately, the changes shown with CT occur quite late in dementia; only after considerable brain changes have already happened. Another important problem with use of CT not to be overlooked, is that volumetric assays have been less reliable, predominantly because of the poorer grey/white matter discrimination and scan angle (since scanning in any non-axial plane is not possible) (de Leon 1989). The value of CT is its wide spread availability and as an

alternative for people contraindicated for MRI (due for example, to metallic implants, pacemakers, etc.) (Keyserling 2005). One other consideration of CT is radiation dose, which is approximately 1-3mSv (head scan), prompting specific guidelines for its use in dementia screening (Small 2008). Use of a 3D T1-weighted MRI scan is the traditional method of producing high-resolution brain images similar to CT. Although the resolution in the past has been inferior to CT, the grey/white matter differentiation, multi-planar acquisition and lack of ionizing radiation have made MRI superior to CT for studying structures in dementia (de Leon 1989).

MRI volumetry involves the automatic or manual tracing of brain structures in multiple slices allowing for volume measurements. Since most dementia is associated with progressive brain tissue loss, volume measurements can provide useful information about disease progression. Region specific volume changes may be associated with different dementias. AD is associated with atrophy of the parietal lobes and the medial temporal lobe (including the hippocampus) as seen by MRI (Vitali 2008). There is also overall brain volume loss and increase in ventricular size (Brewer 2009). Hippocampus volume is a consistent and predictable marker of AD and can sometimes be used to detected risk of conversion from mild cognitive impairment (MCI) to AD (Hampel 2008). A change in hippocampus volume over time is an accurate measure of disease progression and is used as an outcome measure in many AD treatment studies (Bradley 2002; Hampel 2008). Whole brain volume and whole brain to ventricle volume ratios are sensitive but not specific markers of AD severity. More specific findings are changes in cortical thickness or a multivariate principal component analysis (PCA) of brain

deformation (Teipel 2007; Lerch 2008). These methods use automated approaches to brain volumetry and the neuroanatomic correlations of these methods have not been established with pathology (Raz 2007). There is, however, good correlation between automated approaches and manual segmentation (Hsu 2002; Brewer 2009). Since volumetric changes in AD are a central feature of illness progression, volumetric measurements were included in all of the studies presented in this thesis.

3.3 METABOLIC CHANGES IN AD AS MEASURED BY ^{1}H MAGNETIC RESONANCE SPECTROSCOPY (MRS)

Magnetic resonance spectroscopy (MRS) is a MR technique that allows acquisition of spatially prescribed *in vivo* nuclear magnetic resonance (NMR) spectra. Most often, MRS is performed with hydrogen (i.e. proton, ^{1}H) due to the high natural abundance, high gyromagnetic ratio (γ = 42.576MHz/T) and relative simplicity (i.e. the MRI scanner is already tuned to ^{1}H for imaging). Other forms of MRS are called broadband or multinuclear (e.g. ^{13}C, ^{31}P) and have advantages and disadvantages associated with them that are not a part of this thesis. During ^{1}H-MRS acquisition metabolic NMR signatures for a plethora of overlapping metabolites are encoded (de Graaf 2007). This technique allows the probing of various metabolites and xenobiotics present within a voxel of interest. Common ^{1}H-MRS identifiable chemicals of interest include N-acetylaspartate (NAA), choline (Cho), creatine (Cr), alanine (Ala), lactate

(Lac), myoinositol (mI), glutamate (Glu), glutamine (Gln), glucose (Gc) (Soares 2009) and sometimes gamma-Aminobutyric acid (GABA).

AD is associated with a decrease in NAA (a marker of neuronal cell viability) and an increase in mI (a marker of inflammation) (Schuff 2002). There is also a correlation between choline and cognitive improvement with AD treatment (Schmidt 2009). These findings are in keeping with the pathology of AD. Degenerative diseases like AD can also have increased Glu due to impaired reuptake at the synapse (Hu 2007).

Another method of MRS called chemical shift imaging (CSI) allows evaluation of metabolites over a 2 or 3 dimensional volume of the whole brain rather than focusing on one voxel. This technique is also called multivoxel MRS as data acquisition involves spatially encoding multiple voxels over the prescribed volume. Results are often qualitative rather than quantitative. This method can be technically quite difficult due to the sensitivity to motion (Schmidt 2008) and the difficulty in getting a large homogenous B_0 over the entire acquisition volume (i.e. difficult to achieve a perfectly homogenous shim over such a large volume). Since some of the documented changes observed in AD patients using MRS are quite subtle, CSI measures have not found consistent results in assessing dementias (Valenzuela 2001). Overall, however, single voxel ^{1}H-MRS provides some robust markers of AD (lower NAA and higher mI) and as such was included in our study as a comparator to functional methods.

Analysis of MR spectra is challenging due to the overlapping resonances, especially in the narrow banded ^{1}H-MR spectra, which only covers roughly 5-7ppm. Analysis used to be done through individual peak assignment (by hand) and subsequence

deconvolution. More recently a number of algorithms have been developed that use a linear combination of NMR basis sets for each metabolite. The most noted of these is LCmodel (Provencher 1993). There are a few others, however, such as Java Magnetic Resonance User Interface (jMRUI) (Mandal 2012) or Totally Automatic Robust Quantitation in NMR (TARQUIN) (Wilson 2011).

3.4 Iron Changes in AD as Measured by Susceptibility Weighted Imaging (SWI)

Susceptibility weighted imaging (SWI) is a high-resolution 3D gradient echo MRI method, with flow compensation in all three orthogonal planes, that enhances contrast from local tissue susceptibility variations. This allows assessment of regional brain iron deposition and the detection of iron rich microbleeds. Development of brain microbleeds is associated with risk of progressive cognitive impairment (Werring 2010). Microbleeds may be secondary to cerebral amyloid angiopathy and are detectable by SWI. Since SWI is sensitive to a very small amount of iron, some deposits may actually represent iron in senile plaques associated with AD (Ayaz 2010). Histopathology has shown that SWI hypointensities correlated with microbleeds that are associated with cerebral amyloid angiopathy, seen in up to 95% of patients with AD (Schrag 2009).

In addition to microbleeds, phase shift measurements using SWI are sensitive to iron concentrations and thus SWI can be used to quantify iron in the brain. Using SWI, iron concentration in the brain was found to correlate with cognition and risk of dementia

(Kirsch 2009). Increased iron may be a result of overloaded axonal and neuronal iron transport mechanisms (Kirsch 2009). Improved mesencephalon imaging with SWI may help visualization pathology in this region (Manova 2009). The same is true of iron content in the basal ganglion (Bartzokis 2000; Sehgal 2005). SWI is a robust MRI technique to measure iron in the brain. Since iron is central to the pathogenesis of AD, we compared SWI to our measures of functional connectivity.

3.5 FUNCTIONAL CONNECTIVITY IN AD

Traditional fMRI involves task-based brain activations. Memory encoding tasks during fMRI have shown decreased activation of the hippocampus in patients with AD when compared to controls. There is increased activation in the medial parietal and posterior cingulate regions and this may represent a dedifferentiation of memory tasks or compensatory activation (Sperling 2003). Patients with AD also exhibit decreased lateralization during cognitive tasks, more prominently than with normal aging. Tasks that preferentially activate one side of the brain are seen to have activations bilaterally, further suggesting dedifferentiation (Minati 2007) or compensatory mechanisms (Han 2009).

As described in Chapter 2, resting state BOLD (rsBOLD) can also be used to study brain function in health and disease. Although analysis of rsBOLD varies, general patterns of functional connectivity remain constant and there is specific disruption of these patterns in dementia (Liu 2008). AD is associated with a decrease in functional synchrony in the

hippocampus (Li 2002). ICA and seed-based methods of rsBOLD analysis have revealed decreased connectivity in the posterior cingulate and hippocampus (Greicius 2004; Sorg 2007) and well as prefrontal-parietal networks (Wang 2007). These changes can distinguish AD from controls (with a sensitivity of 85% and specificity of 77%) and may predict conversion from MCI to AD (Greicius 2004). Brain network disruptions correlate with disease severity in AD (Broyd 2009; Fleisher 2009). Resting state BOLD has also been shown to correlate with fluorodeoxyglucose positron emission tomography (FDG-PET), a marker of brain activity (Perrin 2009) and these findings are not accounted for by brain atrophy (He 2007). Resting state network (RSN) analysis thus provides a reproducible measure of functional connectivity in AD.

3.6 FRACTAL DIMENSION IN AD

Since neuronal loss and disconnectivity are likely related to changes in signal complexity, one of the earlier clinical applications of fractal analysis of BOLD data observed AD (Maxim 2005) and normal aging (Wink 2006). Aging is associated with a decrease in FD (increase in Hurst exponent). This effect was exaggerated by cholinergic blockade (effectively mimicking AD) (Wink 2006). The comparison of AD to healthy age matched controls showed AD causes a significant global reduction in FD as measured using magnetoencephalography (MEG) (Gómez 2009). These preliminary studies opened the door to FD analysis in AD and this thesis takes the next steps to explore this further.

Using AD as a clinical population to study RSN and FD has two main uses. First, comparing rsBOLD changes to already established measures of AD pathology such as volumetry, MRS and SWI gives us a 'yard stick' with which to measure the accuracy, utility and limitation(s) of these novel techniques. If favorable, FD can be further applied to other brain pathologies, including mental illness. Secondly, FD analysis can offer details about fMRI signal not available to other established methods. Because of this, FD may unveil novel information about AD pathology in early stages of illness.

CHAPTER 4

PROJECT HYPOTHESIS, OBJECTIVES AND METHODS

4.1 HYPOTHESIS

The brain is inherently complex. In fact it is best described as a "complex system" (Bullmore 2009). Complex systems are incredibly non-linear and are not easily characterized. The brain is described as a complex system because it is continually adapting to multitudes of internal and external stimuli, all at differing intensities and frequencies, which are then rapidly processed to generate an appropriate output (scaled in time, space, amplitude, phase and frequency). A complex system is a healthy system as complexity drives the ability for adaptation. A linear system can not, and does not dynamically adapt as a complex system does (Bassingthwaighte 1994). Therefore the work proposed in this project revolved around the hypothesis that rsBOLD signal complexity, as measured through temporal fractal dimension (FD), relates to severity of AD and functional connectivity. In essence, a sick brain loses the ability to adapt and hence becomes less complex. The measure of FD was chosen as the BOLD signal is already a complex mixture of blood flow, metabolism, oxygenated hemoglobin:deoxygenated hemoglobin (oHb:dHb) concentration and blood volume, all at unknown and rapidly varying values. Additional hypotheses included the following: 1) Reduced BOLD signal complexity correlates with reduced regional brain volume (i.e. if neurons were dying, this is reflected in brain volume loss and hence reduced network complexity); 2) Regional brain iron content is increased when brain rsBOLD signal is less complex (i.e. it is already well understood that elevated brain iron is linked with

many brain diseases such as AD); and 3) Metabolic indices of AD (i.e. decreased NAA and increased mI) scale with loss of BOLD signal complexity.

4.2 METHODS

AD subjects for this study were recruited by Dr. William Molloy from St. Peter's Centre for Studies in Aging, Hamilton Ontario. These subjects were part of a larger drug trial of AD (DARAD Trial) (Yavuz 2009), but subjects approached for the MRI study were not taking any drug from the study that would bias MRI results (they were effectively on placebo). Age matched healthy controls (NC) were recruited from the spouses of study subjects, allowing for relatively close matching in age, accessibility to the study centre and day-to-day environmental exposures. Although most AD agreed to return for rescanning 9-12 months later, the DARAD trial was terminated early and only a small proposition of subjects had been in the study for >9 months. Therefore, only about a quarter of AD subjects had repeat scans in our study.

For the FD validation scans (chapter 5) where some the scans were quite long, we chose healthy volunteers. Despite subject and scanner accessibility, we could not scan subjects for hours at a time. Therefore, some the validation data was extrapolated from longer single subject scans. The details of this are explained in chapter 5. Since the work overlapped with another graduate student working on FD in the same lab (Wardlaw 2008), it was this student's FD method we originally focussed on (chapters 5 and 6).

After this, our lab started to refine the FD method (Elzibak 2011), leading us to use the FD algorithm described by Eke *et al* (Eke 2002) (chapter 7).

When choosing a region of interest (ROI) for our MRS study (chapter 6), we proposed a grey matter structure that was i) relatively homogeneous, ii) not bounding air, fluid or bone interfaces that could cause artefacts in the MRS and FD measurements, and iii) was involved in the pathology of AD. Our initial choice was the hippocampus. However, the results from an optimized MRS stimulated echo acquisition mode (STEAM) sequence and FD in our first subject showed too much susceptibility artefact to justify continuing. Our second choice was the putamen, which was our successful ROI for future scans.

We used a STEAM sequence that was optimized to concurrently measure glutamate, glutamine and GABA in addition to NAA and mI. This method originally proposed by Hu *et al.* (Hu 2007) and was implemented by a graduate student in our lab (Sheffield 2010). Our approach used a cubic MRS voxel, and to obtain sufficient SNR, the voxel was larger than the width of the putamen ($8cm^3$). This introduced the potential of partial voluming which could not be avoided, unless we had a transmit SENSE MR platform with spatially programmed volume selective RF. FD analysis was also prescribed to the same cubic voxel to ensure an accurate comparison of FD and MRS. When not constrained by an MRS voxel, measurement of FD in the putamen used a precisely outlined ROI for each subject (chapter 7).

Measuring resting state networks (RSN) in the brain complimented studying network complexity with FD analysis. We designed the study (chapter 7) to compare

connectivity in the DMN to FD within the DMN (in the posterior cingulate cortex, PCC) and outside of it (in the putamen). The putamen was chosen to allow for consistency with our previous study (chapter 6), and the PCC is the central DMN and also involved in AD pathology. Both the PCC and the putamen fall within the same axial acquisition plane, so FD could easily be measured from both ROIs from our high frequency (TR=250ms), low special coverage (3 slices) BOLD scan.

The final study (chapter 8) describes the evaluation of how iron deposition may alter brain network connectivity. Iron content was calculated from susceptibility weighted images (SWI). SWI post-processing was done using a GE Functool plug-in (General Electric Healthcare, Milwaukee WI) written in-house. The results from this plug-in were compared to results from the SPIN software developed by Dr. Mark Haacke (Haacke 2010) and was found to be equivalent. The methods for SWI analysis are described in chapter 8.

The last chapter of the thesis (chapter 9) distils the experimental results into one story and provides suggested future directions.

CHAPTER 5

TEMPORAL FRACTAL DIMENSION (FD)

STABILITY OF BOLD FMRI

Brain Fractal Blood-Oxygen Level Dependent (BOLD) Signals: The Effect of MRI Acquisition Parameters on Temporal Fractal Dimension (FD) Stability

Mohammed A. Warsi, B.Sc., M.Sc., M.D., FRCP(C), Alexander M. Weber, B.Sc., M.Sc., Michael D. Noseworthy, M.Sc., Ph.D., P.Eng.

5.1 CONTEXT OF THE PAPER

FD is a relatively new measure of rsBOLD and for this reason stability as a brain metric requires exploration. It is understandable that signal complexity can vary with signal parameters. Therefore brain FD was measured when key imaging acquisition parameters were altered. This included how rsBOLD signals were acquired (spiral vs. EPI), length of data collected and data temporal resolution. In the third paper (chapter 7) intra-subject scan-to-scan reproducibility was evaluated. Additionally, all acquisition factors were explored for both methods used in this thesis for measuring FD (i.e. FD_{RD} and FD_{PS}) highlighting each method's strengths and weaknesses.

5.2 DECLARATION STATEMENT

Mohammed Ali Warsi and Alex Weber, as principle co-authors, wrote the article, performed analysis and created figures and tables as appropriate. Contributions by

Mohammed Ali Warsi warranted his name as first author. Michael D. Noseworthy, as corresponding author, described the need for and initiated the study on FD stability, wrote the first versions of the FD analysis program using Matlab (Mathworks, Natick, MA), provided guidance, funding and advice. Furthermore he was instrumental in proofreading/editing and submitting the manuscript for publication.

This paper has been submitted for publication to the journal *Visualization, Image Processing and Computation in Biomedicine.*

5.3 PAPER

Brain Fractal Blood-Oxygen Level Dependent (BOLD) Signals: The Effect of MRI Acquisition Parameters on Temporal Fractal Dimension (FD) Stability

Mohammed A. Warsi, B.Sc., M.Sc., M.D., FRCP(C)[1-3], Alexander M. Weber, B.Sc., M.Sc.[1,3], Michael D. Noseworthy, M.Sc., Ph.D., P.Eng.[1-7*]

[1]*School of Biomedical Engineering, McMaster University, Hamilton, Ontario, Canada.*
[2]*Department of Psychiatry and Behavioural Neuroscience, Hamilton, Ontario, Canada.*
[3]*Brain-Body Institute, St. Joseph's Healthcare, Hamilton, Ontario, Canada.*
[4]*Electrical & Computer Engineering, McMaster University, Hamilton, Ontario, Canada.*
[5]*Medical Physics & Applied Radiation Sciences, McMaster University, Hamilton, Ontario, Canada.*
[6]*Diagnostic Imaging, St. Joseph's Healthcare, Hamilton, Ontario, Canada.*
[7]*Department of Radiology, McMaster University, Hamilton, Ontario, Canada.*

**Corresponding Author Address:*
Dr. Michael D. Noseworthy, Ph.D., P.Eng.
Director, Imaging Research Centre,
St. Joseph's Healthcare, 50 Charlton Ave. East
Hamilton, Ontario, Canada. L8N 4A6
Phone: +1 1(905) 522-1155 x35218
Email: nosewor@mcmaster.ca

ABSTRACT

Fractal analysis of the temporal patterns in functional magnetic resonance imaging (fMRI) brain data has recently gained momentum in assessing diseased and pharmacokinetically altered brain. However, there is no agreed upon standard method of acquisition and analysis. Therefore, we examined the fractal dimension (FD) of the brain's blood oxygen level dependent (BOLD) signal over time, with varying time-points, MRI k-space filling techniques, repetition times (TR), and scan lengths. Furthermore, fractal dimension was determined with two different approaches: relative dispersion (FD_{RD}), and power spectrum (FD_{PS}) techniques. At a reduced number of time points, FD_{RD} is resistant to differing TR. FD_{PS} is time-point invariant at a low TR (250ms). With constant scan times, FD_{PS} is the least variable. Our results show there are some constraints to FD measurement in the brain that require a certain amount of consistency in technique when comparing multiple scans. But within these constraints, FD can provide a reliable method to examine brain resting state BOLD signal.

KEY WORDS

functional magnetic resonance imaging, blood oxygen level dependent (BOLD), MRI, brain, fractal, resting state

INTRODUCTION

Fractals are non-differentiable functions that exist where Euclidean systems fail and their dimension exceeds that of topological dimensions (i.e. is non-Euclidean). Fractals exhibit self-similarity at multiple scales. They are found in biological and physiological systems, some examples being: the surface area of the Romanesque broccoli[1], pulmonary blood flow[2], EEG patterns[3], and DNA base-pair sequences[4].

As opposed to Euclidean geometry, whose structures have topological dimensions that are integers, fractal structures have fractional dimensions. For example, one of the earliest fractals described was the Koch curve, the dimension of which is 1.2613. The definition of a fractal dimension (FD), given by Mandelbrot[5] is:

$$FD = \frac{\log(N)}{\log(r)} \qquad \textbf{eqn. 1}$$

where ***N*** is the number of unit lengths in a basic recurring pattern, and ***r*** is a scale ratio, or number of unit lengths over the pattern's base (**Fig. 1**). However, this equation is impractical in biological systems where ***N*** and ***r*** are hard to define. Alternatively, FD can be calculated using an indirect method that estimates the value from the slope of a relationship between two parameters (detailed below).

Figure 1. Part of Koch's curve. On the left, the first iteration of Koch's curve is shown, where N is equal to the unit lengths (4), and r is equal to the number of unit lengths that will cover the base (3). The center and right graphs show the second and third iteration (with N=16, r=9 and N=64, r=27, respectively). All of the graphs have an FD value of 1.2619 (logN/logr).

Since the 1990s, it has been known that time-signals from functional magnetic resonance imaging (fMRI) blood oxygen level dependent (BOLD) signals can be modeled using fractal mathematics[6]. These patterns have long memory, or are positively auto-correlated, in time. This auto-correlation is denoted using FD or the Hurst exponent (H), a scaled variant to FD. Values of FD between (but not including) 1 and 1.5 are said to be negatively auto-correlated; between 1 and 1.5, positively auto-correlated; and a value of FD=1.5 indicates a time-series made up of white noise (i.e. truly random).

There are many methods of determining FD from a time series, only two of which will be discussed in detail here (for a full review see Bassingthwaighte[7]). The first method[8] determines data relative dispersion (RD) and is best suited for consistently sampled data. Signal FD_{RD} can be calculated from RD (standard deviation divided by mean of the signal) using:

$$FD = 1 - \frac{\log[RD(m)/RD(m_0)]}{\log(m/m_0)} \qquad \textbf{eqn. 2}$$

where FD is the fractal dimension, ***m*** is the scale of measurement used to calculated ***RD***, and $\boldsymbol{m_0}$ is an assigned reference value. For mathematical simplicity $\boldsymbol{m_0}$ is assigned a value of 1.0. This approach is done by pooling and taking the mean of adjacent values from the original set, progressively reducing the size of the new data set. FD_{RD} is then estimated by finding $\boldsymbol{\alpha}$: the negative slope of log(RD) plotted against log(group size); where $FD_{RD} = 1 - \alpha$. The FD can also be obtained using signal frequency or power, accomplished by first applying a Fourier transform to the data. Next, the absolute power spectrum (PS) of the signal is obtained, by squaring the absolute value of the complex waveform, which in turn is inversely related to the frequency raised to the power of $\boldsymbol{\beta}$:

$$|PS|^2 = f^{-\beta} \qquad \textbf{eqn. 3}$$

FD_{PS} is then calculated from:

$$FD_{PS} = \frac{(3-\beta)}{2} \qquad \textbf{eqn. 4}$$

This holds true for most physiological signals where $\boldsymbol{\beta}$ <1 and the signal is classified as having a fractional Gaussian pattern (fGn)[9]. When $\boldsymbol{\beta}$ is negative for fractal signals they are often referred to as 1/f processes.

Schepers *et al.* compared four different techniques to calculate FD on simulated data with known H values[10]. The four FD techniques included: RD; PS; Hurst's original method for determining the H exponent, referred to as the rescaled range analysis (R/S); and correlation analysis (C). Their analysis showed the RD method often under-estimates

the H value, such that FD is biased toward a 1.5 value as it takes into account correlations over large temporal distances. They further showed that RD is well suited for long signals. They concluded the PS method gave least biased results, with lowest variance, for both short and long signals (defined as 512 and 32768 time-points respectively).

Fractal analysis of brain BOLD signals has been successfully applied to the study of Alzheimer's disease[11, 12], acute pharmacological challenge[13], attention deficit-hyperactivity disorder[14], cognitive tasks[15], and autism[16]. Thus, in recent years, the application of fractal analysis in brain applications has become a useful and potentially powerful method. These studies, however, each used a frequency domain fractal analysis method, with similar TR times (~1100ms) and analyzed the same number of time-points (512) (**Table 1**).

Table 1: Table comparing approaches for fractal BOLD changes in the brain. These 5 are the only ones, to the best of our knowledge, and have all used almost identical methods.

Published Study	Time-points	FD Analysis Method	Repetition Time
Maxim, 2005	512	Frequency domain	1,100
Wink, 2006	512	Frequency domain	1,100
Anderson, 2006	512	Frequency domain	1,000
Wink, 2008	512	Frequency domain	1,100
Lai, 2010	512	Frequency domain	1,302

No study has yet been published that evaluates brain BOLD fractal signal properties over various acquisition schemes. Even though researchers use similar analysis techniques and MRI parameters, there has yet to be an investigation showing fractal signal dependencies (if any) on these parameters. Therefore, we performed the

following variations in BOLD scanning to determine effects on fractal signal characteristics: MRI k-space filling method (spiral vs. EPI), length of repeat time (TR) or sampling frequency (TR^{-1}), number of temporal points (TP) and total length of scan (LS). A lower TR is sensitive to signal higher frequency components but at the expense of spatial coverage. Finally, we also evaluated the fractal stability of the signal over time.

MATERIALS AND METHODS

The study was approved by our local research ethics committee, in accordance with the declaration of Helsinki. Healthy young-adult subjects (five male and two female; all between the ages of 25 to 35) were scanned using a GE 3T Signa HD MRI system and 8-channel phased array head RF coil (GE Healthcare, Milwaukee WI). Subjects were assigned to various BOLD scan parameters as described in **Table 2**.

Table 2: Number of subjects of each type of scan. Some subjects participated in more than one scan.

Scan Type	Repetition Time	Slices	Time-points	Subjects	Section
EPI	250	3	6666	2	6
			2048	5	4, 5
		1	8192	1	1, 2, 3
	2000	24	256	5	4
Spiral	250	3	2048	4	5

Following a 3-plane localizer scan, a 3D T1-weighted sequence (fSPGR IR prepped α=12°, TE/TR/TI = 2.1/7.5/450ms, FOV=24cm, 320x192 matrix, 2mm thick, 90 slices, interpolated to 180 i.e. 1mm thick) was used to prescribe BOLD image acquisition

through the largest cross sectional area of the basal ganglia, parallel to the AC-PC line (i.e. anterior-posterior commissure). During all BOLD scans, subjects were asked to remain still, keep their eyes open, not sleep, and not think of anything in particular (i.e. be 'at rest' as best as possible). fMRI scans were done using either EPI or spiral-based k-space acquisitions. However, both were single readout trajectory (single shot EPI, or single interleaf spiral) and both used the following same acquisition parameters: TE=35, FOV=24cm, 64 ×64matrix, 5mm thick slices. Differences between k-space filling strategies are detailed below.

To test variations in scan TR, TP and LS, EPI scanning was performed. This was done with either short TR (α=70°, TR=250ms) with a range of 1-3 slices and 2048 to 8192 time points, or a long TR (α=90°, TR=2000ms) with 24 slices and 256 time points (see **table 2** for details). For all scans the first 10 seconds (40 acquisitions for TR=250ms, and 20 for TR=2000ms) were discarded to allow for signal/T1 relaxation equilibration.

It was not feasible to scan single subjects enough times to get FD data representing multiple different repetition times (TR), scan lengths (LS) and number of temporal data points (TP). These variations were therefore calculated from single scans lasting 34.13 minutes (1 slice, 8192 time points, TE/TR=35/250ms, α=70°, FOV=24cm, 64×64matrix, 5mm thick slices) and varying TR, LS and TP was done artificially taking into consideration the following relationship, LS=TR×TP. This approach removed any potential scan-to-scan variation effect. Thus either TR, TP or LS were able to be constant while varying the others.

1) Constant Repeat Time (TR)

We extracted BOLD data with the following number of time-points: 32, 64, 128, 256, 512, 1024, 2048, 4096, and 8192. The time-points were taken by truncating our single slice EPI brain BOLD scan, keeping TR constant (TR=250ms).

2) Constant Number of Time Points (TP)

Using the same large EPI data set, TR time was varied by extracting every *n*th time point, such that if a TR of 500 was desired, every second time-point was used (i.e. the TR was 250ms). A comparison was made with TR values of 250 (every point), 500 (every 2^{nd} point), 1000 (every 4^{th} point) and 2000ms (every 8^{th} point). Data was truncated to 1024 time points (the constant or maximum size of the data set, i.e. 8192) and this analysis was redone with 256 time points.

3) Constant Scan Length (LS)

We compared the effect on FD of varying TR and the number of temporal points to keep scan time constant at 34m 8s. Varied TRs (TR = 250, 500, 1000 and 2000ms) were extracted as before, by taking every *n*th time point, but the data was not truncated for length of scan. Subsequently as TR increased, TP decreased (TP = 8192, 4096, 2048, 1024). This analysis was redone with a shorter scan length (8min. 32s) (TP = 2048, 1024, 512, 256).

4) Constant Scan Length (LS) in Multiple Subjects

The extrapolated result from the short scan (8min. 32s) was compared with short scans in 5 health subjects (three male, two female; all between the ages of 25 and 35 years). For these 5 subjects, 2 scans, each of 8min. 32s were performed at 2 different TRs

(TR=250 / TP=2048 and TR=2000 / TP= 256). Co-registered single slice FD maps were calculated for 5 subjects scans for both TR values. FD_{RD} and FD_{PS} values were obtained for an ROI covering a large portion of white and grey matter (**Fig. 2**).

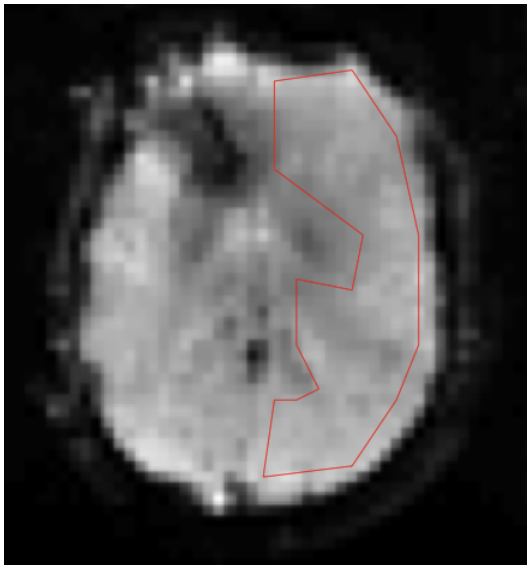

Figure 2. Right Hemisphere ROI. The ROI chosen for analysis had a total of 321 voxels.

5) k-Space Filling Strategies

Two k-space filling strategies were used: EPI and spiral. EPI scans were done using the standard GE Healthcare EPI product scan. Spiral acquisition was performed using a single interleaf spiral scan (spiral-out, 4858 points, reconstructed to 64x64 using a Kaisser-Bessel convolution kernel, beta=11.525, window width=2.5mm)[17].

6) Temporal Stability

The last avenue explored was how resting brain BOLD signal changes over time. Two subjects were scanned using our standard EPI BOLD sequence (TR=250ms). A total of 6666 temporally contiguous BOLD images were acquired over 28 minutes at a

sampling rate of 4Hz (1/TR). A sliding window of 2048 data points was evaluated over the 6666 data points. The sliding window (i.e. 512s, or 8.5minutes) was shifted by an intervals of 46 points (i.e. 11.5sec) to obtain 100 temporally shifted FD maps. PS and RD were analyzed over an entire slice as well as within a single region of interest drawn around the putamen.

Analysis

Fractal analysis was performed using in-house programs written in Matlab (v.7.10, The Mathworks, Natick MA). Motion (translational and rotational) during the scan was assessed and corrected using AFNI[18]. Motion was not corrected for scans testing stability of signal over time. Self-similarity of the time and frequency domain was evaluated pixel-wise[19], resulting in fractal maps of FD using relative dispersion (FD_{RD}) and power spectrum analysis (FD_{PS}). Accuracy of the line of best fit for the slope of the log-log plots were considered significant at $P<0.05$. The proportion of voxels with significant fitting, within a given ROI, was expressed as a percentage. A high percentage was interpreted as most voxels having fractal time signal.

The FD_{PS} and FD_{RD} maps were skull stripped (removing background), warped into Talairach coordinates and spiral and EPI scans were compared with a one-way ANOVA using AFNI[18].

RESULTS

Varying Temporal Acquisition Characteristics

Constant Repeat Time (TR)

With TR constant and scan length increased by increasing the number of time points (TP), both FD_{PS} and FD_{RD} approached unity, more so FD_{RD} than for FD_{PS} (**Fig. 3**). FD_{PS} appeared more stable for midrange values of TP while having the greatest deviation with the very low TP range.

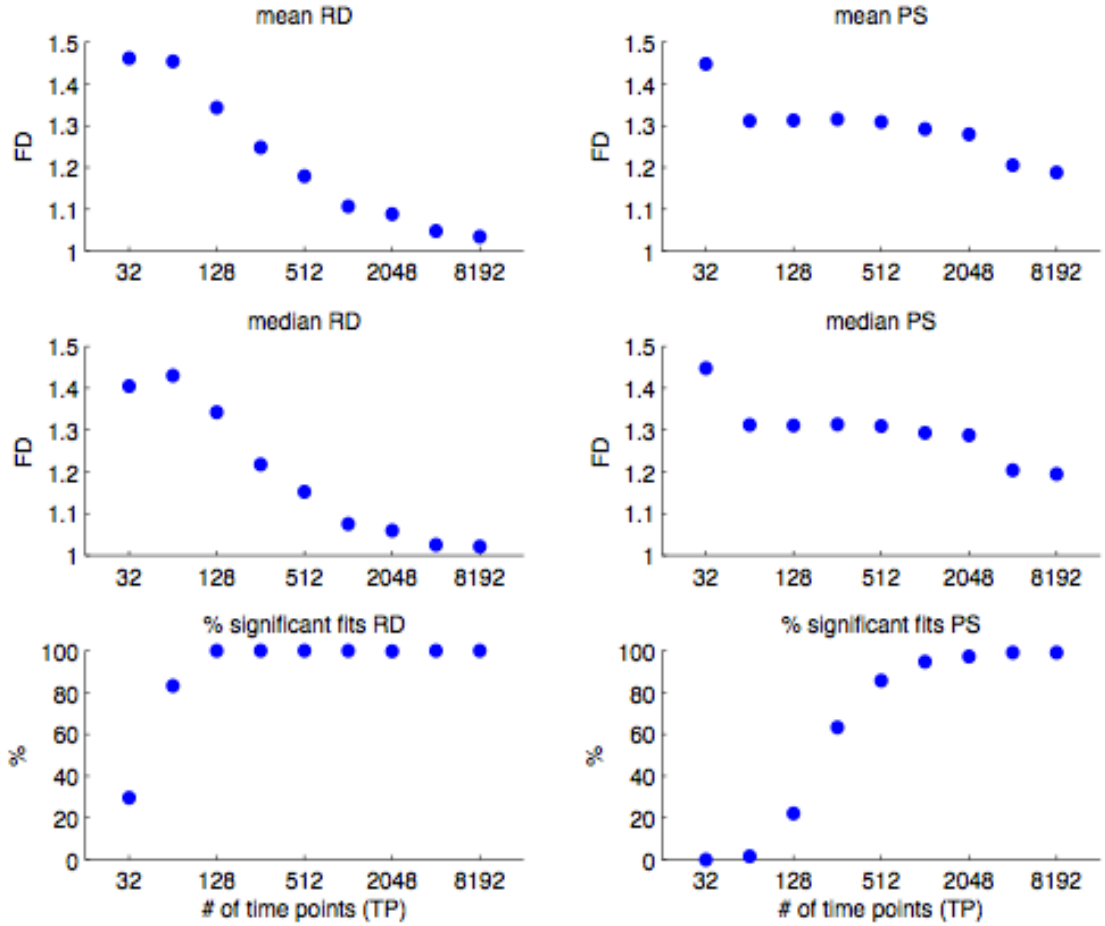

Figure 3. Fractal behaviour over varying time-points (TR=250ms). All x-axes represent the number of time points. The y-axes for the top four figures represent the FD. The y-axes for the bottom two figures represent percentage of voxels with significant log-log fits.

Constant Number of Time Points (TP)

With TP constant at 1024, and TR ranging from 250 to 2000ms, the length of time was between 4min. 16s and 34min. 8s. Varying the TR resulted in increased mean (from 1.05 to 1.14) and median (1.03 and 1.13) FD_{RD}, while the percent significant fits remained similar to before (~100%) (**Fig. 4**). Both mean and median FD_{PS} similarly decreased (from 1.3 to ~1.13), while the percent significant fits increased slightly from 94 to 100%.

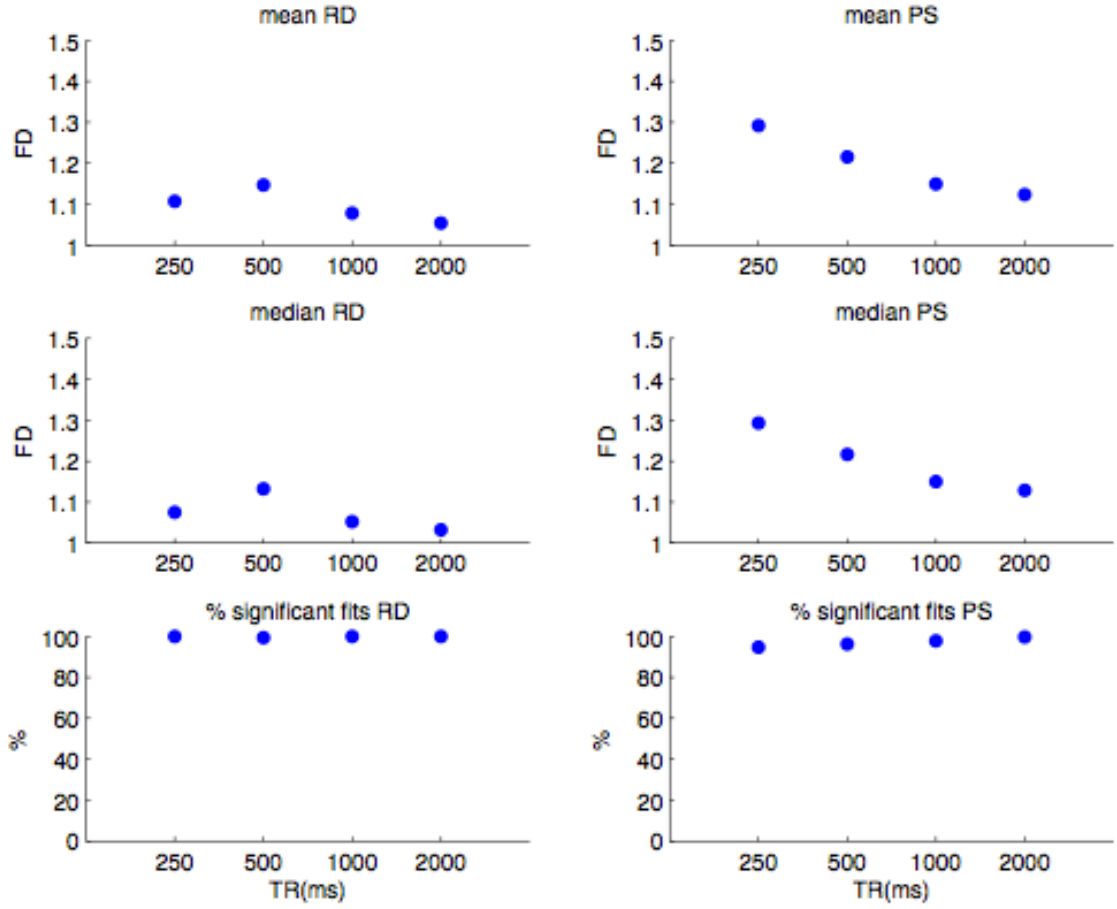

Figure 4. Fractal behaviour over varying repetition times (1024 time-points). All x-axes represent the TR(ms). The y-axes for the top four figures represent the FD. The y-axes for the bottom two figures represent percentage of voxels with significant log-log fits.

With TP constant at 256 and TR ranging from 250 to 2000ms, the total scan length was between 1min. 4s and 8min. 32s. Here TR did not appreciably alter FD_{RD} in relation to its mean (~1.22), median (~1.19) or even the percent of significant fits (~100%) (**Fig. 5**). As for FD_{PS}, the FD for both the mean and median decreased from 1.3 to ~1.13, while the percent of significant fits increased from 63 to 91%.

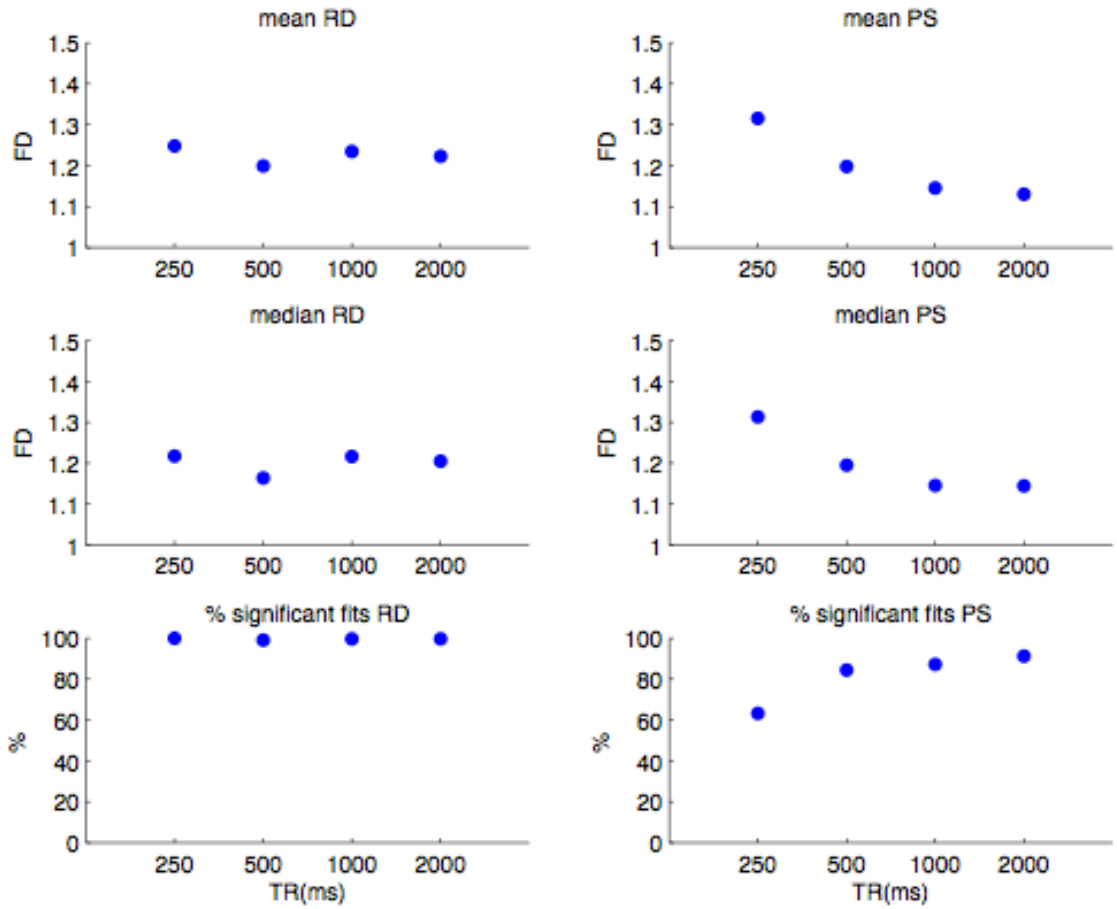

Figure 5. Fractal behaviour over varying repepition times (256 time-points). All x-axes represent the TR(ms). The y-axes for the top four figures represent the FD. The y-axes for the bottom two figures represent percentage of voxels with significant log-log fits.

Constant Scan Length (LS)

With constant LS (34min. 8s) FD_{RD} is almost equal to 1 (**Fig. 6**). FD_{PS}, on the other hand, still maintains a mean value around 1.17 (range: 1.12 to 1.21), which appears to decrease as TR is increased (and the number of time-points decreases). The percentage of significant line fits remained constant around 99%. With LS reduced to 8min. 32s, FD_{RD} value increased from 1.09 to 1.22 as the TR was increased and time-points were reduced from 8192 to 1024 (**Fig. 7**). The percentage of voxels with significant fits stayed constant at approximately 100%. FD_{PS} decreased from 1.28 to 1.13, while the percentage of significant fits also decreased, from 97 to 91%.

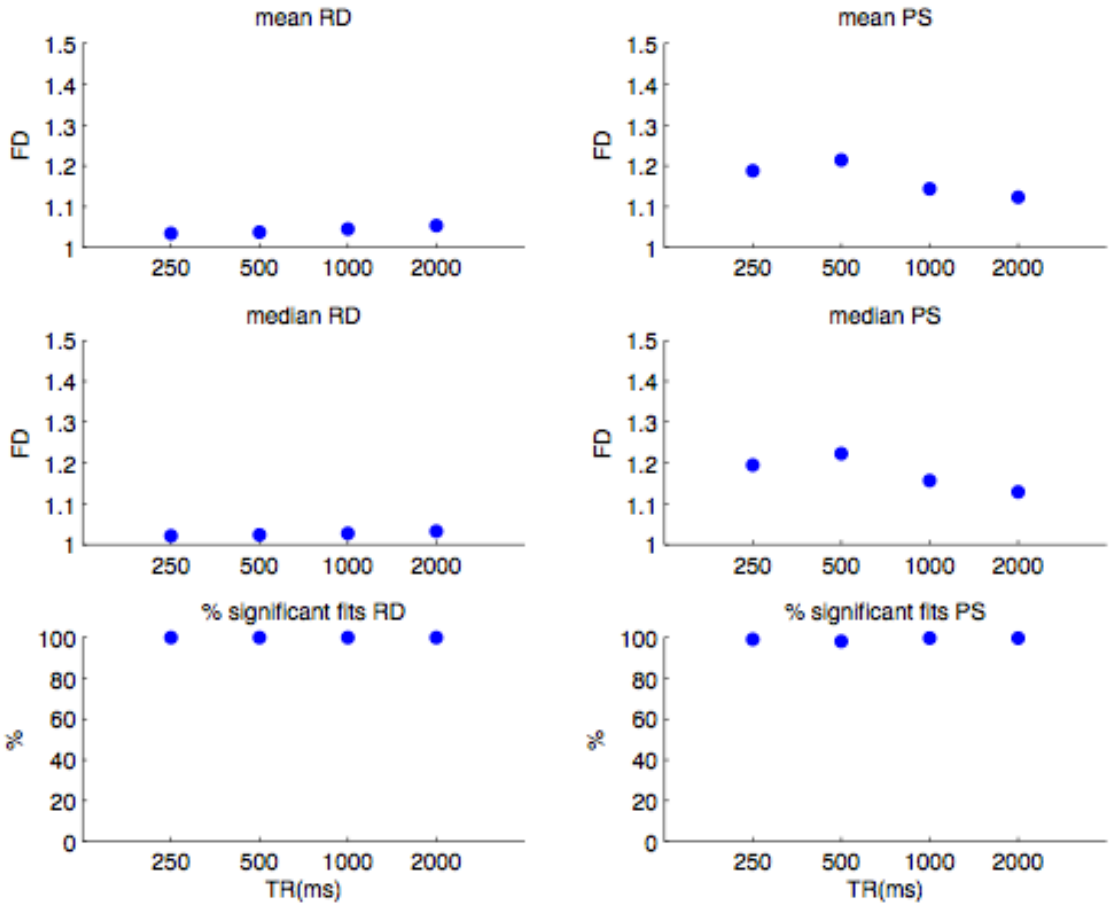

Figure 6. Fractal behaviour over varying time-points and repetition times (34min. scan length). All x-axes represent the TR(ms). The y-axes for the top four figures represent the FD. The y-axes for the bottom two figures represent percentage of voxels with significant log-log fits.

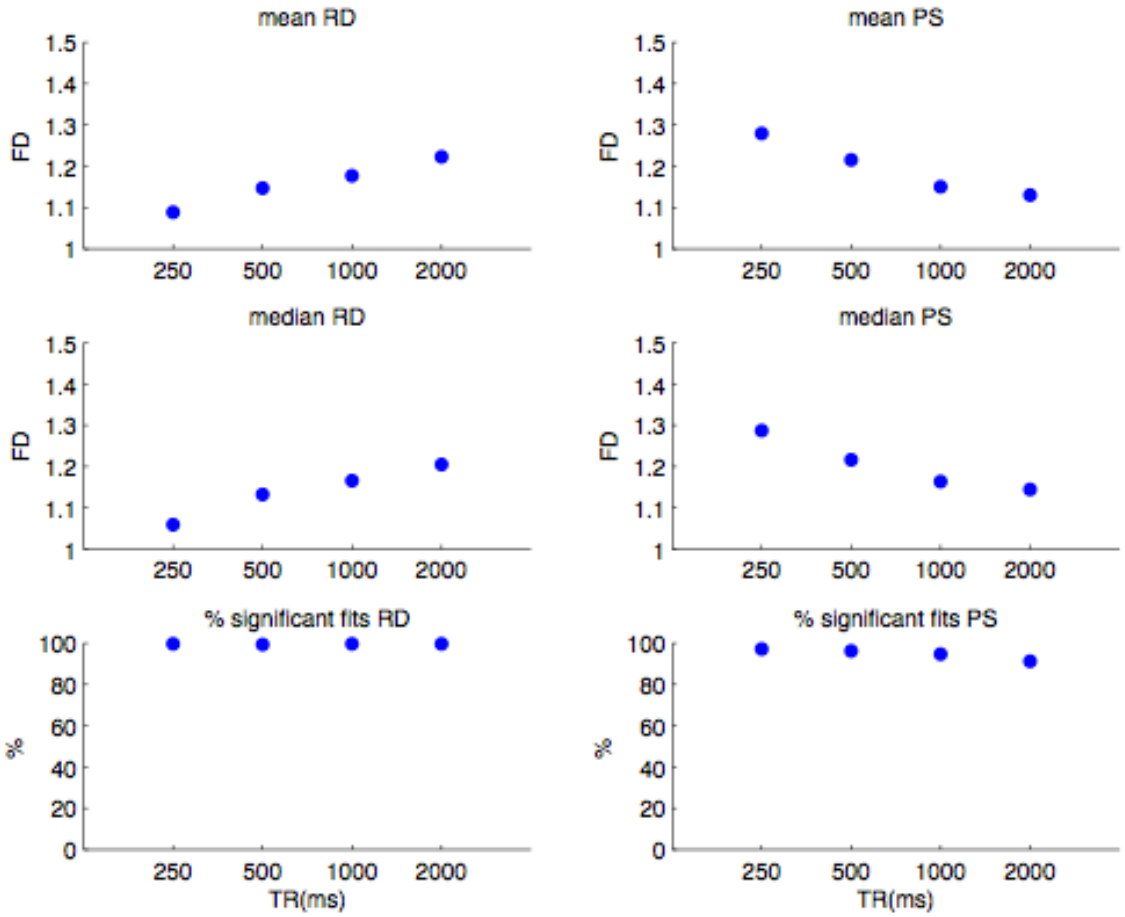

Figure 7. Fractal behaviour over varying time-points and repetition times (8min. 32s scan length). All x-axes represent the TR(ms). The y-axes for the top four figures represent the FD. The y-axes for the bottom two figures represent percentage of voxels with significant log-log fits.

Constant Scan Length in Multiple Subjects

Unlike the extracted TR variants described above, in the data acquired in 5 different subjects, FD_{RD} were very similar at both TR values (i.e. close to 1.16), with most of the voxels having significant fits (> 99%) (**Fig. 8**). Values of FD_{PS} differed from the extracted TR comparison, with a higher FD value at the higher repetition time (1.12 at TR=250 and 1.17 at TR=2000). Also unlike the extracted TR comparison, the percent of

voxels with a significant fit decreased from 97 to 84% (TR=250 to TR=2000ms). There was no statistical difference between FD_{RD} or FD_{PS} values for the two different TRs in the 5 subjects.

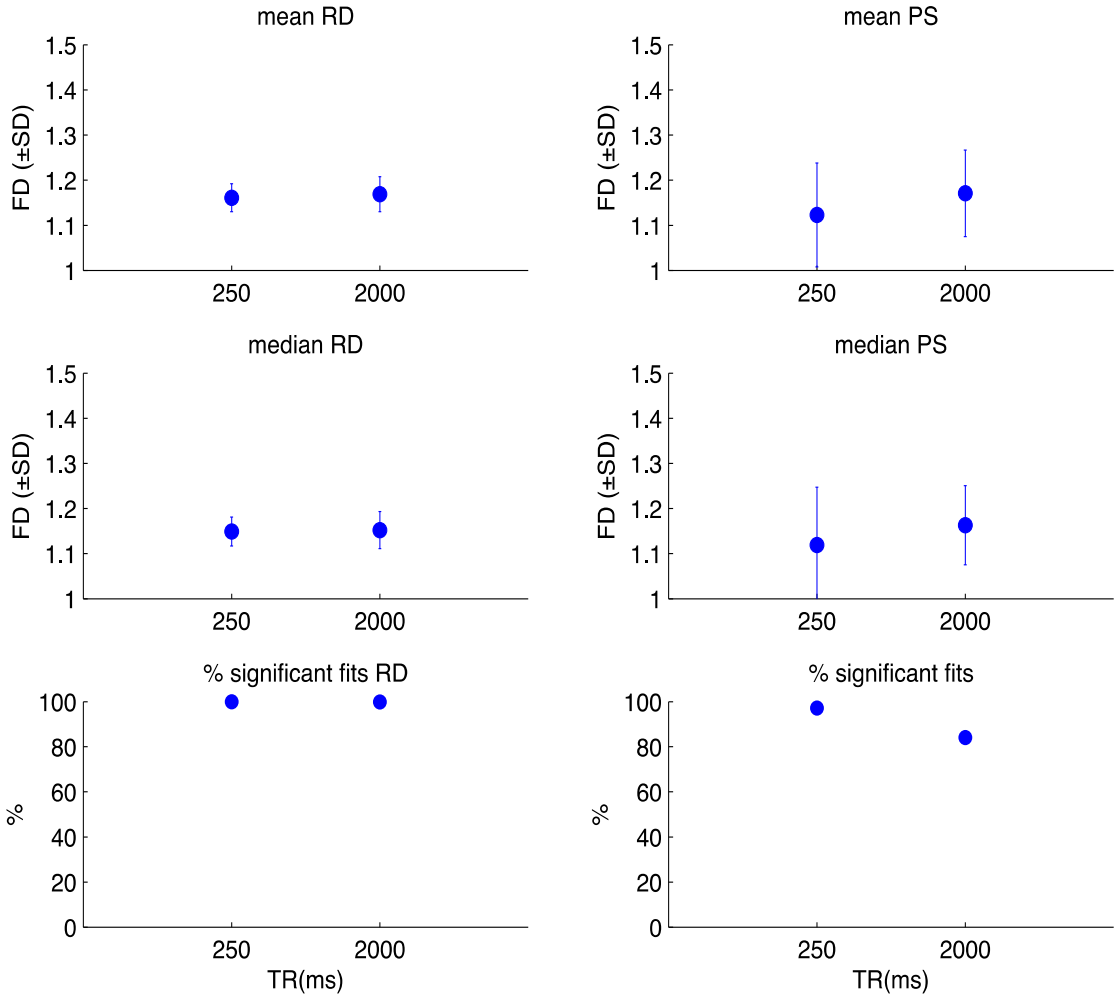

Figure 8. Fractal behaviour (mean and median ±SD) from 5 subjects. All x-axes represent the TR(ms). The y-axes for the top four figures represent the FD. The y-axes for the bottom two figures represent percentage of voxels with significant log-log fits.

k-Space Filling Strategies

EPI and spiral FD maps showed minor differences within individual subjects on visual inspection (**Fig. 9**). While spiral scans were less susceptible to Nyquist ghosting artifacts (i.e. these artifacts are more benign in spiral), these scans were more susceptible to field inhomogeneities. The fact that Nyquist ghosting is easy to see in EPI and dispersed in the background of spiral is shown clearly on the RD maps (**Fig. 9**): the noise from spiral is more structured (i.e. the ghosting is blurred over the whole background) than EPI, likely leading to reduced FD_{RD}. A comparison of EPI and spiral in four subjects using a one-way ANOVA demonstrated no statistically significant difference between FD values for both PS and RD methods (**Fig. 10**). The RD map shows a very slight (not significant) increase in F values along one edge of the head, possibly the result of subtle subject motion.

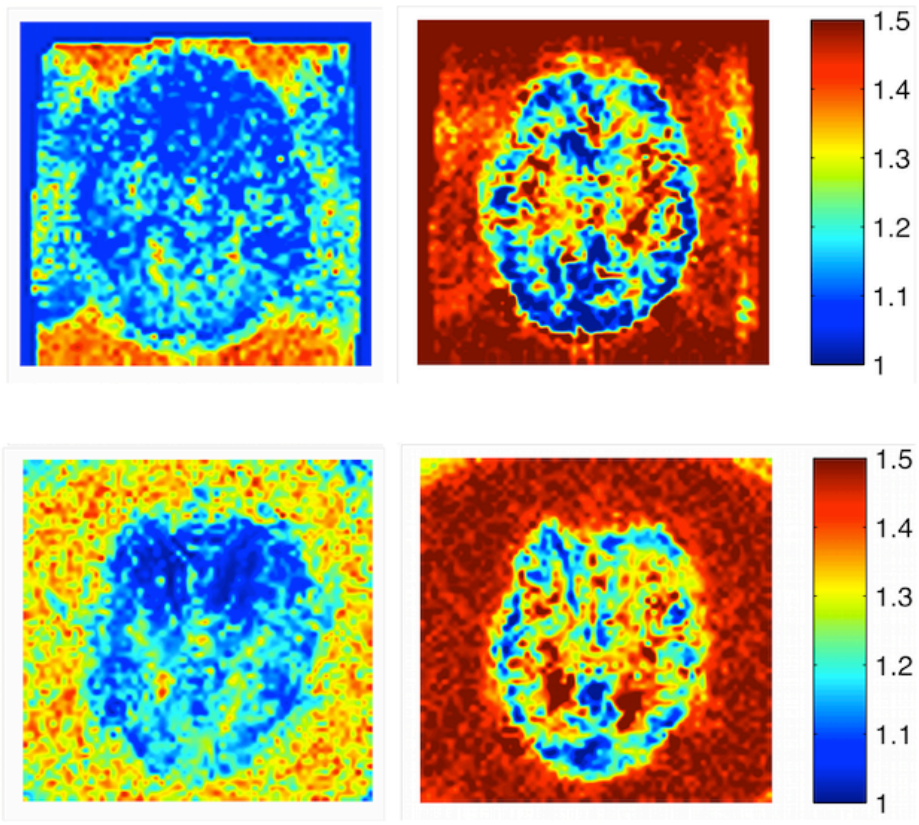

Figure 9. FD maps from single subject showing Nyquist ghosting from EPI scans (a and b) and inhomogeneity artifact from frontal sinuses in spiral (c and d).

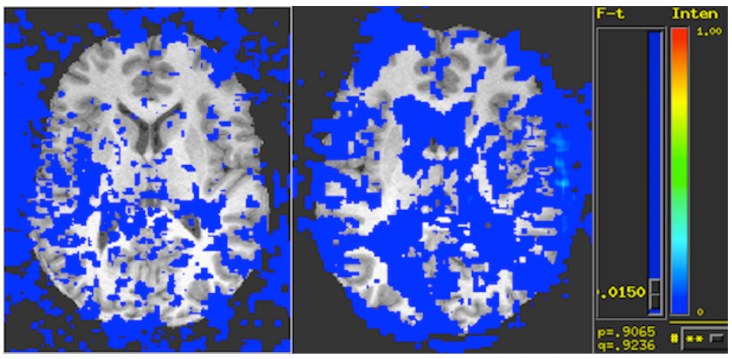

(a) EPI vs spiral - PS (b) EPI vs spiral - RD

Figure 10. One-way ANOVA comparing FD maps from EPI vs spiral for PS analysis (a) and RD analysis (b). Threshold for F statistic set at 0.015 (p = 0.9) demonstrated no voxels with statistically significant difference between EPI and spiral.

Temporal Stability

Although whole slice FD_{PS} and FD_{RD} did not show Gaussian distributions, their distributions did stay consistent over time (**Fig. 11**). FD_{PS} values were heavily weighted towards 1.5 (random), likely due to the inclusion of air (noise) in the axial slice. FD_{RD} peaked in the middle of the FD range. This difference in background noise values was also noted in individual scans (**Fig. 9**). The chosen ROI (putamen), however, was Gaussian distributed, both for FD_{RD} and FD_{PS} (**Fig. 12**). Scans from subject 2 showed a wider range in FD_{RD} as well as more motion during the scan (**Fig. 13**).

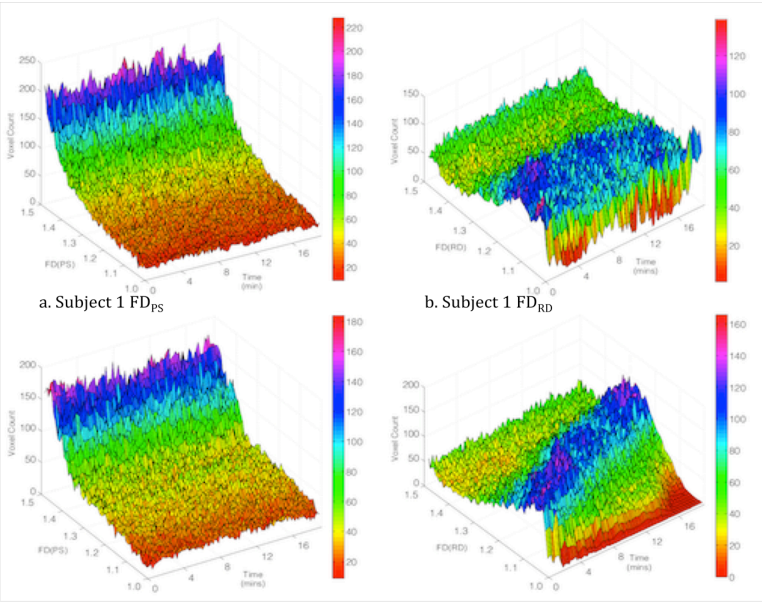

Figure 11. Histogram plots through entire axial slice for two subjects (subject 1:a-b, subject 2:c-d). x axis = FD value, y axis = number of pixels within given FD range, z axis = time (minutes).

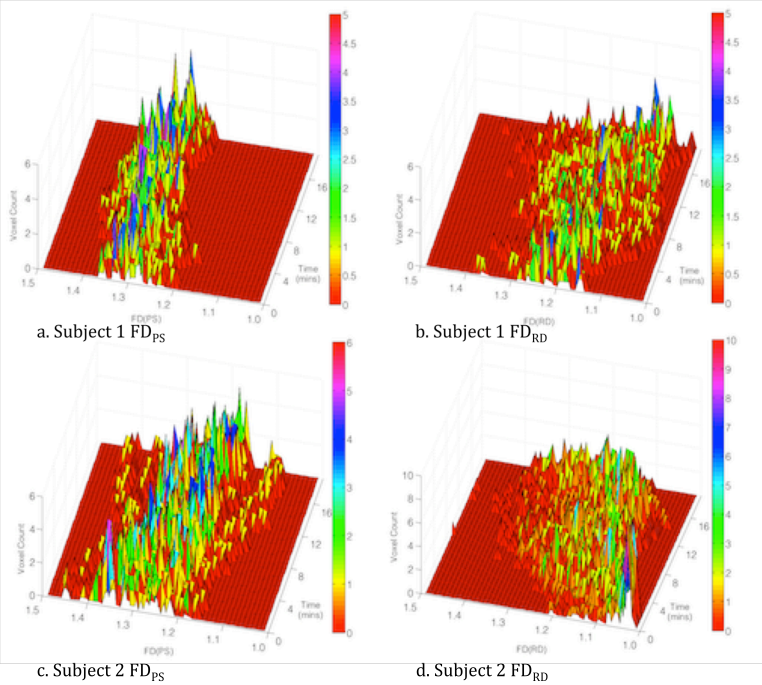

Figure 12. Histogram plots through prescribed ROI (putamen) for two subjects (subject 1:a-b, subject 2:c-d).with the x axis = FD value, y axis = number of pixels within given FD range, z axis = time (minutes).

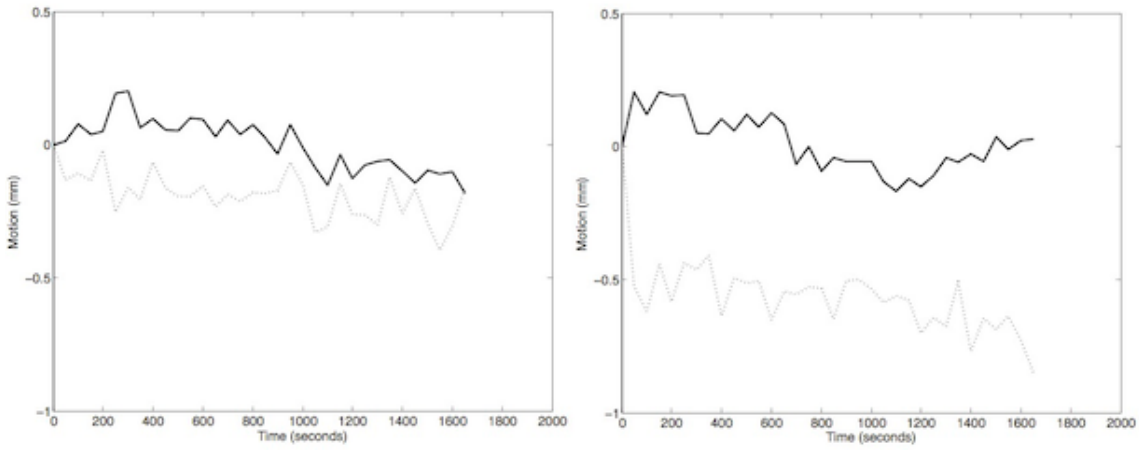

Figure 13. Motion in anterior-posterior (solid line) and left-right (dotted line) direction through the course of the scan for 2 subjects (a=subject 1, b=subject 2). Subject 1 showed less movement than subject 2.

DISCUSSION

To our knowledge, this is the first paper to evaluate the fractal properties of brain BOLD signals over various scanning parameters using both power spectrum and relative dispersion analysis methods. The stability of FD values seems to differ from parameter to parameter. We have attempted to characterize these changes so that future FD acquisition can maximize the reliability of FD_{RD} and FD_{PS} measurement.

When the TR was kept constant and scan length was increased, the FD value progressively moved closer to unity, especially for FD_{RD} and to a much lower extent for FD_{PS}. It is likely that, had more time-points been acquired, the FD_{RD} value would have settled on a value of 1. Were this to happen, BOLD signal would be assumed ordered, as opposed to complex or random. Although at first this may seem to contradict the thesis that brain BOLD signal is fractal in nature, this may only be true when observing scales lower than the 30 minute level (0.25s x 8192 time-points = ~30m). This is the case for many natural fractal phenomena. For instance, in spatial analysis of fjordian coast lines fractal properties break down once the spatial scale goes beyond a certain zoom level: either when we get to the soil level, or the continental level.

The FD value determined using the PS method does not appreciably change whether scales of 64, 128, 256, 512, 1024, or 2048 time-points were used, having only changed from 1.31 to 1.27. Thus, from 16 seconds to 8.5 minutes the brain BOLD signal remains consistently self-similar (i.e. fractal), based on the power spectrum. For FD_{PS} it may not be necessary to obtain a large number of time-points when fewer may do the job

(with a TR of 250 ms). For $FD_{RD,}$ it seems very important to keep the number of time points constant between scans, since changes in TP can have a large effect on FD_{RD}.

When TP was kept constant, changes in TR do not have a large effect on $FD_{RD.}$ This supports the idea that FD is constant at different scales of measurements. FD_{PS} also seems independent of TR except for higher values of FD when the TR is very low (250ms). This is likely due to the frequency of cardiac pulsatility, one of the contributing sources to BOLD signal variation, which becomes aliased throughout BOLD power spectrum when sampled at low frequency (high TR). In our method, we did not filter out this frequency component. However, this is one solution that has previously been employed[9, 20]. Thus, the RD method, although dependent on how many time-points are acquired, appears independent of TR; while the PS method gives the opposite result: independent of the time-points, but dependent on the TR.

At longer scan lengths (constant LS), FD_{RD} remains low but stable with changes in TR, despite changes in TP. There was a slight drift upwards in FD_{RD} as TP decreased (TR increased) for the shorter scan length (8m 32s). This drift was not as dramatic as observed when scan length was varied (with TR constant), suggesting changes in scan length has strong influence on FD_{RD}, rather than TR or TP. FD_{PS} also remained relatively stable through variations in TP and TR, while LS was kept constant. Furthermore FD_{PS} was similarly influenced by low TR when TP was kept constant. The percent significant voxel-wise fits remained constant around 99%. These results suggest FD_{PS} is relatively stable despite changes in TP, TR or LS but is influenced at the extremes of these measurements (especially low TR or very low TP).

From the extracted data, it can be concluded that at a reduced number of time points (e.g. 256), FD_{RD} is very resistant to changing TRs. FD_{PS} is time-point invariant at a low TR (250ms). With constant scan times, FD_{PS} is the least variable.

A comparison between repeated scans with different acquisition parameters gave similar results to that extracted from a single long high frequency scan. Both FD_{RD} and FD_{PS} were relatively stable with changes in TR and TP while LS was kept constant over 8min 32s. The values for FD_{RD} and FD_{PS} were similar (between 1.1 and 1.2) but the values of FD_{PS} had a wider Gaussian distribution in our 5 subjects compared to FD_{RD}. Unlike our extracted data, lower TR did not increase FD_{PS}. These findings are very promising for allowing full-brain (20-30 slice) BOLD scans, which require long TRs (2000ms) over [clinically more feasible] shorter scan times (~10mins).

The distribution of FD remains relatively stable through the course of a long scan. FD_{RD} has less stability than FD_{PS}, and maybe more greatly influenced by subject motion. Subject non-respiratory motion is aperiodic . This would not be reflected as self-similarity at any scale of frequency and would therefore have less influence on FD_{PS}. Relative dispersion is very sensitive to outliers and therefore motion would influence FD_{RD}. The effect of motion on fMRI FD is also highlighted in the changes in FD after motion correction[11].

The filling of functional MRI k-space was done using either Cartesian echo planar imaging (EPI) or spiral based readouts. There have documented differences between the two, for example, off resonance spins may cause blurring and ringing in spiral versus a shift in the phase encode direction with EPI causing ghosting in that direction[21]. Also,

oversampling, or early sampling the center of k-space with spirals can result in better signal to noise ratio (SNR). In comparing these two different acquisition methods of BOLD fMRI with respect to FD mapping, we found no significant difference. Thus FD analysis may be immune to some of the artifact and SNR differences between EPI and spiral.

CONCLUSION

There are various subtle differences in the methods by which FD analysis can be performed in the brain. We have shown that, while some of the differences are benign, other differences can have a significant effect of the precision and reliability of FD values. This highlights the fact that FD values are methodologically dependent (i.e. RD versus PS), and are dependent upon number of temporal points (TP) used, scan length (LS), motion and repetition time (TR). These factors highlight the limitations of brain FD mapping including the need to avoid too little (RD and PS) or too many (RD) time-points, too long scan lengths (RD) and high repetition-time (TR 2000 for PS of measured data). These parameters should be kept consistent when comparing different scans or subjects. On the other hand, FD measurements have been shown to be robust over time, and not sensitive to scan type (spiral vs EPI).

Fractal dimension mapping of BOLD fMRI signals provide a new method to observe the functioning brain at rest. Presence of a temporal fractal pattern in resting blood flow illuminates the underlying order in the perceived ‘noise’ when the brain is at

'rest', whereas traditional BOLD fMRI has sought to either eliminate resting BOLD signal or attempt to 'regress out' some of it's components in generalized linear models.

REFERENCES

1. Strogatz SH. Complex systems: Romanesque networks. Nature. 2005 Jan 27;433(7024):365-6.

2. Glenny RW, Robertson HT. Fractal modeling of pulmonary blood flow heterogeneity. J Appl Physiol. 1991 Mar;70(3):1024-30.

3. Xu N, Xu JH. The fractal dimension of EEG as a physical measure of conscious human brain activities. Bull Math Biol. 1988;50(5):559-65.

4. Havlin S, Buldyrev SV, Bunde A, Goldberger AL, Ivanov P, Peng CK, Stanley HE. Scaling in nature: from DNA through heartbeats to weather. Physica A. 1999 Nov 1;273(1-2):46-69.

5. Mandelbrot B. How long is the coast of britain? Statistical self-similarity and fractional dimension. Science. 1967 May;156(3775):636--8.

6. Zarahn E, Aguirre GK, D'Esposito M. Empirical analyses of BOLD fMRI statistics. I. Spatially unsmoothed data collected under null-hypothesis conditions. Neuroimage. 1997 Apr;5(3):179-97.

7. Bassingthwaighte JB, Liebowitch LS, West BJ. Fractal Physiology: Oxford University Press; 1994.

8. Glenny RW, Robertson HT, Yamashiro S, Bassingthwaighte JB. Applications of fractal analysis to physiology. J Appl Physiol. 1991 Jun;70(6):2351--67.

9. Eke A, Hermán P, Bassingthwaighte JB, Raymond GM, Percival DB, Cannon M, Balla I, Ikrényi C. Physiological time series: distinguishing fractal noises from motions. Pflügers Archiv : European journal of physiology. 2000 Mar 01;439(4):403-15.

10. Schepers HS, van Beek JHGM, Bassingthwaighte JB. Four Methods to Estimate the Fractal Dimension from Self-Affine Signals. IEEE Engineering in Medicine and Biology. 1992 Jan 1;11(2):57-64.

11. Maxim V, Sendur L, Fadili J, Suckling J, Gould R, Howard R, Bullmore E. Fractional Gaussian noise, functional MRI and Alzheimer's disease. Neuroimage. 2005 Mar 1;25(1):141-58.

12. Warsi M, Molloy W, Noseworthy M. Correlating brain blood oxygenation level dependent (BOLD) fractal dimension mapping with magnetic resonance spectroscopy (MRS) in Alzheimer’s disease. Magnetic Resonance Materials in Physics, Biology and Medicine. 2012:1-10.

13. Wink AM, Bernard F, Salvador R, Bullmore E, Suckling J. Age and cholinergic effects on hemodynamics and functional coherence of human hippocampus. Neurobiol Aging. 2006 Oct 1;27(10):1395-404.

14. Anderson CM, Lowen SB, Renshaw PF. Emotional task-dependent low-frequency fluctuations and methylphenidate: Wavelet scaling analysis of 1/f-type fluctuations in fMRI of the cerebellar vermis. J Neurosci Methods. 2006 Feb;151(1):52--61.

15. Wink A-M, Bullmore E, Barnes A, Bernard F, Suckling J. Monofractal and multifractal dynamics of low frequency endogenous brain oscillations in functional MRI. Hum Brain Mapp. 2008 Jul 1;29(7):791-801.

16. Lai M-C, Lombardo MV, Chakrabarti B, Sadek SA, Pasco G, Wheelwright SJ, Bullmore ET, Baron-Cohen S, Consortium MA, Suckling J. A shift to randomness of brain oscillations in people with autism. Biol Psychiatry. 2010 Dec;68(12):1092--9.

17. Glover GH, Lai S. Self-navigated spiral fMRI: interleaved versus single-shot. Magnetic resonance in medicine : official journal of the Society of Magnetic Resonance in Medicine / Society of Magnetic Resonance in Medicine. [Comparative Study]. 1998 Apr 01;39(3):361-8.

18. Cox RW. AFNI: software for analysis and visualization of functional magnetic resonance neuroimages. Comput Biomed Res. 1996 Jun 1;29(3):162-73.

19. Wardlaw G, Wong R, Noseworthy MD. Identification of intratumour low frequency microvascular components via BOLD signal fractal dimension mapping. Phys Med. 2008 Jun 1;24(2):87-91.

20. Fougere PF. On the Accuracy of Spectrum Analysis of Red Noise Processes Using Maximum Entropy and Periodogram Methods: Simulation Studies and Application to Geophysical Data. J Geophys Res. 1985;90(A5):4355-66.

21. Sangill R, Wallentin M, Østergaard L, Vestergaard-Poulsen P. The impact of susceptibility gradients on cartesian and spiral EPI for BOLD fMRI. Magma (New York, NY). [Evaluation Study]. 2006 Aug 01;19(3):105-14.

CHAPTER 6

BOLD FD VS. MRS IN AD

Correlating Brain Blood Oxygenation Level Dependent (BOLD) Fractal Dimension Mapping with Magnetic Resonance Spectroscopy (MRS) in Alzheimer's Disease

Mohammed A. Warsi, B.Sc., M.Sc., M.D., FRCP(C), William Molloy, MB BCh, MRCP(I), FRCP(C), Michael D. Noseworthy, Ph.D., P.Eng.

6.1 CONTEXT OF THE PAPER

The FD method was used to study signal complexity in the brains of patients with Alzheimer's Dementia (AD). Although hippocampus is a well-known area for study of AD, the putamen was chosen as the region of interest (ROI), due to reduced susceptibility artefacts, while still exhibiting AD pathology (de Jong 2008). The same ROI was used for MRS measurement of AD markers including N-acetyl aspartate (NAA), myoinositol (mI) and glutamate (glu) using an optimized stimulated echo acquisition mode (STEAM) sequence (Hu 2007). Volumetry of major brain regions was done using NeuroQuant, an automated segmentation tool (Brewer 2009). This study allowed us to compare FD to reliable measures of AD disease progression.

6.2 DECLARATION STATEMENT

Mohammed Ali Warsi as principle author wrote the article, performed analysis and created figures and tables as appropriate. Michael D. Noseworthy, as corresponding author, hypothesized the use of FD in assessing AD, wrote the first versions of the FD analysis program using Matlab (Mathworks, Natick, MA), provided guidance, funding and advice, and performed proofreading/editing and submission of the manuscript for publication. Dr. William Molloy provided clinical geriatric assessment, patient recruitment, guidance and commentary.

This paper has been published in the journal *Magnetic Resonance Materials in Physics, Biology and Medicine*. Permission to reproduce this work was obtained from Springer Publishing on 8th August 2012.

6.3 PAPER

Magn Reson Mater Phy
DOI 10.1007/s10334-012-0312-0

RESEARCH ARTICLE

Correlating brain blood oxygenation level dependent (BOLD) fractal dimension mapping with magnetic resonance spectroscopy (MRS) in Alzheimer's disease

Mohammed A. Warsi · William Molloy · Michael D. Noseworthy

Received: 19 July 2011 / Revised: 15 February 2012 / Accepted: 2 March 2012

Abstract
Objectives To correlate temporal fractal structure of resting state blood oxygen level dependent (rsBOLD) functional magnetic resonance imaging (fMRI) with in vivo proton magnetic resonance spectroscopy (^{1}H-MRS), in Alzheimer's disease (AD) and healthy age-matched normal controls (NC).
Materials and methods High temporal resolution (4 Hz) rsBOLD signal and single voxel (left putamen) magnetic resonance spectroscopy data was acquired in 33 AD patients and 13 NC. The rsBOLD data was analyzed using two types of fractal dimension (FD) analysis based on relative dispersion and frequency power spectrum. Comparisons in FD were performed between AD and NC, and FD measures were correlated with ^{1}H-MRS findings.
Results Temporal fractal analysis of rsBOLD, was able to differentiate AD from NC subjects ($P = 0.03$). Low FD correlated with markers of AD severity including decreased concentrations of *N*-acetyl aspartate ($R = 0.44$, $P = 0.015$) and increased myoinositol (mI) ($R = -0.45$, $P = 0.012$).
Conclusion Based on these results we suggest fractal analysis of rsBOLD could provide an early marker of AD.

Keywords Fractals · Magnetic resonance imaging · Magnetic resonance spectroscopy

Introduction

At rest, many physiological processes seem to exhibit random, low amplitude fluctuations. Physiological "noise" has long been thought to be hiding important information. However, any underlying pattern has been difficult to characterize due to the seeming randomness of noise.

M. A. Warsi · M. D. Noseworthy
School of Biomedical Engineering, McMaster University, Hamilton, ON, Canada

M. A. Warsi · M. D. Noseworthy
Department of Psychiatry and Behavioural Neuroscience, Hamilton, ON, Canada

M. A. Warsi · M. D. Noseworthy
Brain-Body Institute, St. Joseph's Healthcare, Hamilton, ON, Canada

W. Molloy
St. Peter's Centre for Studies in Aging, Hamilton, ON, Canada

Present Address:
W. Molloy
Department of Gerontology and Rehabilitation, University College Cork, Cork, Ireland

M. D. Noseworthy
Electrical and Computer Engineering, McMaster University, Hamilton, ON, Canada

M. D. Noseworthy
Medical Physics and Applied Radiation Sciences, McMaster University, Hamilton, ON, Canada

M. D. Noseworthy (✉)
Imaging Research Centre, St. Joseph's Healthcare, 50 Charlton Ave., East Hamilton, ON L8N 4A6, Canada
e-mail: nosewor@mcmaster.ca

M. D. Noseworthy
Department of Radiology, McMaster University, Hamilton, ON, Canada

Published online: 24 March 2012

Chaos theory has been able to unravel complex systems leading to patterning that was never before apparent. These patterns have been compared to other patterns in nature such as the branching of trees, the architecture of snowflakes or the shape of coastlines. The patterns are described as fractal, where gross patterns are repeated for recursively smaller scales. Specifically, in many physiological systems the power (p) of a noise signal is related to its frequency (f) with a $1/f^{\alpha}$ relationship [1]. This "pink noise" has been observed, for example in brain electroencephalography (EEG) signals [2], and recently, resting state blood oxygen level dependent (rsBOLD) signal from magnetic resonance imaging (MRI) [3].

Power and frequency of physiologic noise are related by the variable α. This parameter can be scaled to represent standard variables such as the Hurst exponent (H), as measured by power spectral analysis (H_{PS}), or the fractal dimension (FD_{PS}). In the brain, noise follows a fractional Gaussian model and α is related to H_{PS} and FD_{PS} as follows [4]:

$$\alpha = 2H_{PS} - 1 \quad (1)$$

$$\alpha = -2FD_{PS} + 3. \quad (2)$$

Another measure of signal complexity that uses fractal analysis is relative dispersion (RD), which changes with measurement scale (MS). Similar to the power-frequency relationship in FD_{PS}, the signal spread or RD follows a $1/MS^{\beta}$ relationship. β can also be scaled to represent the Hurst exponent (H_{RD}) and fractal dimension (FD_{RD}) [5, 6]:

$$\beta = 1 - FD_{RD} \quad (3)$$

$$\beta = H_{RD} - 1. \quad (4)$$

In our study, we used both power spectral analysis (FD_{PS}) and relative dispersion (FD_{RD}) as scaled measures of α and β. The fractal dimension of a temporally varying signal represents a degree of complexity of the signal. FD of 1.5 represents complex noise while an FD of 1.0 represents a "simple" pattern such as a sine wave.

Simple signals (low FD) often represent "ill health". Low signal complexity represents a lack of adaptability and this is true for signals in the heart, brain and other organs [7, 8]. In the brain, signal complexity is thought to represent a degree of global connectivity [8]. Areas with multiple inputs from other brain regions are likely to have a more complex signal and therefore a higher FD. Therefore degenerative brain illness should be associated with a decrease in signal complexity (low FD). This has been validated with EEG measurements of brain activity and also been shown true for complexity of rsBOLD signals [3]. Maxim et al. demonstrated that patients with probable early Alzheimer's disease (AD) have significantly higher values of H (i.e. lower FD) in the medial and lateral temporal cortex, dorsal cingulate cortex, premotor cortex, left precentral gyrus and postcentral gyrus. In a study by Wink et al. [9], healthy ageing and cholinergic receptor blockade (mimicking AD) were both associated with significant increase in H or lower FD. Lower biosignal complexity can also be detected by measuring the Higuchi's fractal dimension of magnetoencephalogram (MEG) in AD [10].

In our study, we correlated FD analysis with in vivo magnetic resonance spectroscopic (MRS) measures in the AD brain. Our measures of metabolite concentrations focused on N-acetyl aspartate (NAA) and myoinositol (mI) which have been validated in AD as measures of disease severity [11]. NAA, a marker of neuronal viability and density, decreases as AD progresses. mI is a marker of gliosis or inflammation. We optimized our MRS acquisition to include secondary measures of glutamate (glu), glutamine (gln) and GABA since change in these neurotransmitters have been linked to AD [12].

Since astrocytes and microglia are involved in AD senile plaque formation, mI is seen to increase in AD. These changes occur in the grey matter and are most evident in the medial temporal lobe [11], hippocampus and deep grey matter structures such as the putamen [13]. Recent Positron Emission Tomography (PET) [14] and quantitative R2 iron quantification [15, 16] studies have also shown changes in the putamen associated with AD. Inhomogeneity of B_0 at the base of the brain can decrease accuracy of MRS measurements, especially in the hippocampus. Also, the putamen is less likely to show volumetric changes in early AD when compared to the hippocampus or amygdala which would contribute to partial voluming effects [17]. Therefore the putamen was chosen as our region of interest (ROI). We hypothesized changes in spectroscopic measures of NAA and mI would be reflected in regional FD scores, in both Alzheimer's and aged-matched normal controls (NC).

Materials and methods

Thirty-three subjects with mild to moderate AD (mean ± SD mini mental state exam (MMSE) = 22 ± 3) and 13 age-matched normal controls (NC) were scanned at rest with eyes open. Diagnosis and severity of illness was also confirmed by clinical exam, Alzheimer's Disease Assessment Scale (ADAS) and Clinical Dementia Rating Scale (CDR). Subjects were recruited from a local geriatric clinic after obtaining informed consent. Aged-matched controls were spouses of AD subjects who did not have AD based on clinical exam by a geriatrician and a screening cognitive exam (Table 1).

A 3T GE Signa HD MRI system and eight-channel phased array head RF coil (General Electric Healthcare,

Table 1 Subject details (mean ± SD)

	AD	NC	*P* value
N	33	13	–
Females	15	8	0.34
Age (y)	76.4 ± 7.8	73.7 ± 6.0	0.22
MMSE[a]	22.3 ± 3.4	28.4 ± 1.1	<0.001
Illness onset (y)	3.5 ± 2.3	–	–
Education (y)	13.1 ± 3.4	–	–
SADAS[b]	18.1 ± 6.9	–	–
CDR[c]	0.98 ± 0.53	–	–

[a] Mini mental status exam

[b] Standardized Alzheimer's disease assessment scale—cognitive subscale

[c] Clinical dementia rating—global score

Milwaukee WI) was used for all imaging and spectroscopy. Head motion was minimized using soft foam pads placed between the subject and head coil. Standard T1 and T2-weighted images were used to prescribe a rsBOLD (gradient echo EPI, $\alpha = 70^{o}$, TE/TR = 35/250 ms, FOV = 24 cm, 64 × 64 matrix, three contiguous 5 mm thick slices) image acquisition through the basal ganglia. 2,400 temporally contiguous BOLD images were acquired over 10 min at a sampling rate of 4 Hz (1/250 ms). Spatial coverage was sacrificed for temporal resolution to allow resolution of higher frequencies not typically evaluated using resting state methods (e.g. cardiac frequency). Motion was assessed by measuring rigid translations and rotations (six degrees of freedom) for each volume in the time course. Motion correction was performed using an iterated linearized weighted least squares algorithm in AFNI [18]. Magnetic resonance spectroscopy data was obtained using a STEAM sequence (TE/TM/TR = 72/6/3,000 ms, NEX = 512, 5,000 Hz spectral bandwidth, 4,096 spectral points, 2 × 2 × 2 cm) optimized for glutamate, glutamine and GABA acquisition [12].

The region of interest (ROI) voxel for MRS was positioned over the center of the left putamen based on the T1 and T2 anatomical images. The scanner coordinates were used to prescribe the MRS ROI to encompass the center of the BOLD slices (Fig. 1).

BOLD data was assessed for nonlinear signal characteristics using in-house programs written in Matlab version 7.9.0.529 (The Mathworks, Natick MA). FD_{RD} analysis was done using nine scales of measurements with corresponding relative dispersions over the middle 2,048 images from the acquired 2,400 volumes, discarding volumes where subjects may be anticipating the beginning or end of the scan. FD_{PS} was measured from the Fourier transform of the temporal data for each voxel. Robust fit of a log–log plot for each pixel generated values for α and β and were rescaled to produce maps of FD_{PS} and FD_{RD} , respectively. *FD* values for each voxel within the ROI were averaged and compared to MRS metabolite concentrations. MRS

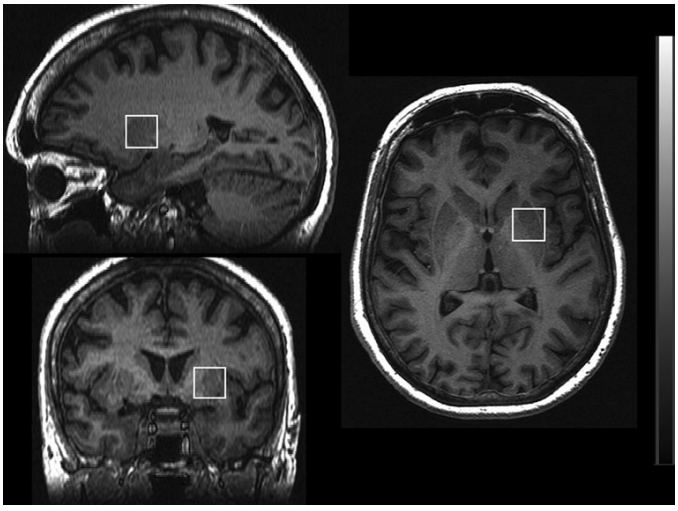

Fig. 1 Placement of ROI for MRS acquisition (putamen). Data from this cubic volume was also extracted for FD post-processing analysis

data was analyzed with LCModel [19] using basis sets developed in-house for this combination of TE/TM [20] which provides absolute metabolite concentrations (represented as a value relative to unsuppressed water, and presented in institutional units, IU). Metabolite concentrations were considered accurate if SD of fit with basis sets was less than 30 %. All acquisition and analysis was done blinded to subject status (AD vs. NC).

Volumetric analysis of whole brain and individual brain structures was performed using NeuroQuant (NQ), a commercial automated segmentation software. NQ volumes have been validated against manually drawn volumes in AD [21]. Volumes of the putamen, caudate and thalamus were compared for AD versus NC using a two-tailed unpaired Student's t test. Grey matter (GM), amygdala and hippocampal volumes were also compared.

In addition, structural data was analysed with FSL-VBM, a voxel-based morphometry analysis [22, 23] carried out with FSL tools [24]. FSL-VBM was carried out on SHARCNET (Shared Hierarchical Academic Research Computing Network), a network cluster of high performance computers from a consortium of Canadian academic institutions with over 8,000 CPUs available for computation [25]. Brain-extraction was performed using the FSL brain extraction tool [26] followed by tissue-type segmentation [27]. MNI152 standard space was used to align grey-matter partial volume images using the affine registration tool FLIRT followed by nonlinear registration using FNIRT which uses a b-spline representation of the registration warp field [28–30]. Native grey matter images were then non-linearly re-registered to the resultant study-specific template. Partial volume images were then modulated by dividing by the Jacobian of the warp field. An isotropic Gaussian kernel with a sigma of 3 mm was used to smooth the modulated segmented images. Permutation-based non-parametric testing, correcting for multiple comparisons across space, was used to apply voxelwise GLM.

Anatomical scans were realigned to a standard template (Talairach) using AFNI [18]. Transformation parameters were used to warp the FD maps into standard space allowing for intra subject comparison of FD maps and group analysis. Voxel by voxel two-tailed unpaired Student's t test (corrected for multiple comparisons) was used to compare FD maps of AD versus NC aligned in standard space.

Statistical analysis was done using the statistics toolbox of Matlab and SPSS (version 17, SPSS Inc., Chicago, IL, USA). Two-tailed un-paired Student's t test, with unequal sampling, was used for comparing FD values between subject groups. Pearson's correlation coefficient was used for comparing FD with MRS metabolite concentrations (specifically NAA and mI). Level of significance was set at $P < 0.05$, although specific P values are reported. A Jarque–Bera test, which takes into consideration both skewness and kurtosis, was used to confirm normality of FD and MRS data. Motion in AD versus NC was evaluated by comparing variance of translation and rotation using a general linear model multivariate analysis.

Results

All participants were able to complete the FD BOLD study (AD: $n = 33$, NC: $n = 13$) but two AD subjects were unable to complete the MRS study (scan series was terminated early due to claustrophobia) (MRS AD $n = 31$). Voxel-wise parametric maps of FD_{RD} and FD_{PS} showed significant fits to BOLD data within the selected ROI for all subjects ($P < 0.01$) confirming a linear multiscale relationship (i.e. fractal). Significant fitting of NAA, using LCModel [19] was observed in 30 AD (11 for NC) subjects, while mI was significantly fit in 29 AD subjects (12 for NC). Fewer MRS scans had reliable measures of glu (26 AD, 12 NC), gln (11 AD, 2 NC) and GABA (3 AD, 1 NC). Gln and GABA were therefore exclude from analysis. SHARCNET performed VBM analysis on multiple processors totaling 1.3 years of CPU time (95 % of allocated) while utilizing 0.57 TB of memory.

FD comparisons of AD versus NC

Statistical maps of FD comparing AD to NC are shown (Fig. 2). FD maps though the mid section showed some significant differences in FD in the putamen, caudate and thalamus. Statistical analysis showed AD subjects had a significantly lower mean FD_{PS} in the region of interest (ROI) voxel placed over the left putamen, when compared to NC ($P = 0.03$). The mean ± SD FD_{PS} for AD was 1.08 ± 0.12 compared to 1.15 ± 0.11 for normal controls. Low FD_{PS} (or FD_{RD}) signifies a simpler (i.e. less complex) signal. Mean FD_{RD} was also reduced in AD compared to NC, although this was not statistically significant. A comparison of FD in the specific voxel over the putamen showed that AD subjects had lower FD_{RD} in this region (Fig. 3). Motion did not significantly differ in AD versus NC ($P = 0.192$).

When comparing the concentrations of NAA, mI and glu between groups, no significant differences were detected (mean ± SD NAA: AD = 7.7 ± 1.7 IU, NC = 8.3 ± 2.2 IU; mean ± SD mI: AD = 6.3 ± 1.7 IU, NC = 5.9 ± 1.1 IU; mean ± SD glu: AD = 3.1 ± 2.3 IU, NC = 2.8 ± 1.5 IU).

A comparison of volumes obtained from NQ in AD versus NC showed no significant difference in the volumes of the putamen, caudate or thalamus ($P > 0.10$). There was a significant difference in GM, amygdala and hippocampal volumes ($P < 0.001$) (AD < NC). GM differences were

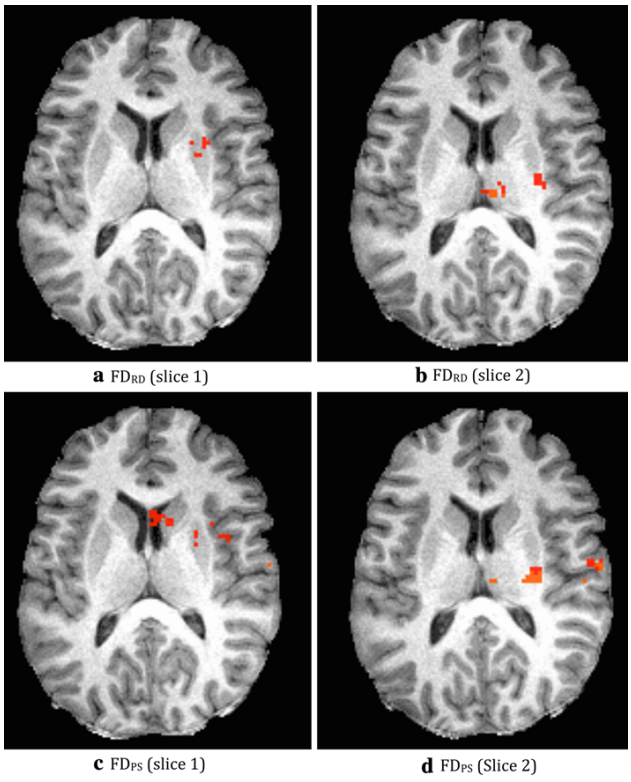

Fig. 2 Statistical maps (voxel-wise *t* test) comparing FD maps of AD versus NC. Differences are seen in the putamen, caudate and thalamus in both FD_{RD} (**a**, **b**) and in FD_{PS} (**c**, **d**)

seen between AD and NC in the temporal-parietal region but did not reach statistical significance (Fig. 4).

Comparing FD to MRS in AD

For AD subjects, significant correlation between FD_{PS} and NAA ($R = 0.44$, $P = 0.015$), and FD_{RD} and NAA ($R = 0.38$, $P = 0.041$) were found (Fig. 5). Furthermore a significant negative correlation between FD_{RD} and mI values was noted ($R = -0.45$, $P = 0.012$) but not FD_{PS} ($R = 0.03$, $P > 0.05$) (Fig. 5). The correlations were not seen ($P > 0.05$) in NC for FD_{RD} (NAA $R = 0.14$, mI $R = -0.22$) nor FD_{PS} (NAA $R = 0.07$, mI $R = -0.25$) (Fig. 6). There was also no correlation between FD_{RD} or FD_{PS} and glu ($P > 0.05$).

Metabolite values were measured using LCModel that reports concentration values based on standardization to the signal from water. Alternatively, NAA and mI can be measured as a ratio to creatine (Cr) that assumes the Cr level is constant and independent of disease state. This assumption has been recently challenged [31] and Cr concentration correlates with FD values [32].

MMSE scores did not correlate significantly with FD_{RD}, FD_{PS} nor MRS changes.

Discussion

Fractals are a curious design seen extensively in nature. Self-similarity at different scales of measurement is seen in the geography of coastlines, branching patterns of trees and in many physiological signals. In the brain, discovery of a fractal pattern in resting blood flow illuminates the underlying order in the perceived 'noise' when the brain is

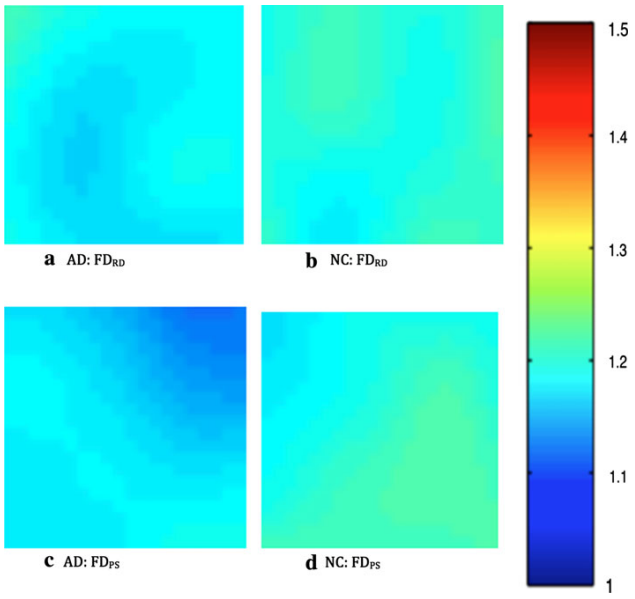

Fig. 3 Comparison of BOLD FD_{RD} (**a**, **b**) and FD_{PS} (**c**, **d**) map values, from only the MRS region of interest (ROI). The resultant images are average FD maps for all subjects in the AD (**a**, **c**) and NC (**b**, **d**) groups. Overall, the AD group had clearly lower *FD* values in this region of interest

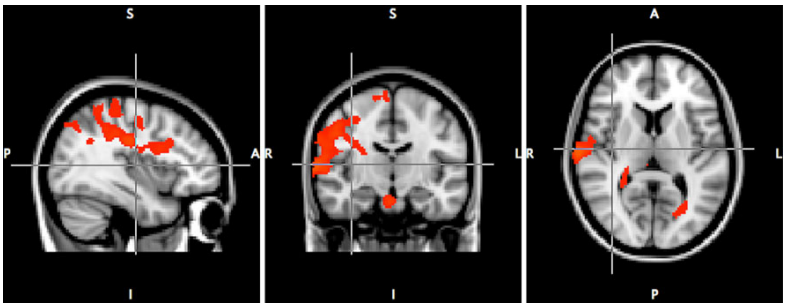

Fig. 4 VBM analysis showing regional structural differences between AD and NC. The values were not statistically significant at the 95 % level of confidence. However, the images reflect regions leading to significance. These results were not surprising given the AD group was diagnosed as early onset

at 'rest', whereas traditional BOLD fMRI has always sought to eliminate the resting BOLD signal for analysis. This has captured the imagination of many scientists and the scientific community as a whole. A recent cover article in *Scientific American* on "The Brain's Dark Energy" [33] discussed complex processes in the brain at rest. Similarly the cover article in *Science Illustrated* explored the same topic [34]. The idea that the brain is busy at work, even when we are not consciously processing information or involved in any task, opens the door to the exploration of the subconscious mind. Resting BOLD analysis also allows us to explore BOLD signal without the confounding complications of functional paradigms, and their associated assumptions, in traditional fMRI.

FD in resting BOLD represents temporal brain order or disorder. Areas of the brain that are healthy are associated

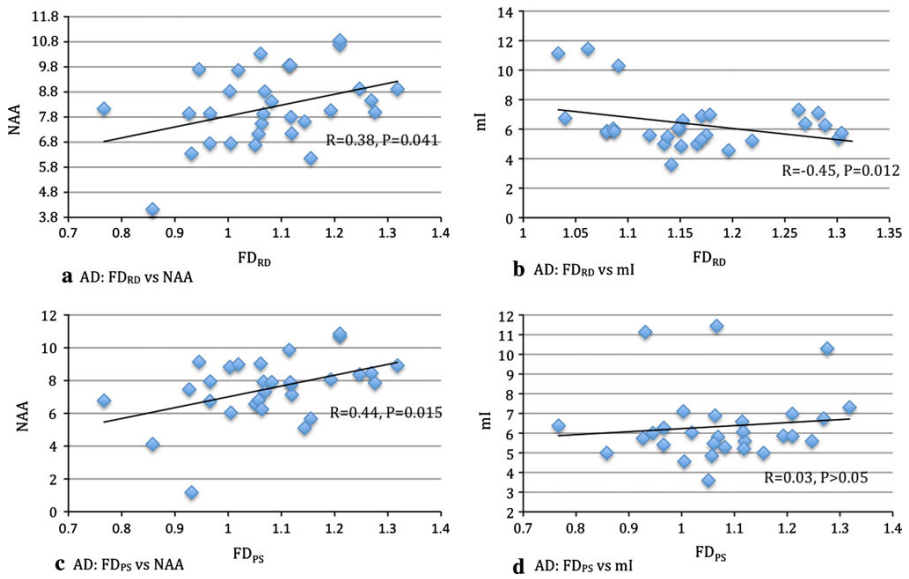

Fig. 5 Previous investigators have shown reduced *N*-acetyl aspartate (NAA) and increased myoinositol (mI) in Alzheimer's disease, as measured using magnetic resonance spectroscopy (MRS). Low fractal dimension (FD), measured in the MRS ROI, correlated with these biochemical markers of AD severity (**a**, **b**, **c**) except for FD_{PS} and mI (**d**)

with more complex signals, likely due to the interconnectivity with other brain areas. In this study, we found that the BOLD signal in the brain is less complex in AD compared to NC as evident from lower *FD* values. We suggest that this brain area (the deep grey matter) may have fewer connections with other parts of the brain compared to NC. This notion is supported by some of the EEG work by Maxim et al. [3].

We specifically chose the basal ganglion because the deep grey matter has been implicated in AD, and this region is away from the skull, making MRS measurements more precise. MRS is sensitive to inhomogeneity of the MRI magnetic field, which is more pronounced at the interface between brain tissue and bone. For this reason, other deep brain structures such as the hippocampus are also problematic.

This is the first study to compare *FD* to MRS in AD. MRS has previously shown utility in providing validated markers of AD disease severity. As expected, lower *FD* correlated with AD severity. Patients with 'unhealthy' ordered brain BOLD signal patterns had higher mI and lower NAA. One reason why reduced BOLD signal complexity correlates with disease severity may be related to neuronal loss. AD is associated with a progressive loss of neurons, especially in the grey matter [35]. When an area of interest loses neurons, there is less connectivity to other areas of the brain. This is also supported by observations of resting BOLD default networks in AD [36]. With fewer neuronal connections, a region of interest will have fewer inputs modifying local basal activity and therefore would be associated with a less complex BOLD signal (i.e. lower *FD*). Similarity of BOLD *FD* to previously reported EEG findings suggests neuronal networks are the primary contributor. This is supported by the decrease in *FD* observed after cholinergic receptor blockade which causes a decrease in neuronal signaling without changing vascular density [8]. Thus, lower *FD* values highlight a reduction in neuronal connectivity consistent with neuronal loss in AD.

Although *FD* may be related to neuronal connectivity it could also be influenced by vascularity. There is evidence for this from *FD* mapping of tumours. Low frequency components of T2* signals are related to vasomodulation in the microvascular environment in tumours [37, 38]. Hypervascular tumours are associated with lower FD values [39]. This is a result of the BOLD fluctuations being dominated by low frequency components (microvasculature) rather than high frequency components (perfusion and large vessel flow) [39]. AD is associated with a moderate

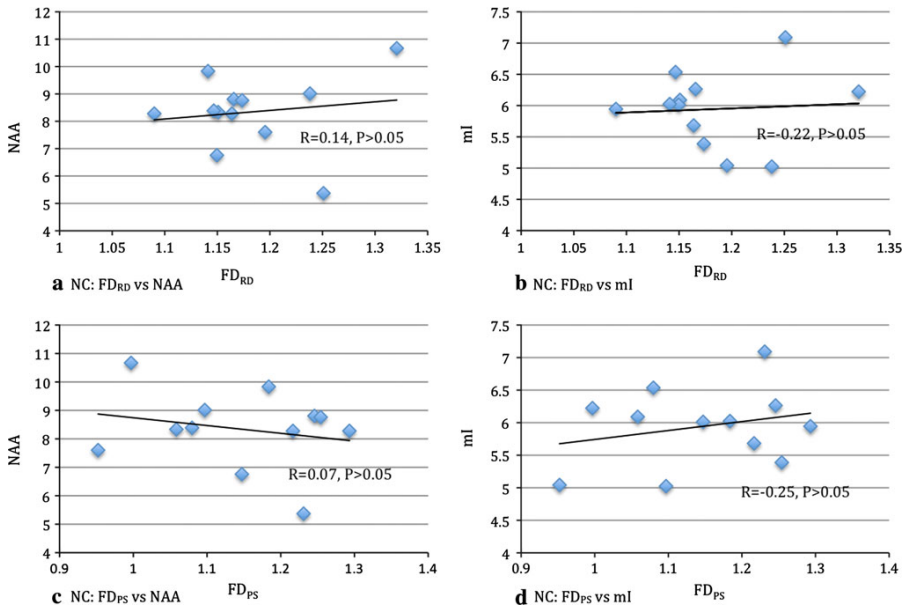

Fig. 6 NAA and mI did not correlate with FD_{RD} nor FD_{PS} in normal controls (NC)

increase in grey matter vascularity [40] thus it is possible that lower *FD* values may be related to changes in vascularity rather than neuronal networks. As *FD* is applied to more pathology, it will become clearer exactly what is being measured. Postmortem pathology correlation with *FD* could help clarify the vascularity contributions.

The subjects had early AD and, thus, MMSE scores were in the mild to moderate range. There were differences in GM, amygdala and hippocampal volumes, but not yet in the putamen, caudate or thalamus. MRS findings were not significantly different between AD and NC, although NAA was lower and mI was higher in AD as expected. Lack of statistical significance may reflect the lower number of NC subjects and more likely the mild disease severity. The significant correlation of FD to NAA and mI and the significant difference between FD in AD versus NC may suggest that FD is more sensitive to early changes in AD when compared to MMSE or MRS but likely not more sensitive than volumetric based discrimination (such as hippocampal volumetrics [41]). This would have to be validated with a comparison of FD with more complete neurocognitive tests for AD.

A comparison of FD to MRS necessitated a cubic ROI due to the limitations of MRS acquisitions. Bias from volumetric changes were minimized by using a large deep gray matter structure such as the putamen, where much of the MRS voxel is homogeneous. Future studies should focus on FD measurements in ROIs that include particular brain structures. The optimized STEAM sequence for MRS was unable to provide useful information about glu, gln or GABA in this study and a standard PRESS sequence would likely have been sufficient to provide accurate measures of NAA and mI. Also, not every comparison of MRS to FD gave significantly correlated results (FD_{PS} did not correlate with mI) which may be a result of some inconsistency in FD measurement. This is also highlighted in the range of FD values found in normal controls, suggesting that FD is influenced by measures other than severity of AD or clinical status.

Spatial range of the imaging data was sacrificed for high temporal resolution; a TR of 250 ms allowed collection of only three brain slices. This limits the discussion of whole brain connectivity but allows for a more robust analysis of higher frequency BOLD components including cardiac

($\sim$1 Hz) components as the TR satisfies the Nyquist criterion for this physiological frequency. Future studies may examine how FD relates to whole brain connectivity with a comparison to resting state networks.

Conclusion

We suggest that spatial *FD* maps may provide a sensitive measure of regional neuronal loss in AD. Our *FD* changes were seen in mild to moderate AD. Therefore, *FD* mapping may detect early signs of AD pathogenesis.

Acknowledgments This work was supported by the Canadian Institute of Health Research (CHIR) FRN79779 (WM) and the Ontario Graduate Scholarship in Science and Technology Fund Raymond Moore Scholarship (MAW).

References

1. Wink A-M, Bullmore E, Barnes A, Bernard F, Suckling J (2008) Monofractal and multifractal dynamics of low frequency endogenous brain oscillations in functional MRI. Hum Brain Mapp 29(7):791–801
2. Song IH, Lee SM, Kim IY, Lee DS, Kim SI (2005) Mutifractal analysis of electroencephalogram time series in humans. Lect Notes Comput Sci 3512:921–926
3. Maxim V, Sendur L, Fadili J, Suckling J, Gould R, Howard R, Bullmore E (2005) Fractional Gaussian noise, functional MRI and Alzheimer's disease. Neuroimage 25(1):141–158
4. Kiviniemi V, Remes J, Starck T, Nikkinen J, Haapea M, Silven O, Tervonen O (2009) Mapping transient hyperventilation induced alterations with estimates of the multi-scale dynamics of BOLD signal. Front Neuroinform 3:18
5. Bassingthwaighte JB, Liebovitch LS, West BJ (1994) Fractal measures of heterogeneity and correlation. In: Fractal physiology. Oxford University Press, New York, NY, pp 63–107
6. Eke A, Herman P, Kocsis L, Kozak LR (2002) Fractal characterization of complexity in temporal physiological signals. Physiol Meas 23(1):R1–R38
7. Goldberger AL, Amaral LA, Hausdorff JM, Ivanov P, Peng CK, Stanley HE (2002) Fractal dynamics in physiology: alterations with disease and aging. Proc Natl Acad Sci USA 99(Suppl 1):2466–2472
8. Suckling J, Wink AM, Bernard FA, Barnes A, Bullmore E (2008) Endogenous multifractal brain dynamics are modulated by age, cholinergic blockade and cognitive performance. J Neurosci Methods 174(2):292–300
9. Wink AM, Bernard F, Salvador R, Bullmore E, Suckling J (2006) Age and cholinergic effects on hemodynamics and functional coherence of human hippocampus. Neurobiol Aging 27(10): 1395–1404
10. Gómez C, Mediavilla A, Hornero R, Abásolo D, Fernández A (2009) Use of the Higuchi's fractal dimension for the analysis of MEG recordings from Alzheimer's disease patients. Med Eng Phys 31(3):306–313
11. Schuff N, Capizzano AA, Du AT, Amend DL, O'Neill J, Norman D, Kramer J, Jagust W, Miller B, Wolkowitz OM, Yaffe K, Weiner MW (2002) Selective reduction of N-acetylaspartate in medial temporal and parietal lobes in AD. Neurology 58(6): 928–935
12. Hu J, Yang S, Xuan Y, Jiang Q, Yang Y, Haacke EM (2007) Simultaneous detection of resolved glutamate, glutamine, and gamma-aminobutyric acid at 4 T. J Magn Reson 185(2):204–213
13. de Jong LW, van der Hiele K, Veer IM, Houwing JJ, Westendorp RGJ, Bollen ELEM, de Bruin PW, Middelkoop HAM, van Buchem MA, van der Grond J (2008) Strongly reduced volumes of putamen and thalamus in Alzheimer's disease: an MRI study. Brain 131(Pt 12):3277–3285
14. Koivunen J, Scheinin N, Virta JR, Aalto S, Vahlberg T, Nagren K, Helin S, Parkkola R, Viitanen M, Rinne JO (2011) Amyloid PET imaging in patients with mild cognitive impairment: a 2-year follow-up study. Neurology 76(12):1085–1090
15. Qin Y, Zhu W, Zhan C, Zhao L, Wang J, Tian Q, Wang W (2011) Investigation on positive correlation of increased brain iron deposition with cognitive impairment in Alzheimer disease by using quantitative MR R2′ mapping. J Huazhong Univ Sci Technol Med Sci 31(4):578–585
16. Zhu WZ, Zhong WD, Wang W, Zhan CJ, Wang CY, Qi JP, Wang JZ, Lei T (2009) Quantitative MR phase-corrected imaging to investigate increased brain iron deposition of patients with Alzheimer disease. Radiology 253(2):497–504
17. Vitali P, Migliaccio R, Agosta F, Rosen HJ, Geschwind MD (2008) Neuroimaging in dementia. Semin Neurol 28(4):467–483
18. Cox RW (1996) AFNI: software for analysis and visualization of functional magnetic resonance neuroimages. Comput Biomed Res 29(3):162–173
19. Provencher SW (1993) Estimation of metabolite concentrations from localized in vivo proton NMR spectra. Magn Reson Med 30(6):672–679
20. Sheffield P, Noseworthy MD (2010) Simultaneously assessed GABA/Glutamate/Glutamine concentration gender differences at 3.0T. In: Proceedings of the 17th scientific meeting, International Society for Magnetic Resonance in Medicine, Honolulu, p 940
21. Brewer JB, Magda S, Airriess C, Smith ME (2009) Fully-automated quantification of regional brain volumes for improved detection of focal atrophy in Alzheimer disease. AJNR Am J Neuroradiol 30(3):578–580
22. Ashburner J, Friston KJ (2000) Voxel-based morphometry—the methods. Neuroimage 11(6 Pt 1):805–821
23. Good CD, Johnsrude IS, Ashburner J, Henson RN, Friston KJ, Frackowiak RS (2001) A voxel-based morphometric study of ageing in 465 normal adult human brains. Neuroimage 14(1 Pt 1):21–36
24. Smith SM, Jenkinson M, Woolrich MW, Beckmann CF, Behrens TE, Johansen-Berg H, Bannister PR, De Luca M, Drobnjak I, Flitney DE, Niazy RK, Saunders J, Vickers J, Zhang Y, De Stefano N, Brady JM, Matthews PM (2004) Advances in functional and structural MR image analysis and implementation as FSL. Neuroimage 23(Suppl 1):S208–S219
25. Bauer M (2007) High performance computing: the software challenges. In: Proceedings of the 2007 international workshop on Parallel Symbolic Computation, London, pp 11–12
26. Smith SM (2002) Fast robust automated brain extraction. Hum Brain Mapp 17(3):143–155
27. Zhang Y, Brady M, Smith S (2001) Segmentation of brain MR images through a hidden Markov random field model and the expectation-maximization algorithm. IEEE Trans Med Imaging 20(1):45–57
28. Jenkinson M, Smith S (2001) A global optimisation method for robust affine registration of brain images. Med Image Anal 5(2):143–156
29. Jenkinson M, Bannister P, Brady M, Smith S (2002) Improved optimization for the robust and accurate linear registration and motion correction of brain images. Neuroimage 17(2):825–841
30. Rueckert D, Sonoda LI, Hayes C, Hill DL, Leach MO, Hawkes DJ (1999) Nonrigid registration using free-form deformations:

application to breast MR images. IEEE Trans Med Imaging 18(8):712–721
31. Ongür D, Prescot AP, Jensen JE, Cohen BM, Renshaw PF (2009) Creatine abnormalities in schizophrenia and bipolar disorder. Psychiatry Res 172(1):44–48
32. Warsi MA, Molloy DW, Standish T, Wardlaw G, Noseworthy MD (2010) BOLD Signal Fractal Dimension Mapping in AD Demonstrates Increase Microvascular Activity and Metabolism When Combined With Spectroscopy. In: Proceedings of the 17th scientific meeting, International Society for Magnetic Resonance in Medicine, Honolulu, p 4242
33. Raichle ME (2010) The brain's dark energy. Sci Am 302(3): 44–49
34. Jannot M (2010) How are we wired? Sci Illus 3(2):32–38
35. Lerch JP, Pruessner JC, Zijdenbos A, Hampel H, Teipel SJ, Evans AC (2005) Focal decline of cortical thickness in Alzheimer's disease identified by computational neuroanatomy. Cereb Cortex 15(7):995–1001
36. Liu Y, Wang K, Yu C, He Y, Zhou Y, Liang M, Wang L, Jiang T (2008) Regional homogeneity, functional connectivity and imaging markers of Alzheimer's disease: a review of resting-state fMRI studies. Neuropsychologia 46(6):1648–1656
37. Baudelet C, Cron GO, Ansiaux R, Crokart N, DeWever J, Feron O, Gallez B (2006) The role of vessel maturation and vessel functionality in spontaneous fluctuations of T2*-weighted GRE signal within tumors. NMR Biomed 19(1):69–76
38. Baudelet C, Ansiaux R, Jordan BF, Havaux X, Macq B, Gallez B (2004) Physiological noise in murine solid tumours using T2*-weighted gradient-echo imaging: a marker of tumour acute hypoxia? Phys Med Biol 49(15):3389–3411
39. Wardlaw G, Wong R, Noseworthy MD (2008) Identification of intratumour low frequency microvascular components via BOLD signal fractal dimension mapping. Phys Med 24(2):87–91
40. Kalaria RN, Cohen DL, Premkumar DR, Nag S, LaManna JC, Lust WD (1998) Vascular endothelial growth factor in Alzheimer's disease and experimental cerebral ischemia. Brain Res Mol Brain Res 62(1):101–105
41. Barnes J, Bartlett JW, van de Pol LA, Loy CT, Scahill RI, Frost C, Thompson P, Fox NC (2009) A meta-analysis of hippocampal atrophy rates in Alzheimer's disease. Neurobiol Aging 30(11):1711–1723

CHAPTER 7

BOLD FD VS. RSN IN AD

Fractal Dimension Compared to Resting State Network Analysis of BOLD MRI in Alzheimer's Disease.

Mohammed A. Warsi, B.Sc., M.Sc., M.D., FRCP(C), William Molloy, MB BCh, MRCP(I), FRCP(C), Michael D. Noseworthy, M.Sc., Ph.D., P.Eng.

7.1 CONTEXT OF THE PAPER

In the following manuscript (chapter 7) a further refined method for fractal dimension (FD) analysis was implemented. In chapters 5 and 6 the FD calculation was based on a publication of this technique (Wardlaw 2008) that assumes the signal exhibits fractional Gaussian noise (fGn). Previous reports of FD analysis methods had proposed an algorithm to challenge the assumption of complete fGn signal (Eke 2002) and allowed us to filter out non-fGn (i.e. fractional Brownian noise, fBm) signals that represented approximately 22% of the rsBOLD signal in ROIs. This method was presumed to increase the accuracy of FD analysis.

This new approach for measuring FD was compared to functional connectivity in the default mode network (DMN), a known network affected by AD (Greicius 2004). Having established FD reduction in AD (chapter 6), we tested the hypothesis that this reduction was related to brain functional connectivity. DMN connectivity was compared to FD in areas within the DMN (posterior cingulate cortex) and outside of the network

(putamen). We expected the reduction in network connectivity would correlate with reduced FD.

7.2 DECLARATION STATEMENT

Mohammed Ali Warsi as principle author wrote the article, performed analysis and created figures and tables as appropriate. Michael D. Noseworthy, as corresponding author, hypothesized the use of FD in assessing Alzheimer's, wrote the first versions of the FD analysis program using Matlab (Mathworks, Natick, MA), provided guidance, funding and advice, and performed proofreading/editing and submission of the manuscript for publication. Dr. William Molloy provided clinical geriatric assessment, patient recruitment, guidance and commentary.

This paper has been submitted for publication to the *Journal of Psychiatry and Neurosciences*.

7.3 PAPER

Fractal Dimension Compared to Resting State Network Analysis of BOLD MRI in Alzheimer's Disease.

Mohammed A. Warsi, B.Sc., M.Sc., M.D., FRCP(C)[1,2,3], William Molloy, MB BCh, MRCP(I), FRCP(C)[4], Michael D. Noseworthy, M.Sc., Ph.D., P.Eng.[1,2,3,5,6,7,8*]

[1] *School of Biomedical Engineering, McMaster University, Hamilton, Ontario, Canada.*

[2] *Department of Psychiatry and Behavioural Neuroscience, Hamilton, Ontario, Canada.*

[3] *Brain-Body Institute, St. Joseph's Healthcare, Hamilton, Ontario, Canada.*

[4] *Department of Gerontology and Rehabilitation, University College Cork, Ireland.*

[5] *Electrical & Computer Engineering, McMaster University, Hamilton, Ontario, Canada.*

[6] *Medical Physics & Applied Radiation Sciences, McMaster University, Hamilton, Ontario, Canada.*

[7] *Diagnostic Imaging, St. Joseph's Healthcare, Hamilton, Ontario, Canada.*

[8] *Department of Radiology, McMaster University, Hamilton, Ontario, Canada.*

**Corresponding Author Address:*

Dr. Michael D. Noseworthy, Ph.D., P.Eng.

Director, Imaging Research Centre,

St. Joseph's Healthcare, 50 Charlton Ave. East

Hamilton, Ontario, Canada. L8N 4A6

Phone: +1 1(905) 522-1155 x35218

Email: nosewor@mcmaster.ca

Abstract:

Background: We investigated temporal fractal structure of BOLD-fMRI in Alzheimer's disease (AD) and age-matched controls (NC). Relative dispersion fractal dimension (FD_{RD}), a measure of signal complexity, was compared to default mode network (DMN) connectivity using resting-state network (RSN) analysis.

Methods: 38 mild/moderate AD subjects (MMSE=22±3) and 16 NC were scanned at rest. Nine AD returned 10.31±1.96 months later. BOLD-fMRI acquisitions focused on high temporal sampling (TR=250ms, 3 slices, 2400 time-points) for FD analysis and expanded spatial coverage (TR=2000ms, 24 slices, 300 time-points) for RSN analysis. DMN nodes included posterior cingulate cortex (PCC), medial prefrontal cortex (MPC), lateral parietal cortex (LPC) and hippocampal formation (HF) and were used to calculate normalized correlation (Z-values).

Results: FD_{RD} in putamen correlated with that in PCC ($r=0.83$, $p<0.001$) and FD_{RD} was consistent between baseline and follow-up (putamen: $r=0.81/p=0.015$, PCC: $r=0.69/p=0.058$). NC had higher FD_{RD} than AD and FD_{RD} was lower at follow-up but not statistically significant. DMN Z values were significantly lower in AD than in NC ($p=0.004$). DMN mean Z-values correlated with FD_{RD} in PCC ($r=0.33$, $p=0.043$) and RSN Z values correlated with the HF for both putamen ($r=0.31$, $p=0.049$) and PCC ($r=0.32$, $p=0.046$).

Limitations: FD_{RD} was only measured in a small brain area. Also, patients were in early stages of illness so differences in FD_{RD} and RSN compared to NC was likely subtle.

Conclusions: FD_{RD} relates to functional connectivity and is a reliable and reproducible measure of complexity. FD_{RD} decreases as AD progresses and unlike RSN, FD_{RD} is not limited to functional networks.

Introduction:

Resting state blood oxygen level dependent (BOLD) MRI has revealed that spatially separated areas of the brain are activating in synchrony thus displaying functional connectivity[1]. Through RSN analysis, the default mode network (DMN) consistently appears to be one of the strongest functional networks in the brain[2]. The DMN is a network connecting the posterior cingulate cortex (PCC) to the medial prefrontal cortex (MPC), left and right lateral parietal cortex (l-LPC and r-LPC) and the left and right hippocampal formation (l-HF and r-HF)[3]. Certain pathologies seem to have characteristic DMN changes and can be seen in schizophrenia, Alzheimer's disease (AD) and multiple sclerosis[4]. In AD, there is a decrease in connectivity between the nodes of the DMN, most significantly between the PCC and HF[5]. This may relate to the involvement of DMN in episodic memory processing[6].

Another method of characterizing BOLD fMRI signal at rest is to study the complexity of the signal in the time domain using fractal dimension mapping (FD)[7]. FD analysis of resting state BOLD signal characterizes the complexity on a scale from 1 (ordered signal) to 1.5 (disordered or random). Although FD can also characterize negative autocorrelation ($1.5 < FD < 2.0$), this is not normally seen in physiological systems[8].

In many physiological systems the power ($\boldsymbol{p}$) of a noise signal is related to its frequency ($\boldsymbol{f}$) with a $\boldsymbol{1/f^{\beta}}$ relationship[9] and can be scaled to a value of FD of the BOLD power spectrum (FD_{PS}). In systems exhibiting fractional Gaussian noise (fGn) such as the brain, relative dispersion (FD_{RD}) provides a more accurate measure of FD due to

marked bias of FD_{PS} in the lower range of $\boldsymbol{\beta}$ values[10]. Similar to the power-frequency relationship in $\boldsymbol{FD_{PS}}$, the signal spread or relative dispersion (RD) follows a $\boldsymbol{1/MS^{\alpha}}$ relationship where $\boldsymbol{MS}$ is the measurement scale[11,12]. Therefore RD was our main measure of FD in this study. The limited spatial coverage of high frequency (low TR) allowed us to measure FD in areas both within the DMN (PCC) and external to it (putamen) but not the hippocampus.

Objectives

We sought to characterize the FD signal in the brain and compare it to functional connectivity measures with RSN. We chose to study subjects with Alzheimer's disease (AD) since this population has well characterized changes in the DMN. We hypothesized that signal complexity as measured by FD_{RD} would be different in normal controls (NC) compared to AD and that this change in complexity would be related to changes in functional connectivity as measured by RSN.

Methods:

In a study approved by our research ethics board, 38 subjects with mild to moderate AD (MMSE=22±3) and 16 age and gender matched NC were recruited. A small number (9 subjects) with AD agreed to return for a repeat scan 10.31±1.96 months later. Diagnosis and severity of illness was also confirmed by clinical exam, Alzheimer's Disease Assessment Scale (ADAS) and Clinical Dementia Rating Scale (CDR). Subjects were recruited from a local geriatric clinic after obtaining informed consent. Aged

matched controls were spouses of AD subjects who did not have AD based on clinical exam by a geriatrician and a screening cognitive exam (Table 1).

Table 1: Subject Details (Mean±SD)

	AD	NC	P Value
N	38	16	-
Females	18	10	0.32
Age (y)	76.8±7.6	74.1±5.7	0.16
MMSE[1]	22.1±3.2	28.6±1.2	<0.001
Illness onset (y)	3.5±2.2	-	-
Education (y)	13.0±3.4	-	-
SADAS[2]	18.0±6.8	-	-
CDR[3]	0.96±0.53	-	-

[1] Mini Mental Status Exam

[2] Standardized Alzheimer's Disease Assessment Scale – Cognitive Subscale

[3] Clinical Dementia Rating – Global Score

Standard T1 and T2-weighted images, acquired using a GE Signa HD 3.0Tesla MRI (General Electric Healthcare, Milwaukee WI) and 8 channel phased array head coil, were used to prescribe BOLD image acquisitions (echo planar imaging (EPI) TE = 35ms, FOV=24cm, 64x64 matrix, 5mm thick slices). FD scans had high temporal frequency (α

=70°, TR=250ms, 3 slices, 2400 time points) while RSN scans had large spatial coverage (α =90°, TR=2000ms, 24 slices, 300 time points). Motion correction was performed using an iterated linearized weighted least squares algorithm in AFNI[13], which considered the head as a rigid body (6 degrees of freedom). FD regions of interest (ROI) were prescribed in the putamen and posterior cingulate cortex (PCC) using template masking in AFNI and confirmed visually (Figure 1).

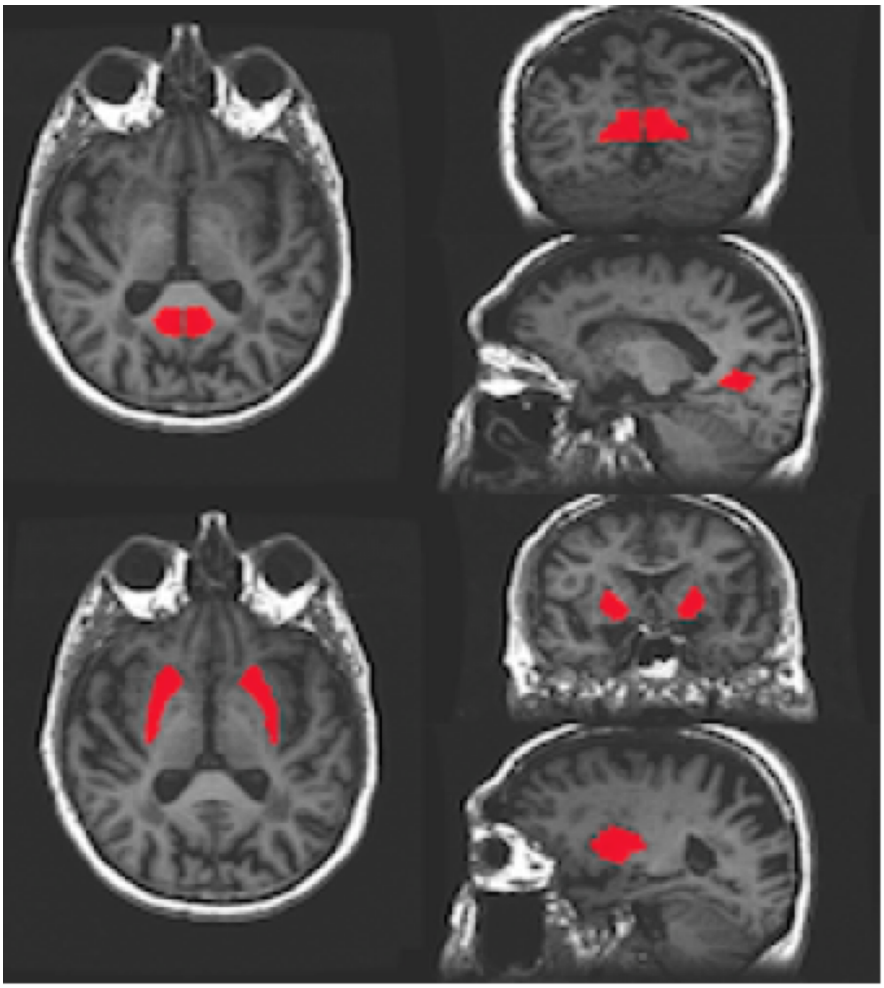

Figure 1: Masks of the PCC and putamen produced by ANFI[13] and used to prescribe ROIs for FD analysis in one subject.

FD Calculations

High temporal resolution BOLD data was assessed for nonlinear signal characteristics with in-house programs written in Matlab (v.7.9, The Mathworks, Natick MA). The analysis followed two pipelines: FD analysis of the power spectrum (FD_{PS}) and through relative dispersion (FD_{RD}). FD analysis was done using the method of Eke *et al.*[10]. Using this approach the BOLD signal is first characterized as either fractional Gaussian noise (fGn) or fractional Brownian motion (fBm) using the power spectral density (PS). Signals that can not clearly be classified as either required signal summation conversion (SSC) for further characterization. fGn signals were quantified using relative dispersion fractal analyses (FD_{RD}). Although fBm signals could be characterized using scaled windowed variance (SWV) analyses, fBm in brain BOLD signal is not meaningful and may represent non-physiological noise[8] and these voxels were therefore not included in the analysis.

FD_{RD} analysis was done using 9 scales of measurement over the middle 2048 images from the acquired 2400 volumes, discarding volumes where subjects may be anticipating the beginning or end of the scan. Signal FD_{RD}, at each voxel, was calculated from RD (standard deviation divided by mean of the signal) using:

$$FD = 1 - \frac{\log[RD(m)/RD(m_0)]}{\log(m/m_0)} \qquad \text{(eqn. 1)}$$

where FD is the fractal dimension, m is the scale of measurement used to calculated RD, and m_0 is an assigned reference value. For mathematical simplicity, m_0 is assigned to a value of 1.

We have found the FD_{RD} approach to be temporally stable over this time period using a sliding window approach[14]. The Matlab iteratively reweighted least squares linear regression algorithm 'robustfit' was used, with a bisquare weighting function, to calculate the slope, $\boldsymbol{\alpha}$, through log(RD) vs. log(scale) and FD_{RD} was determined using $FD_{RD} = 1 - \alpha$. This was performed voxel-wise to produce maps of FD_{RD}. FD_{PS} was measured from the Fourier transform of the temporal data for each voxel. As with FD_{RD} , FD_{PS} was calculated from the negative slope of the log-log plot (β) for each voxel (eqn. 2). FD_{RD} values for each voxel within the ROI were averaged.

$$\beta = -2FD_{PS}+3 \qquad \text{(eqn. 2)}$$

RSN method

Whole brain BOLD data was analyzed for resting state functional networks (RSN) using methods described by Van Dijk *et al.*[3]. Data was converted to standardized space (Talairach) and resampled to 2mm isotropic voxels. A Gaussian kernel with full-with-half-max (FWHM) of 6mm was used for spatial smoothing. Temporal filtering of components greater than 0.08Hz and less than 0.001Hz was performed to eliminate high frequency noise and low frequency drift, respectfully. Time series were extracted from

the 6 nodes of the DMN. These nodes were defined in standard space as described by Van Dijk *et al.* (2010). All processing steps were done using AFNI [13].

The extracted time series from the PCC was correlated with other nodes of the DMN using Pearson's correlation. These correlations were normalized to produce standard scores (Z values) for each node (eqn. 3) using Fisher's *r*-to-*z* transformation[15], which could then be compared between subjects and correlated with other measures such as FD_{RD}.

$$Z = 0.5 \cdot \ln\left[\frac{1+r}{1-r}\right] \qquad \text{(eqn. 3)}$$

Overall functional connectivity in the DMN was also represented by the mean Z values from all nodes in for given subject.

Volumetric analysis of whole brain and individual brain structures was performed using NeuroQuant (NQ)[16], a commercial automated segmentation software. NQ volumes have been validated against manually drawn volumes in AD[16]. Volumes of the putamen, caudate and thalamus were compared between AD and NC using a 2 tailed unpaired Student's t-test. Grey matter (GM), amygdala and hippocampal volumes were similarly compared.

Anatomical scans were realigned to a standard template (Talairach) using AFNI[13]. Transformation parameters were used to warp all FD maps into standard space allowing for intra subject comparison of FD maps and group analysis.

Statistical analysis was done using the statistics toolbox of Matlab and SPSS (version 17, SPSS Inc., Chicago, IL, USA). Two-tailed unpaired Student's t-test, with unequal sampling, was used for comparing FD_{RD} values and RSN Z values between

subject groups. Pearson's correlation coefficient was used for comparing FD_{RD} with RSN Z values, with the significance threshold set at $p<0.05$. A Jarque–Bera test, which takes into consideration both skewness and kurtosis, was used to confirm normality of FD and RSN data. Motion in AD compared to NC was evaluated by comparing variance of translation and rotation using a general linear model multivariate analysis. All acquisition and analysis was done blinded to subject status (AD vs. NC).

Results:

All subjects were able to complete the full brain RSN scans (AD: n=38, NC: n=16) but two AD subjects were unable to complete the FD scans because of early scan termination due to claustrophobia (AD: n=36, NC=16). All 9 AD subjects that returned for follow-up completed RSN and FD scans. A comparison of volumes obtained from NQ in AD compared to NC showed no significant difference in the volumes of the putamen, caudate or thalamus. However, there was a significant difference in GM, amygdala and hippocampal volumes ($p<0.001$) (AD < NC).

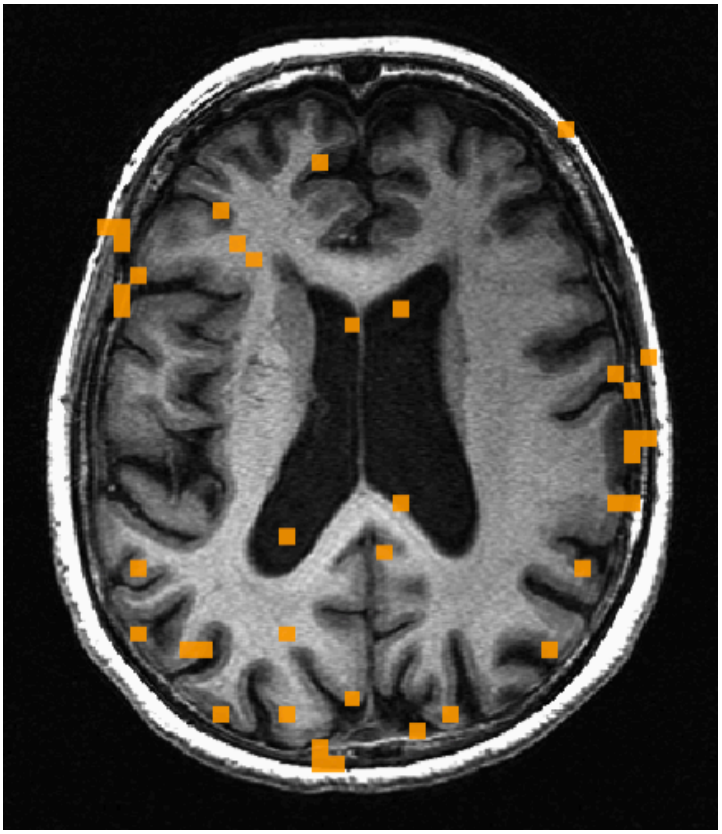

Figure 2: Map of fBm voxels in one subject. Voxels exhibiting fBm characteristics appeared randomly throughout the imaged slice with no apparent anatomical relevance. The percentage of fGn voxels in the ROIs was maximal at 100% and minimal at 58.6%. The number of fBm voxels did not correlate with any outcome measures and was consistent between AD and NC.

FD analysis

Voxel-wise parametric FD maps showed significant fits to BOLD data within the selected ROI for all subjects ($p<0.01$) confirming a linear multiscale relationship (i.e. fractal). PS analysis from all voxels within the ROIs for all subjects revealed most voxels exhibited fGn patterns (78.0±13.0% in putamen, 72.1±13.3% in PCC). There was no specific pattern or clustering of fBm signal although many of the voxels aligned with the CSF or margins (Figure 2). This confirmed FD_{RD} as the appropriate method of FD

quantification. The percentage of fGn signal did not correlate with any of the outcome measures. FD_{RD} was compared between the two ROIs (putamen and PCC) and were found to correlate with each other ($r=0.83$, $p<0.001$) (Figure 3). FD appeared consistent between baseline and follow-up and had significant correlation of FD_{RD} for the Putamen ($r=0.81$, $p=0.015$) and trended towards significance in the PCC ($r=0.69$, $p=0.058$) (Figure 4). There was a mean lowering for FD_{RD} in AD over time (putamen and PCC change in FD=0.01) and compared to NC, FD_{RD} was lower in AD (putamen and PCC change in FD=0.02) but these comparisons were not statically significant. There was no correlation between FD_{RD} values and volumes of putamen, PCC or hippocampus.

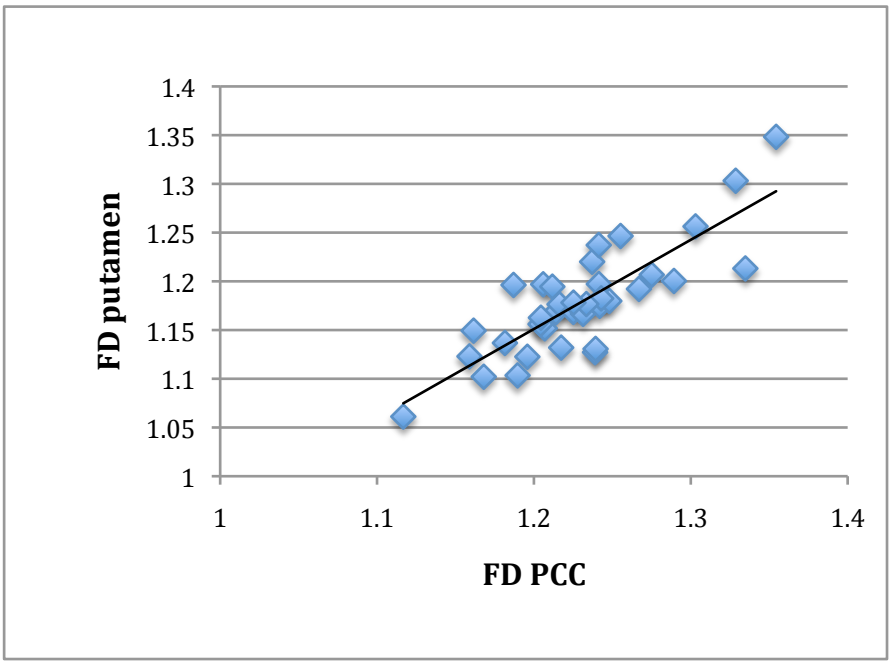

Figure 3: FD_{RD} values between the two ROIs (PCC and putamen) shows strong correlation with each other ($r=0.83$, $p<0.001$).

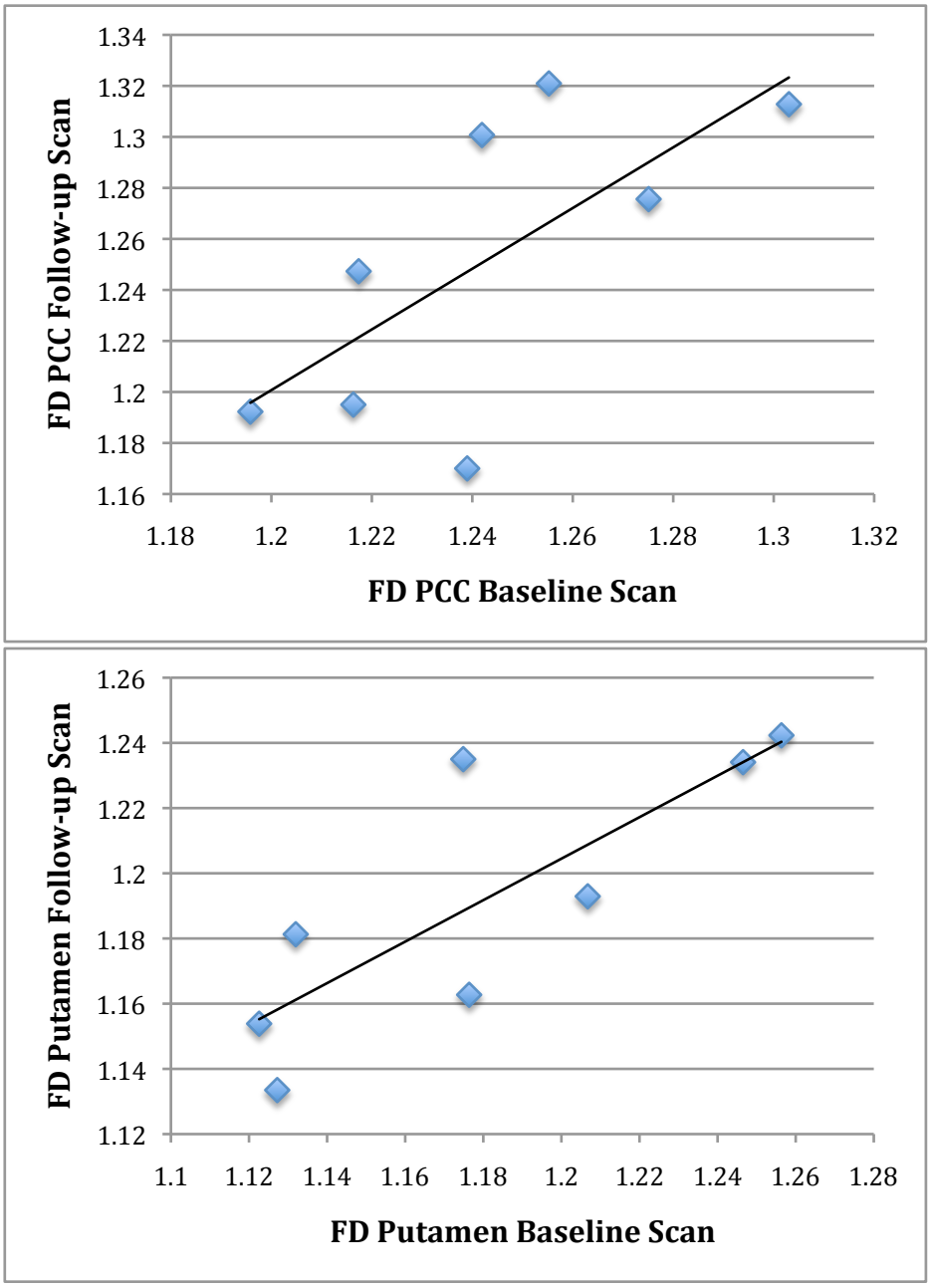

Figure 4: Correlations between FD_{RD} at baseline and FD_{RD} follow-up in the Putamen (r=0.81, p=0.015) and the PCC (r=0.69, p=0.058).

RSN

The range of Z value correlations for the DMN in AD (mean±std: 0.37±0.20) was in keeping with previously published data[17,3]. DMN Z values were significantly lower in NC (mean±std: 0.65±0.32) compared to DMN in AD (p=0.004) (Figure 5). Bilateral nodes correlated with each other (HF-left vs HF-right: r=0.53, p<0.001, LPC-left vs LPC-right: r=0.50, p=0.002) (Figure 6). Z values in the HF, MPC and LPC did not correlated with each other.

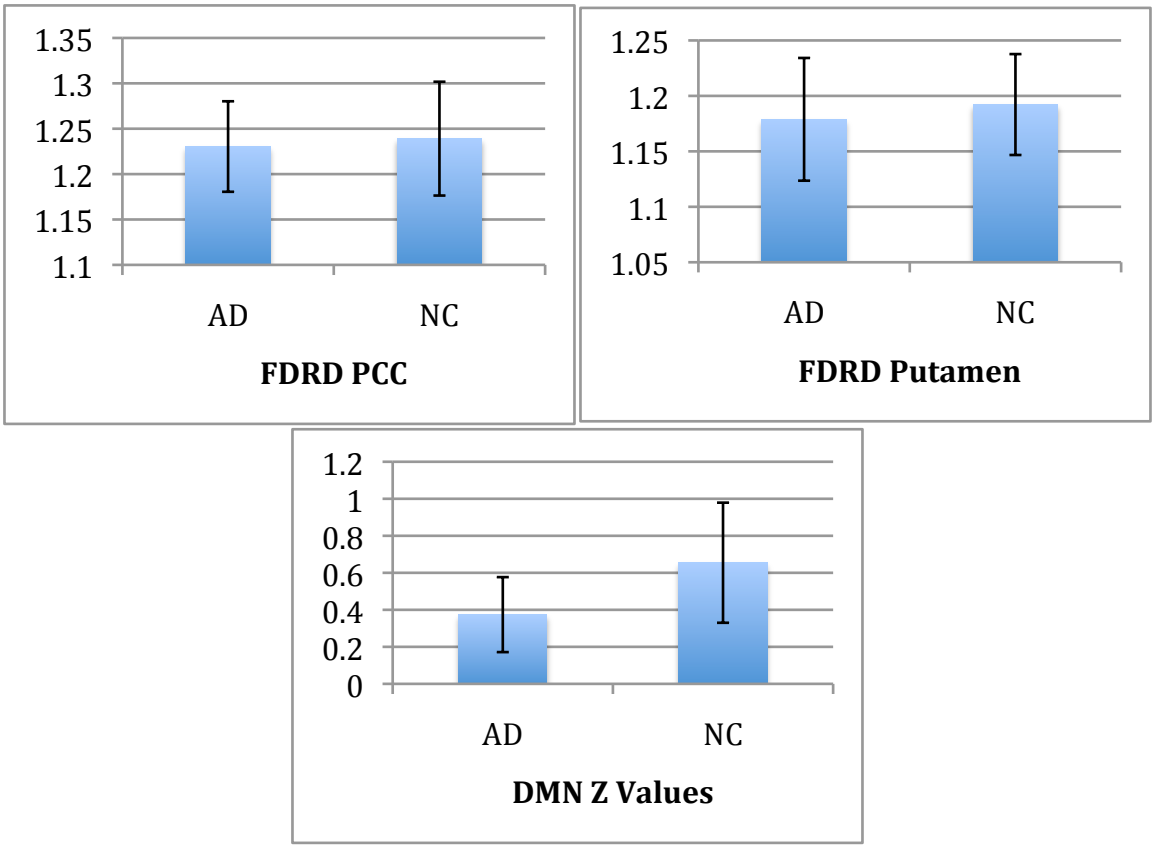

Figure 5: FD_{RD} in the PCC and putamen, as well as the mean Z values for the DMN were lower in NC when compared to AD. This difference was statistically significant for the DMN (p=0.004).

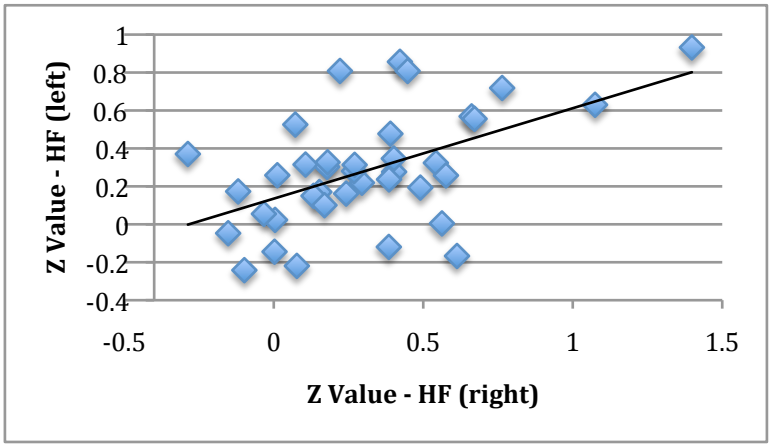

A

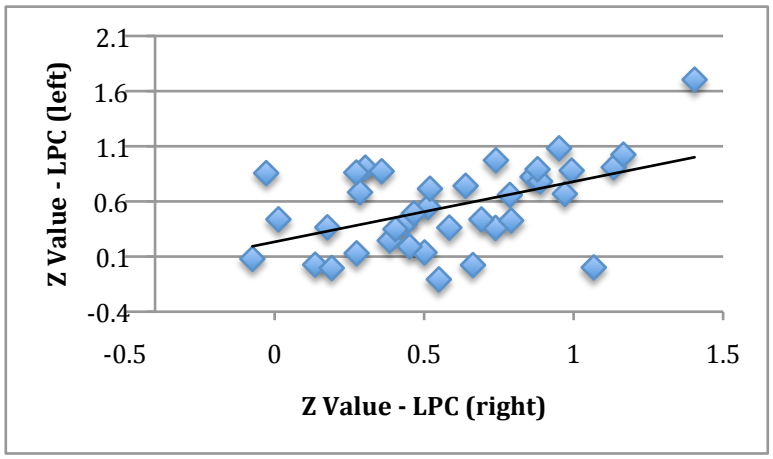

B

Figure 6: DMN Z values correlated between the left and right HF (r=0.53, p<0.001) (Fig 6A) and left and right LPC (r=0.50, p=0.002) (Fig 6B).

FD compared to RSN

Mean Z values for the DMN significantly correlated with FD_{RD} in the PCC (r=0.33, p=0.043) and trended towards significance in the putamen (r=0.27, p=0.081) (Figure 7). There was also significant correlation between FD_{RD} and RSN in the hippocampal formation (HF) (FD_{RD} in putamen vs. RSN in HF: r=0.31, p=0.049, FD_{RD} in

PCC vs. RSN in HF: r=0.32, p=0.046) (Figure 7). FD_{RD} did not significantly correlate with other individual nodes of the DMN (FD_{RD} vs. MPC and LPC).

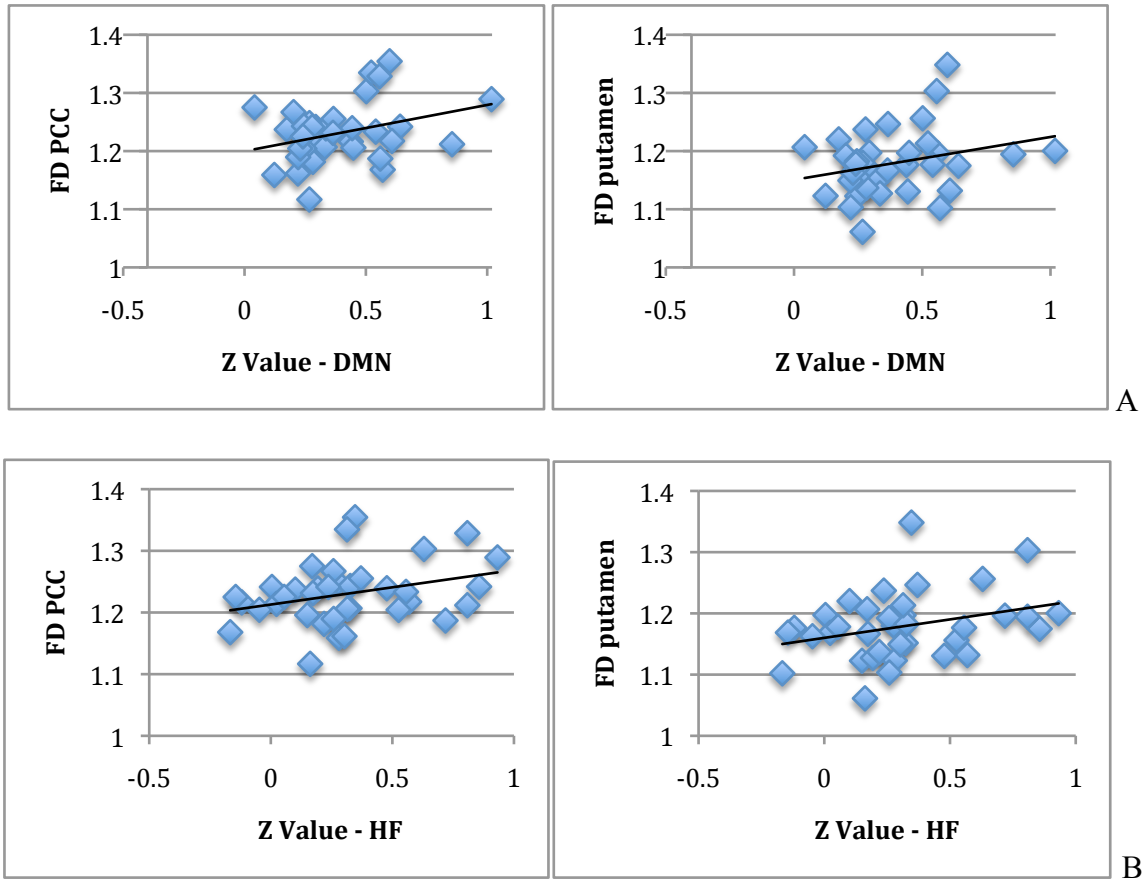

Figure 7: Correlations of FD_{RD} to the Mean Z values for the DMN in the PCC (r=0.33, p=0.043) and the putamen (r=0.27, p=0.081) (Fig 7A) and correlations with RSN (HF) in FD_{RD} PCC (r=0.32, p=0.046) and in FD_{RD} putamen (r=0.31, p=0.049) (Fig 7B).

Discussion:

This study highlights FD analysis as a useful tool to analyze signal complexity in physiological systems like the brain and demonstrates that FD_{RD} values can be applied to various ROIs with consistent results. FD relates to functional connectivity in the brain.

Since their discovery[18], there have been great efforts to characterize the functional networks in normal and pathological brains. RSN analysis involves two major methods. The first is the seed based method where a single voxel in a BOLD time series is compared to all the other voxels to find significant correlations in time. This can be done to study networks where one point (the seed voxel) is known or predetermined[19]. The second method of RSN analysis involves comparing each brain voxel to every other voxel and identifies networks without any *a priori* model or seed placement. This method uses independent component analysis (ICA) to identify multiple networks[19]. Both methods of RSN analysis find the DMN as being a major network that seems to be ubiquitous across subjects[4] and through time[20] and both find deficiencies in the DMN of AD. Using seed based analysis, we were able to correlate RSN to FD, a measure of complexity.

Fractals are patterns that have self similarity at multiple scales. For example, the branching pattern of trees is similar from the trunk to leaflet level. Scaled self-similarity can also occur in time, for example the variation brain EEG signal over minutes is similar in pattern to the changes at the millisecond scale[21]. This fractal pattern is also seen in resting state fMRI. Signal complexity such as cardiac ECG signal has been related to physiological health[22]. Power and frequency of physiologic noise are related by the variable $\boldsymbol{\beta}$. This parameter can be scaled to represent standard variables such as the Hurst exponent ($\boldsymbol{H}$), as measured by power spectral analysis ($\boldsymbol{H_{PS}}$), or the fractal dimension ($\boldsymbol{FD_{PS}}$).

Physiological systems can produce fractal patterns that are either static (fractional Gaussian noise – fGn) or non-static (fractional Brownian motion – fBm). BOLD signals

from the brain mostly exhibit fGn[23]. fBm is thought to relate to non-physiological noise such as motion artifacts[8]. Power spectral density (PS) can be used to sort fGn from fBm and can also provide and estimate of FD (FD_{PS}). Most of the brain BOLD signal follows a fGn pattern rather than fBm in our study, which is consistent with other studies of brain BOLD FD[8,9]. fBm signals represent high $\boldsymbol{\beta}$ values with contributions from CSF signal[9] or patient motion[8] and our subjects had fBm mainly in the ventricles and at the brain margins. The CSF contribution to fBm may explain the higher proportion of fBm caught within the PCC ROI vs. the putamen.

Brain changes in AD occur in the grey matter and are most evident in the medial temporal lobe, hippocampus and deep grey matter structures such as the putamen[24]. Recent positron emission tomography (PET)[25] and quantitative R2 iron quantification[26,27] studies have also shown changes in the putamen associated with AD. FD in the putamen also correlates with changes in magnetic resonance spectroscopy (MRS) in AD[28]. Inhomogeneity of main MRI field (B_0) at the base of the brain can decreased accuracy of BOLD measurements due to susceptibility artifact, especially in the hippocampus, and was therefore not chosen for FD analysis. Also, the putamen is less likely to show volumetric changes in early AD when compared to the hippocampus or amygdala which would contribute to partial voluming effects[29]. Therefore the putamen was chosen as our region of interest (ROI). When patients are AC-PC aligned in the scanner, the PCC lies within the same axial plane as the putamen, allowing up to have this second ROI within the 3 axial slices of FD image acquisition. PCC has been implicated in the pathology of AD through MRS[30] and PET[31] studies.

Previous AD changes have been attributed to changes in neuronal connectivity[23]. We studied the relationship of FD_{RD} in AD to functional connectivity using RSN. The direct correlation between the two suggests that a decrease in FD_{RD} is related to a decrease in connectivity. This includes FD_{RD} in areas connected to the DMN (PCC) as well as areas unrelated to the DMN (putamen) and suggests that FD_{RD} may be an indirect measure of functional connectivity. Since FD is a measure of signal complexity, this makes sense. Areas with less functional connectivity likely have less neuronal input modulating the signal pattern. Therefore, these areas will have lower signal complexity and subsequently lower FD. Other studies have pharmacologically mimicked a decrease in neuronal connectivity and shown a reduction in FD[32]. The most robust changes in DMN for AD are seen it the hippocampus[5] and in our study the changes in HF RSN correlated with FD.

FD is not subject to the node constraints of RSN analysis and can therefore be applied to any area of the brain. In this fashion, FD has previously been used to assess signal complexity in various brain regions, including a comparison of GM to WM[9] and compared to MRS findings in AD[28]. Resting BOLD analysis also allows us to explore BOLD signal without the confounding complications of functional paradigms, and their associated assumptions, in traditional fMRI.

One measure of reliability of FD_{RD} measurements was the reproducibility in subjects. When subjects were rescanned, their FD values were very similar to baseline approximately 10 months earlier. This suggests that FD_{RD} is a consistent trait in AD brains. There was a slight decrease in FD_{RD} over this time period, which is consistent

with the idea that FD_{RD} decreased with AD disease severity[28]. This is further reinforced by FD_{RD} values in NC being lower than AD. These differences were not significant, likely due to early stage of illness in the subjects; MMSE scores were in the mild to moderate range. There were differences in GM, amygdala and hippocampal volumes, but not yet in the putamen, caudate or thalamus.

The utility of FD analysis of resting state BOLD need not be limited to the study of AD. Signal complexity is an important component of schizophrenia, depression, anxiety and disorders of childhood[33]. With the development of more objectives measure of personality, brain signal complexity has also been used to characterize personality disorders[34]. Most of these studies have utilized EEG, an accessible technology with excellent temporal resolution but limited spatial information. Signal patterns from EEG are even being used to help predict treatment response to therapeutics [35]. FD of resting BOLD could offer a complimentary approach to these methods.

Limitations:

We were unable to measure FD in areas of the brain such as the hippocampus due to imaging parameter constraints. Spatial range of the imaging data was sacrificed for high temporal resolution; a TR of 250ms allowed collection of only three brain slices. However, this allows for a more robust analysis without aliasing of higher frequency BOLD components including cardiac (~1Hz) components, as the TR satisfies the Nyquist criterion for this physiological frequency. Although FD analysis could be performed on whole brain resting BOLD data (TR of 2000ms), the dominant cardiac signal would

appeared aliased. Although patients with mild to moderate AD allowed us to study the early changes in AD, some differences from NC were not very robust, not allowing us to find statistically significant changes in some parameters for the number of subjects studied.

Conclusion:

We conclude that FD_{RD} is related to functional connectivity and is a reliable and reproducible measure of signal complexity. Unlike RSN, FD_{RD} can be applied to any area of the brain and is not limited to functional networks. There may be some reduction in FD_{RD} as AD progresses. In the future, FD_{RD} could be compare to structural connectivity using diffusion tensor imaging or to EEG temporal signal.

References:

1. Biswal BB, Van Kylen J, Hyde JS. Simultaneous assessment of flow and BOLD signals in resting-state functional connectivity maps. *NMR Biomed*. 1997;10(4-5):165-170.

2. Greicius MD, Srivastava G, Reiss AL, et al. Default-mode network activity distinguishes Alzheimer's disease from healthy aging: evidence from functional MRI. *Proc Natl Acad Sci USA*. 2004;101(13):4637-4642.

3. Van Dijk KRA, Hedden T, Venkataraman A, et al. Intrinsic functional connectivity as a tool for human connectomics: theory, properties, and optimization. *J Neurophysiol*. 2010;103(1):297-321.

4. Rosazza C, Minati L. Resting-state brain networks: literature review and clinical applications. *Neurological sciences : official journal of the Italian Neurological Society and of the Italian Society of Clinical Neurophysiology*. 2011;32(5):773-785.

5. Sorg C, Riedl V, Mühlau M, et al. Selective changes of resting-state networks in individuals at risk for Alzheimer's disease. *Proc Natl Acad Sci U S A*. 2007;104(47):18760-18765.

6. Vincent JL, Snyder AZ, Fox MD, et al. Coherent spontaneous activity identifies a hippocampal-parietal memory network. *J Neurophysiol*. 2006;96(6):3517-3531.

7. Wardlaw G, Wong R, Noseworthy MD. Identification of intratumour low frequency microvascular components via BOLD signal fractal dimension mapping. *Phys Med*. 2008;24(2):87-91.

8. Maxim V, Sendur L, Fadili J, et al. Fractional Gaussian noise, functional MRI and Alzheimer's disease. *Neuroimage*. 2005;25(1):141-158.

9. Wink A-M, Bullmore E, Barnes A, et al. Monofractal and multifractal dynamics of low frequency endogenous brain oscillations in functional MRI. *Hum Brain Mapp*. 2008;29(7):791-801.

10. Eke A, Hermán P, Bassingthwaighte JB, et al. Physiological time series: distinguishing fractal noises from motions. *Pflügers Archiv : European journal of physiology*. 2000;439(4):403-415.

11. Bassingthwaighte JB, Liebowitch LS, West BJ. Fractal Physiology: Oxford University Press; 1994.

12. Eke A, Herman P, Kocsis L, et al. Fractal characterization of complexity in temporal physiological signals. *Physiol Meas*. 2002;23(1):R1-38.

13. Cox RW. AFNI: software for analysis and visualization of functional magnetic resonance neuroimages. *Comput Biomed Res*. 1996;29(3):162-173.

14. Warsi MA, Noseworthy MD, editors. Stability of brain resting state BOLD fractal dimension (FD) mapping. Proceedings of the 28th Annual Scientific Meeting, European Society of Magnetic Resonance in Medicine and Biology (ESMRMB) 2011; Leipzig, Germany. 28:512.

15. Zar JH. Biostatistical analysis. 4th ed. Upper Saddle River, N.J.: Prentice Hall; 1999.

16. Brewer JB, Magda S, Airriess C, et al. Fully-Automated Quantification of Regional Brain Volumes for Improved Detection of Focal Atrophy in Alzheimer Disease. *AJNR Am J Neuroradiol*. 2009;30(3):578-580.

17. Fleisher AS, Sherzai A, Taylor C, et al. Resting-state BOLD networks versus task-associated functional MRI for distinguishing Alzheimer's disease risk groups. *Neuroimage*. 2009;47(4):1678-1690.

18. Biswal B, Yetkin FZ, Haughton VM, et al. Functional connectivity in the motor cortex of resting human brain using echo-planar MRI. *Magn Reson Med*. 1995;34(4):537-541.

19. Rosazza C, Minati L, Ghielmetti F, et al. Functional Connectivity during Resting-State Functional MR Imaging: Study of the Correspondence between Independent Component Analysis and Region-of-Interest-Based Methods. *AJNR American journal of neuroradiology*. 2012;33(1):180-187.

20. Chou Y-H, Panych LP, Dickey CC, et al. Investigation of Long-Term Reproducibility of Intrinsic Connectivity Network Mapping: A Resting-State fMRI Study. *American Journal of Neuroradiology*. 2012;33:833-838.

21. Song I-H, Lee S-M, Kim I-Y, et al. Multifractal Analysis of Electroencephalogram Time Series in Humans. *Lect Notes Comput Sc*. 2005;3512:921-926.

22. Goldberger AL, Amaral LA, Hausdorff JM, et al. Fractal dynamics in physiology: alterations with disease and aging. *Proc Natl Acad Sci U S A*. 2002;99 Suppl 1:2466-2472.

23. Kiviniemi V. Endogenous brain fluctuations and diagnostic imaging. *Hum Brain Mapp*. 2008;29(7):810-817.

24. de Jong LW, van der Hiele K, Veer IM, et al. Strongly reduced volumes of putamen and thalamus in Alzheimer's disease: an MRI study. *Brain*. 2008;131(Pt 12):3277-3285.

25. Koivunen J, Scheinin N, Virta JR, et al. Amyloid PET imaging in patients with mild cognitive impairment: a 2-year follow-up study. *Neurology*. 2011;76(12):1085-1090.

26. Qin Y, Zhu W, Zhan C, et al. Investigation on positive correlation of increased brain iron deposition with cognitive impairment in Alzheimer disease by using quantitative MR R2' mapping. *J Huazhong Univ Sci Technolog Med Sci*. 2011;31(4):578-585.

27. Zhu WZ, Zhong WD, Wang W, et al. Quantitative MR phase-corrected imaging to investigate increased brain iron deposition of patients with Alzheimer disease. *Radiology*. 2009;253(2):497-504.

28. Warsi M, Molloy W, Noseworthy M. Correlating brain blood oxygenation level dependent (BOLD) fractal dimension mapping with magnetic resonance spectroscopy (MRS) in Alzheimer's disease. *Magnetic Resonance Materials in Physics, Biology and Medicine*. 2012:1-10.

29. Vitali P, Migliaccio R, Agosta F, et al. Neuroimaging in dementia. *Semin Neurol*. 2008;28(4):467-483.

30. Kantarci K, Petersen RC, Boeve BF, et al. 1H MR spectroscopy in common dementias. *Neurology*. 2004;63(8):1393-1398.

31. Herholz K. PET studies in dementia. *Ann Nucl Med*. 2003;17(2):79-89.

32. Wink AM, Bernard F, Salvador R, et al. Age and cholinergic effects on hemodynamics and functional coherence of human hippocampus. *Neurobiol Aging*. 2006;27(10):1395-1404.

33. Coburn KL, Lauterbach EC, Boutros NN, et al. The value of quantitative electroencephalography in clinical psychiatry: a report by the Committee on Research of the American Neuropsychiatric Association. *The Journal of neuropsychiatry and clinical neurosciences*. 2006;18(4):460-500.

34. Williams LM, Sidis A, Gordon E, et al. "Missing links" in borderline personality disorder: loss of neural synchrony relates to lack of emotion regulation and impulse control. *Journal of psychiatry & neuroscience : JPN*. 2006;31(3):181-188.

35. Khodayari-Rostamabad A, Reilly JP, Hasey G, et al., editors. Using pre-treatment EEG data to predict response to SSRI treatment for MDD. Annual International

Conference of the IEEE Engineering in Medicine and Biology Society IEEE Engineering in Medicine and Biology Society Conference; 2010; Buenos Aires. 6103-6106.

CHAPTER 8

SWI VS. RSN IN AD

The Influence of Brain Iron on Resting State Network Connectivity in Alzheimer's Disease.

Mohammed A. Warsi, E Mark Haacke, William Molloy, Michael D. Noseworthy

8.1 CONTEXT OF THE PAPER

Further exploration of the pathogenesis behind network connectivity led us to compare RSN to iron content using susceptibility weighted imaging (SWI). SWI is an *in vivo* MRI technique that can be used to quantify iron. Since iron has been implicated in neuronal degeneration (Pinero 2000), we hypothesized that iron deposition may correlate with degree of network disconnectivity. If a robust correlation was discovered, iron deposition could then be compared to brain FD in AD to investigate the role of iron in reduction of BOLD signal complexity. Since data for SWI had been acquired in 2009, our methods could not incorporate newer methods of iron quantification such as R2* or T2* relaxometry (Haacke 2010; Rodrigue 2012).

8.2 DECLARATION STATEMENT

Mohammed Ali Warsi as principle author wrote the article, performed analysis and created figures and tables as appropriate. Michael D. Noseworthy, as corresponding

author, hypothesized the use of FD in assessing Alzheimer's, wrote the first versions of the FD analysis program using Matlab (Mathworks, Natick, MA), provided guidance, funding and advice, and performed proofreading/editing and submission of the manuscript for publication. Dr. E. Mark Haacke provided methodological instruction, guidance and commentary. Dr. William Molloy provided clinical geriatric assessment, patient recruitment, guidance and commentary.

This paper has been submitted for publication to the journal *Magnetic Resonance Imaging.*

8.3 PAPER

The Influence of Brain Iron on Resting State Network Connectivity in Alzheimer's Disease

Mohammed A. Warsi[1,2,3], E Mark Haacke[1,4,5], William Molloy[6], Michael D. Noseworthy[1,2,3,7,8,9*]

[1]*School of Biomedical Engineering, McMaster University, Hamilton, Ontario, Canada.*

[2]*Department of Psychiatry and Behavioural Neuroscience, Hamilton, Ontario, Canada.*

[3]Imaging Research Centre, St. Joseph's Healthcare, Hamilton, Ontario, Canada.

[4]*Department of Radiology, Wayne State University, Detroit, Michigan, USA*

[5]*Department of Biomedical Engineering, Wayne State University, Detroit, Michigan, USA.*

[6]*Department of Gerontology and Rehabilitation, University College Cork, Ireland.*

[7]*Electrical & Computer Engineering, McMaster University, Hamilton, Ontario, Canada.*

[8]*Medical Physics & Applied Radiation Sciences, McMaster University, Hamilton, Ontario, Canada.*

[9]*Department of Radiology, McMaster University, Hamilton, Ontario, Canada.*

**Corresponding Author Address:*
Dr. Michael D. Noseworthy, Ph.D., P.Eng.
Director, Imaging Research Centre,
St. Joseph's Healthcare, 50 Charlton Ave. East
Hamilton, Ontario, Canada. L8N 4A6
Phone: +1 1(905) 522-1155 x35218
Email: nosewor@mcmaster.ca

ABSTRACT

The brain default mode network (DMN) is disrupted in Alzheimer's disease (AD). Iron deposition, implicated in AD pathogenesis, can be quantified with susceptibility weighted imaging (SWI). We hypothesized that iron deposition may correlate with degree of DMN disconnectivity. Resting state blood oxygen level dependent (BOLD) and SWI MRI scanning was performed on 38 mild/moderate AD and 16 age/gender matched normal controls (NC). DMN nodes included posterior cingulate cortex (PCC), medial prefrontal cortex (MPC), lateral parietal cortex (LPC) and hippocampal formation (HF) and were used to calculate normalized correlation (Z-values). The DMN connectivity was significantly lower in AD compared to NC. Iron was higher in AD, but only significantly in the PCC. There was a direct correlation between iron and DMN network disruption in the PCC and LPC (higher iron content was associated with more functional network disruption). We suggest this link between network disruption and tissue iron content suggests that iron may be responsible for some of the RSN changes seen in early stages of AD.

1. INTRODUCTION

Measurement of brain resting state activity has become a frequently used approach to understand brain functional connectivity in the absence of a defined task [1, 2]. Using resting state analysis of MRI blood oxygen level dependent (BOLD) signals has revealed spatially separated areas activating in synchrony, hypothesized to represent functionally connected brain regions. Some of the functional networks have been linked to structural networks based on anatomical [3] or diffusion tensor imaging (DTI) [4] studies, while other functional networks cannot be linked structurally [5]. Since their discovery in 1995 [1], there have been great efforts to characterize the functional networks in normal and diseased brains. Resting state networks (RSN) seem to be ubiquitous across subjects [6] and through time [7] with one of the most prevalent being the default mode network (DMN).

The DMN consistently appears to be one of the strongest functional networks in the brain. It connects posterior cingulate cortex (PCC) to medial prefrontal cortex (MPC), left and right lateral parietal cortex (l-LPC and r-LPC) and left and right hippocampal formation (l-HF and r-HF). Brain diseases such as Alzheimer's disease (AD) and multiple sclerosis (MS), have characteristic changes in DMN [6]. In AD, there is a decrease in connectivity between the nodes of the DMN, most significantly between the PCC and HF [8], which may relate to DMN involvement in episodic memory processing [9].

Mechanisms behind DMN connectivity disruptions are not clear, especially in what appear to be unrelated brain disorders. However, one common thread between AD

and MS is the increase in brain iron (Fe) content that is routinely observed [10]. AD patients exhibit increased iron in hippocampus, entorhinal cortex, globus pallidus, putamen and caudate [11]. In MS there is a significant increase in plaque [12] iron content. However, other brain regions in MS patients also show increased brain iron content [13]. Brain iron content, once only probed postmortem, is measureable using MRI susceptibility weighted imaging (SWI) [14]. Elevated brain iron levels are hypothesized to relate to free radical induced damage to brain cells and myelin, leading to loss of normal function [11]. Therefore, the objective of this study was to examine whether reduction in DMN functional connectivity relates to brain iron content in Alzheimer's dementia.

2. MATERIALS AND METHODS

In a study approved by our research ethics board, 38 subjects with mild to moderate AD (Mini Mental Status Exam, MMSE=22±3), and 16 age and gender matched normal controls (NC) were recruited. Diagnosis and severity of illness was also confirmed by clinical exam, Standardized Alzheimer's Disease Assessment Scale (SADAS) and Clinical Dementia Rating Scale (CDR). Subjects were recruited from a local geriatric clinic after obtaining informed consent. To minimize environment effects aged matched controls were spouses of AD subjects who did not have AD based on clinical exam by a geriatrician and a screening cognitive exam (**Table 1**).

Table 1. Subject details.

	AD	NC	P Value
N	38	16	-
Females	18	10	0.32
Age (y)	76.8±7.6	74.1±5.7	0.16
MMSE[1]	22.1±3.2	28.6±1.2	<0.001
Illness onset (y)	3.5±2.2	-	-
Education (y)	13.0±3.4	-	-
SADAS[2]	18.0±6.8	-	-
CDR[3]	0.96±0.53	-	-

[1] Mini Mental Status Exam
[2] Standardized Alzheimer's Disease Assessment Scale – Cognitive Subscale
[3] Clinical Dementia Rating – Global Score

2.1 MRI acquisition

Standard T1 and T2-weighted images, acquired using a GE 3T Signa HD MRI and 8 channel phased array RF coil (General Electric Healthcare, Milwaukee WI) were used to prescribe BOLD and SWI image acquisitions. Resting state BOLD data was acquired using echo planar imaging (EPI) with TE=35ms, TR=2000ms, α =90°, FOV=24cm, 64x64 matrix, 24 slices, 5mm thick, 0mm gap, 300 time points). Susceptibility weighted imaging (SWI) was done using TE=20ms, TR=30ms, α =15°, receiver bandwidth=40kHz, 512x256 matrix, ASSET factor=2, 64 slices, 2mm thick (no gap), NEX=1, no Fermi filter and no grad warp compensation.

2.2 Image Analysis

Whole brain resting state analysis was done using the method described by Van Dijk *et al.* [15]. Motion correction was performed using an iterated linearized weighted least squares algorithm in AFNI [16]. Data was converted to standardized space (Talairach) and resampled to 2mm isotropic voxels. A Gaussian kernel with full-with-half-max (FWHM) of 6mm was used for spatial smoothing. Temporal filtering (>0.08 Hz and <0.001 Hz removed) eliminated high frequency noise and low frequency drift and the time series from the 6 nodes of the DMN were extracted. These nodes were defined in standard space as described by Van Dijk *et al.* All processing steps were done using AFNI [16]. The extracted time series from the PCC was correlated with other nodes of the DMN using Pearson's correlation. These correlations were normalized to produce standard scores (Z values) for each node (**eqn. 1**) using Fisher's *r*-to-*z* transformation [15, 17]:

$$Z = 0.5 \cdot \ln\left[\frac{1+r}{1-r}\right] \qquad \textbf{(eqn.1)}$$

where ***r*** is the Pearson's correlation. Overall DMN functional connectivity was also represented by mean Z values from all nodes in for given subject. Mean Z scores were subsequently correlated with brain iron measures performed using SWI.

SWI images were calculated according to Haacke *et al.* (2009), with one difference. In previous work by Haacke *et al.* (2009) a Siemens scanner was used for iron quantification, with phase values which scale from 0 to 4096, where 0 is -π and 4096 is

+π (2048 is zero phase). In their case they calculated that 3 Siemens units (Φ) corresponds to 1 μg of Fe/g tissue where:

$$\Phi = 2048\left[\left(\varphi/\pi\right)+1\right] \qquad \textbf{(eqn. 2)}$$

with φ being iron concentration. We used a GE MRI system where phase units scale between -3142 and +3142 (i.e. -π and +π, respectfully), with 0 representing zero phase. Therefore for the GE system 4.6 phase units corresponds to 1 μg of Fe/g tissue, where the following phase conversion was applied:

$$\Phi = 3142\left(\frac{\varphi}{\pi}\right) \qquad \textbf{(eqn. 3)}$$

Phase reduction of GM relative to CSF or WM is indicative of the GM iron content [18] and these values were compared to RSN values.

Since SWI iron quantification requires at least 100 voxels [18], a sphere of about 150 voxels was placed at the precise DMN coordinates (posterior cingulate cortex, medial prefrontal cortex, lateral parietal cortex, hippocampal formation) (**fig.1**). These spheres were about 2.5mm in diameter and are well within a homogeneous region of these tissues. Two extra sphere ROIs were placed, one in the CSF (in the central sulcus to avoiding flow artifact of the ventricles) and the other in the WM (corpus callosum). These ROIs were also confirmed visually to confirm RSN coordinates [15] corresponded to

appropriate brain regions in our population (**fig.1**). ROIs for the MPC were close to the skull base where one would expect a large phase distortion artifact (due to the proximity of the frontal sinuses). ROIs were visually inspected for presence of microbleeds, defined as homogeneous signal loss <10mm without vessel continuity which would distort the iron quantification [19].

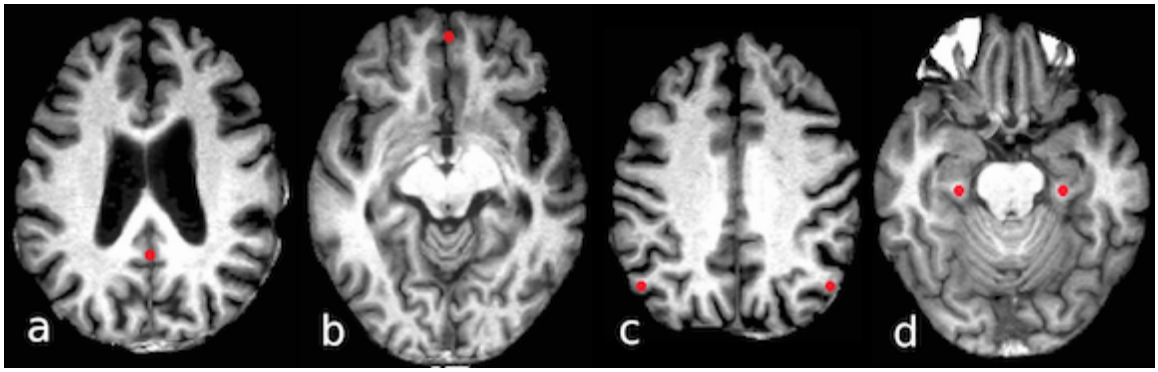

Figure 1. Spherical ROIs placed at the RSN coordinates as defined by Van Dijk *et al.* [15]. These include posterior cingulate cortex (PCC) (a), medial prefrontal cortex (MPC) (b), lateral parietal cortex (LPC) (c) and hippocampal formation (HF) (d).

2.3 Statistical Analysis

Statistical analysis was done using the statistics toolbox of Matlab (v.7.9.0.529 Mathworks, Natick MA) and SPSS (version 17, SPSS Inc., Chicago, IL, USA). Two-tailed unpaired Student's t-test, with unequal sampling, was used for comparing SWI values and RSN Z values between subject groups. Pearson's correlation coefficient was used for comparing SWI with RSN Z values, with the significance threshold set at

P<0.05. A Jarque–Bera test, which takes into consideration both skewness and kurtosis, was used to confirm normality of SWI and RSN ROI data. Motion in AD compared to NC was evaluated by comparing variance of translation and rotation using a general linear model multivariate analysis, as done previously [20]. All acquisition and analysis was done blinded to subject status (AD vs. NC).

3. RESULTS

3.1 Resting State Network (RSN)

The range of Z value correlations for the DMN in AD (mean±std: 0.37±0.20) was in keeping with previously published data [15, 21]. DMN Z values were significantly higher in NC (mean±std: 0.65±0.32) compared to DMN in AD (p=0.004) (**fig. 2**). Bilateral nodes correlated with each other (HF-left vs HF-right: r=0.53, p<0.001, LPC-left vs LPC-right: r=0.50, p=0.002) (**fig. 3**). Z values in the HF, MPC and LPC did not correlate with each other (p>0.05).

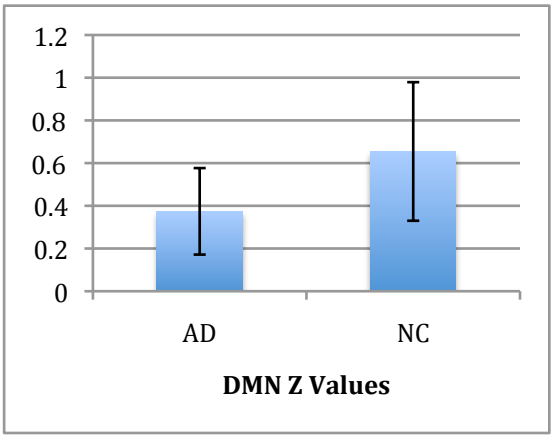

Figure 2. Mean DMN Z values in AD and NC. AD was significantly lower than NC (p=0.004).

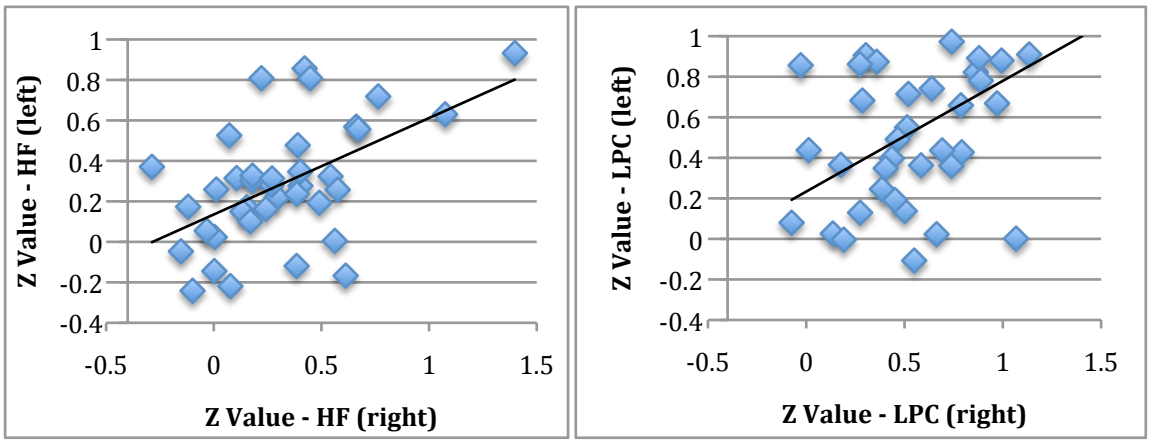

Figure 3. RSN values for bilateral nodes (HF and LPC) have left vs. right correlations (r=0.53; p<0.001 and r=0.50; p=0.002 respectively).

3.2 Susceptibility Weighted Imaging (SWI)

Mean SWI values for iron in the 6 ROIs (4 brain regions) were 10.3 ± 43.1 for AD and 3.5 ± 36.5 for NC (**fig. 4**). Iron in the MPC was significantly different from other

brain regions although, due to artifacts in this region, with a very large SD compared to the mean (**Table 2**). Iron values were significantly higher in AD subjects compared to NC in the PCC ($p<0.05$), but no difference was found between these groups in the either HF, MPC or LPC.

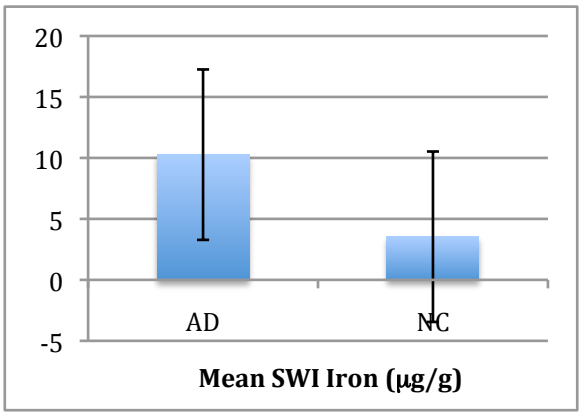

Figure 4. AD has higher mean iron content than NC, but this difference was not significant. There was a large range (SEM shown) likely due to susceptibility artifacts in the MPC.

Table 2. Mean iron content (μg/g ± SD) in individual brain ROIs which include posterior cingulate cortex (PCC), medial prefrontal cortex (MPC), lateral parietal cortex (LPC) and hippocampal formation (HF).

Brain Region	AD	NC	P value
PCC	55.8±32.7	-0.3±18.7	0.013*
MPC[+]	20.4±72.1	-160.9±46.9	0.963
LPC	23.3±12.4	13.9±14.1	0.281
HF	15.4±25.0	-9.3±36.6	0.249

[+]Iron quantity meaningless in MPC due to phase distortion artefacts
* P<0.05

3.3 RSN vs SWI

Connectivity between the PCC and LPC correlated with brain iron values in both the PCC (r=-0.43; p=0.006) and LPC (r=-0.33; p=0.040) (**fig. 5**). This correlation was not seen on other specific nodes of the DMN (e.g. SWI-HF versus RSN-HF) nor did the mean DMN connectivity correlate with iron values in any specific nodes (e.g. SWI-HF versus RSN-mean DMN).

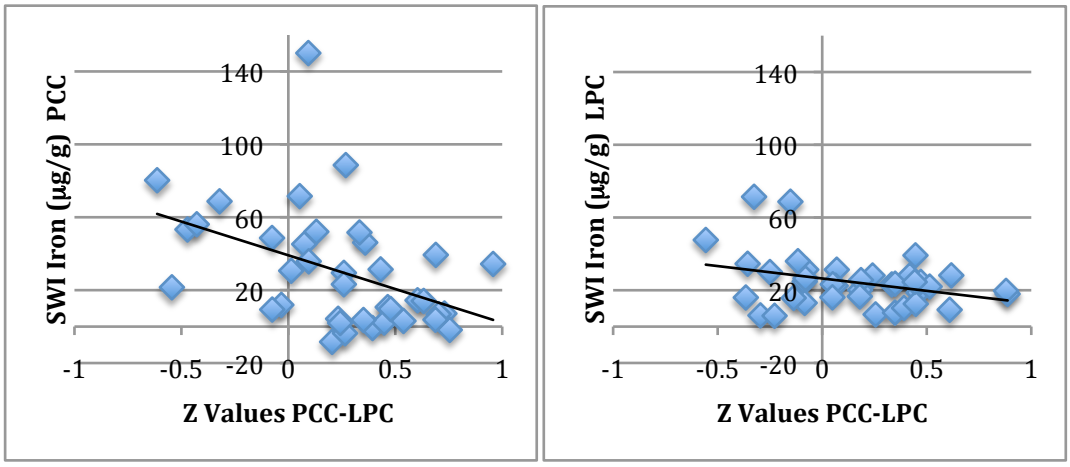

Figure 5. Correlations between iron content and RSN values in the PCC (r=-0.43; p=0.006) and LPC (r=-0.33; p=0.040).

4. DISCUSSION

To our knowledge, this is the first study comparing functional connectivity as measured by RSN analysis, to brain regional iron content. Iron can be found throughout the brain in various forms. We found that AD has higher iron content in the nodes of the DMN as compared to NC, implicating iron in the pathogenesis of network dis-connectivity.

Haemoglobin in red blood cells in a rich source of iron, while non-haeme iron has a role in the electron transport chain of metabolism [11]. Non-haeme iron is transported and stored as transferrin and ferritin respectively. Haemosidrin is the water insoluble form of iron storage, usually formed from ferritin breakdown. All forms of biologically relevant iron can be found in the brain, with deep grey matter structures having the

highest concentration [11]. Iron is an important part of brain biochemistry, functioning in oxidative metabolism (an obligate form of neurometabolism) and synthesis of myelin and neurotransmitters. However iron also plays a key roll in some brain pathologies, especially neurodegenerative diseases, due most likely to its induction of reactive oxygen species through Fenton based chemical reactions [22]. MRI techniques such as SWI allow us to measure iron in the brain *in vivo*. SWI measurements of brain iron have been useful in assessing Parkinson's disease (PD), multiple sclerosis (MS), Alzheimer's disease (AD), and traumatic brain injury (TBI) [10]. SWI amplifies the magnetic field distortions of iron (decrease in T2*), and by doing so, increases the contrast of iron rich areas of the brain. This can he used to highlight vasculature or pathological iron deposits [19]. Vasculature is rich in haeme iron while tissue SWI contrast comes mainly from ferritin and hemosiderin. In addition to quantifying absolute tissue concentrations of iron [23], SWI is useful in comparing intra and inter subject iron concentrations [19].

Our results suggest a link between iron and network disruption. The RSN connectivity and iron values were consistent with values previously obtained in the literature [11, 15, 21], although iron values for MPC were not interpretable, due to elevated phase aliasing, due to susceptibility artifact, which is problematic for this region. The same susceptibility artifact may have also influenced iron values for the HF, but is unlikely to have influenced deeper brain structures such as LPC and PCC. SWI measurements of non-cortical GM structures such as the putamen are even more reliable [18]. Such structures, however, were not relevant to our hypothesis that iron quantity in

the RSN nodes influences functional connectivity because those structures are not involved in DMN connectivity.

There was significant difference in PCC iron between AD and NC, consistent with previously SWI studies demonstrating higher GM iron content in AD [11]. This difference was not demonstrated in the other nodes where we would expect differences in iron, such as the HF, possible due to susceptibility artifacts discussed above.

We were able to demonstrate a correlation between brain iron content in both the PCC and LPC with the functional connectivity between these two nodes. This raises the possibility that functional connectivity may be impaired by iron deposition seen in AD. This study however does not prove any causation but highlights a proportional correlation. It is also possible that phase distortion measured by SWI caused signals in the DMN to desynchronize. Iron content did not correlate with functional connectivity of other nodes. This may be the result of inaccuracy of SWI measurement in the other nodes. Perhaps using other techniques for measuring iron that are less sensitive to phase distortion could tease out more profound differences between AD and NC, leading to further relationship between regional iron content and RSN connectivity. Newer variants of SWI analysis such as susceptibility mapping or T2* relaxation [24] have the potential to improve iron quantification. Future work should be performed to examine correlation of regional brain iron content with other functional networks including deep GM structures such as the basal ganglia resting state network [25].

In summary, examining the correlation of RSN and regional brain iron in mild cognitive impairment could provide valuable information before more severe AD

develops. A prospective study of brain iron and RSN in MCI or early AD may also help shed light on any causation of iron deposition and functional connectivity disruption.

REFERENCES

1. Biswal B, Yetkin FZ, Haughton VM, Hyde JS. 1995. Functional connectivity in the motor cortex of resting human brain using echo-planar MRI. Magn. Reson. Med. 34(4):537-541.

2. Auer DP. 2008. Spontaneous low-frequency blood oxygenation level-dependent fluctuations and functional connectivity analysis of the 'resting' brain. Magn. Reson. Imaging 26(7):1055-1064.

3. van den Heuvel M, Mandl R, Luigjes J, Hulshoff Pol H. 2008. Microstructural organization of the cingulum tract and the level of default mode functional connectivity. J. Neurosci. 28(43):10844-10851.

4. De Luca M, Beckmann CF, De Stefano N, Matthews PM, Smith SM. 2006. fMRI resting state networks define distinct modes of long-distance interactions in the human brain. Neuroimage 29(4):1359-1367.

5. Greicius MD, Supekar K, Menon V, Dougherty RF. 2008. Resting-State Functional Connectivity Reflects Structural Connectivity in the Default Mode Network. Cereb. Cortex 19(1):72-78.

6. Rosazza C, Minati L. 2011. Resting-state brain networks: literature review and clinical applications. Neurol. Sci. 32(5):773-785.

7. Chou Y-H, Panych LP, Dickey CC, Petrella JR, Chen N-K. 2012. Investigation of Long-Term Reproducibility of Intrinsic Connectivity Network Mapping: A Resting-State fMRI Study. AJNR. Am. J. Neuroradiol. 33:833-838.

8. Sorg C, Riedl V, Mühlau M, Calhoun VD, Eichele T, Läer L, Drzezga A, Förstl H, Kurz A, Zimmer C et al. . 2007. Selective changes of resting-state networks in individuals at risk for Alzheimer's disease. Proc. Natl. Acad. Sci. U. S. A. 104(47):18760-18765.

9. Vincent JL, Snyder AZ, Fox MD, Shannon BJ, Andrews JR, Raichle ME, Buckner RL. 2006. Coherent spontaneous activity identifies a hippocampal-parietal memory network. J. Neurophysiol. 96(6):3517-3531.

10. Thomas B, Somasundaram S, Thamburaj K, Kesavadas C, Gupta AK, Bodhey NK, Kapilamoorthy TR. 2008. Clinical applications of susceptibility weighted MR imaging of the brain - a pictorial review. Neuroradiology 50(2):105-116.

11. Haacke EM, Cheng NYC, House MJ, Liu Q, Neelavalli J, Ogg RJ, Khan A, Ayaz M, Kirsch W, Obenaus A. 2005. Imaging iron stores in the brain using magnetic resonance imaging. Magn. Reson. Imaging 23(1):1-25.

12. Haacke EM, Makki M, Ge Y, Maheshwari M, Sehgal V, Hu J, Selvan M, Wu Z, Latif Z, Xuan Y et al. . 2009. Characterizing iron deposition in multiple sclerosis lesions using susceptibility weighted imaging. J. Magn. Reson. Imaging 29(3):537-544.

13. Haacke EM, Garbern J, Miao Y, Habib C, Liu M. 2010. Iron stores and cerebral veins in MS studied by susceptibility weighted imaging. Int. Angiol. 29(2):149-157.

14. Haacke EM, Mittal S, Wu Z, Neelavalli J, Cheng Y-CN. 2009. Susceptibility-weighted imaging: technical aspects and clinical applications, part 1. AJNR. Am. J. Neuroradiol. 30(1):19-30.

15. Van Dijk KRA, Hedden T, Venkataraman A, Evans KC, Lazar SW, Buckner RL. 2010. Intrinsic functional connectivity as a tool for human connectomics: theory, properties, and optimization. J. Neurophysiol. 103(1):297-321.

16. Cox RW. 1996. AFNI: software for analysis and visualization of functional magnetic resonance neuroimages. Comput. Biomed. Res. 29(3):162-173.

17. Zar JH. 1999. Biostatistical analysis. Upper Saddle River, N.J.: Prentice Hall.

18. Haacke EM, Ayaz M, Khan A, Manova ES, Krishnamurthy B, Gollapalli L, Ciulla C, Kim I, Petersen F, Kirsch W. 2007. Establishing a baseline phase behavior in magnetic resonance imaging to determine normal vs. abnormal iron content in the brain. J. Magn. Reson. Imaging 26(2):256-264.

19. Kirsch W, McAuley G, Holshouser B, Petersen F, Ayaz M, Vinters HV, Dickson C, Haacke EM, Britt W, Larseng J et al. . 2009. Serial susceptibility weighted MRI measures brain iron and microbleeds in dementia. J Alzheimers Dis 17(3):599-609.

20. Warsi M, Molloy W, Noseworthy M. 2012. Correlating brain blood oxygenation level dependent (BOLD) fractal dimension mapping with magnetic resonance spectroscopy (MRS) in Alzheimer's disease. Magnetic Resonance Materials in Physics, Biology and Medicine:1-10.

21. Fleisher AS, Sherzai A, Taylor C, Langbaum JBS, Chen K, Buxton RB. 2009. Resting-state BOLD networks versus task-associated functional MRI for distinguishing Alzheimer's disease risk groups. Neuroimage 47(4):1678-1690.

22. Pinero DJ, Connor JR. 2000. Iron in the Brain: An Important Contributor in Normal and Diseased States. The Neuroscientist 6(6):435-453.

23. Ogg RJ, Langston JW, Haacke EM, Steen RG, Taylor JS. 1999. The correlation between phase shifts in gradient-echo MR images and regional brain iron concentration. Magn. Reson. Imaging 17(8):1141-1148.

24. Rodrigue KM, Daugherty AM, Haacke EM, Raz N. 2012. The Role of Hippocampal Iron Concentration and Hippocampal Volume in Age-Related Differences in Memory. Cereb. Cortex.

25. Robinson S, Basso G, Soldati N, Sailer U, Jovicich J, Bruzzone L, Kryspin-Exner I, Bauer H, Moser E. 2009. A resting state network in the motor control circuit of the basal ganglia. BMC Neurosci 10:137.

CHAPTER 9

CONCLUSIONS AND FUTURE DIRECTIONS

9.1 CONCLUDING REMARKS

Alzheimer's disease is a prevalent debilitating illness that brings significant distress to patients and their loved ones. With an aging population, we expect to see a rise in the incidence of AD, with which come great social and economic burden. Early detection and treatment of AD results in better cognitive and functional outcomes (Small 2007). Currently, AD is diagnosed at later stages of illness, while the search for early biomarkers rages on (Kelley 2009).

Fractal dimension (FD) analysis of fMRI BOLD signals offers an *in vivo* method to peer into the brains of AD. FD assessment quantifies the complexity of 100s of billions of interconnected neurons using elements of chaos theory. Our goal was to use FD in the measurement of AD severity. We hoped that changes in BOLD signal complexity might detect neuronal degeneration with equal or greater sensitivity of established biomarkers. We therefore studied FD and AD biomarkers (MRS and volumetry) in mild to moderate dementia. Additionally, we wanted to know more about what FD was measuring. FD is sensitive to neuronal networks, but also to microvasculature. To characterize the neuronal network contribution to FD change, we used resting state network (RSN) analysis of the default mode network (DMN), an already established technique quantifying functional connectivity. We also hypothesized that some of the network disruptions may be the result of increased brain iron deposition, which is often a hallmark feature in AD.

9.2 MAIN FINDINGS AND CONCLUSIONS

The seemingly random "noise" pattern of resting state BOLD signals actually follows a complex characterizable pattern: a fractal. The fractal nature of resting state fMRI is independent of type of MRI acquisition (spiral vs. EPI), scanning frequency (TR) or length of scan. Although the fractal nature does not change, the value of FD is sensitive to some of these parameters (such as TR and scan length) and this need to be kept constant between scans. Once parameters have been established, the FD value is consistent within subjects both in the short term (minutes) and the long term (months).

Reduced FD (i.e. decreased signal complexity) correlated with both increased N-acetyl aspartate (NAA) and decreased myoinositol (mI), as measured by MRS in our population of early AD. Both NAA and mI change with disease severity in AD. It therefore could follow that FD also tracks disease severity in early stages of AD. This was further reinforced with the correlation of FD with RSN connectivity, another index of AD progression. In the AD subjects, there was not a significant range of deep structure volume changes or MMSE scores. In fact, volumes of the putamen did not significantly differ between AD and NC at this stage of illness (while volumes of the hippocampus and cortical grey matter did significantly differ). Nor was there a significant difference between NAA or mI between AD and NC. There was, however a significant difference between FD values. This led us to believe that FD changes in AD correlate with disease

severity (or amount of neuronal disruption and degeneration) and the range of FD change is sufficient to separate AD for NC, at a stage too early for MRS or volumetry to detect.

The two populations (AD and NC) also differed in their detectable iron in the posterior cingulate cortex (PCC). The difference in iron correlated with functional connectivity disruption. It is therefore possible that iron deposition, through Fenton-based chemistry and ensuing lipid peroxidation, is responsible for neuronal damage resulting in network disruption. Conversely, iron may be a marker of neuronal death rather than a cause. A third possibility is that the phase distortion measured by SWI causes de-correlation of previously synchronous signal.

9.3 CONTRIBUTIONS OF THIS WORK

To our knowledge, these are the first studies to compare FD in the brain with MRS and RSN in AD. Using FD to study signal complexity provides novel information about AD signalling, not available using other imaging techniques. We found that brain signal complexity was related to MRS markers of illness severity and to reduced functional connectivity. Although this makes intuitive sense, this has not previously ever been described. Indeed, FD may be more sensitive than some of the established markers to differentiate AD from NC, suggesting changes in AD changes occur before MRS or volumetric changes in need brain structures. Changes in iron deposition also seem to occur early with involvement in (and possibly causation of) network disruption. We now have two new tools (FD and SWI) with which to further explore the pathogenesis of AD

in early stages of illness. It may be the level of detail and complexity provided by FD analysis that is needed to characterize dementia early enough to significantly alter its course.

Despite the long history of FD as a mathematical technique applied to physiological signal, there has been a paucity of FD fMRI studies in clinical populations. We validated and refined the FD technique to be effectively used in clinical studies. We found that FD is consistent in the brain over a period of months (i.e. is a trait rather than a trait feature) and can be applied to different areas of the brain without the constraints and biases of RSN or task-based fMRI studies. We believe this new tool will open up new possibilities of studying illnesses of the brain (or those of the mind) with a measure not previously applied. In fact, this refined method is already planned for application towards other studies starting in Dr. Noseworthy's lab. These include the study of traumatic brain injury, obsessive compulsive disorder (OCD) and alcoholism.

9.4 POSSIBLE APPLICATIONS

The studies herein have shown FD as a sensitive trait measure of pathology in AD in its early stages. This opens the possibility to study other mental illnesses where there are subtle network changes not detectable by volumetry, spectroscopy or other non-invasive imaging techniques. For example, signal changes in depression have led to the recent application of various brain stimulation techniques for treatment such as deep brain stimulation (DBS) (Kennedy 2011) and transcranial magnetic stimulation (TMS) (Hasey

1999). Stimulation targets remain imprecise (Schlaepfer 2010) and a model free characterization of signal complexity could help guide targets. Likewise, schizophrenia is known to be an illness of the brain with only basic network characterization (Lynall 2010). Application of FD analysis could significantly further our understanding of this complex disease.

9.5 FUTURE STUDIES

In creating answers, studies of novel techniques often generate many new questions. Below are studies that address key issues. FD could be measured in an AD population with a wider range of disease states (mild to severe illness). This would allow us to see if there is a progressive decrease in FD and could allow for better comparison of FD to volumetric and cognitive changes. With significant scan-to-scan reproducibility of FD, a prospective study could be designed to follow FD changes through the course of the illness.

In the future, we would also like to further characterize FD with its comparison to SWI and diffusion tensor imaging (DTI). The comparison of FD to SWI is the next logical step after establishing a connection between SWI iron estimation and RSN. DTI analysis would allow us to see if structural network integrity changes affect signal complexity. This would further the hypothesis that FD changes relate to a disruption of network interconnectivity.

As described earlier, EEG is another technique amenable to FD analysis due to the high temporal resolution. Concurrent measurement of FD from BOLD fMRI and EEG would provide invaluable information about the distribution of brain signal complexity differences. We would be able to combine the spatial resolution of MRI with the temporal resolution of EEG, allowing for spatially precise FD measurements down to lower scales of FD measurement.

Finally, with the availability of PET-MRI systems, a comparison of BOLD fMRI FD to PET would be invaluable. This could include [^{18}F]FDG-PET or PET using [^{11}C]-labelled Pittsburgh compound B (PIB), a radiotracer that binds to amyloid in the brain. Both of these methods have bindings that mirror the RSN network activity in the brain (Perrin 2009). Measuring FD at PIB binding regions would reveal how network complexity changes at specific sites of plaque formation. Hypometabolism occurs very early in the illness, sometimes before any other sign or symptom is detectable (Costantini 2008). If FD changes can reliably be detected at sites of [^{18}F]FDG hypometabolism, FD fMRI could be the non-radiotracer successor of PET.

9.6 CONCLUDING STATEMENT

Studies of Alzheimer's disease continue to search for the "holy grail" of prevention or cure. Both these goals remain elusive. Each incremental step towards the understanding and identification of AD brings us all a little closer. We hope that providing a novel look at function in the AD brain is one of those steps in the right

direction. By targeting one of the brain's most basic functions, signalling, we hope to have opened the door into research of subtle brain functional changes responsible for the early pathology of AD. We hope this tool can also be used to explore the same in a variety of mental illnesses and bring us that much closer to cures.

BIBLIOGRAPHY

Ances, B. M., O. Leontiev, et al. (2008). "Regional differences in the coupling of cerebral blood flow and oxygen metabolism changes in response to activation: implications for BOLD-fMRI." Neuroimage **39**(4): 1510-1521.

Attwell, D. and S. B. Laughlin (2001). "An energy budget for signaling in the grey matter of the brain." Journal of Cerebral Blood Flow and Metabolism **21**(10): 1133-1145.

Ayaz, M., A. S. Boikov, et al. (2010). "Imaging cerebral microbleeds using susceptibility weighted imaging: one step toward detecting vascular dementia." J Magn Reson Imaging **31**(1): 142-148.

Bär, K.-J., M. K. Boettger, et al. (2007). "Non-linear complexity measures of heart rate variability in acute schizophrenia." Clin Neurophysiol **118**(9): 2009-2015.

Bartzokis, G. and T. A. Tishler (2000). "MRI evaluation of basal ganglia ferritin iron and neurotoxicity in Alzheimer's and Huntingon's disease." Cell Mol Biol (Noisy-le-grand) **46**(4): 821-833.

Bassingthwaighte, J. B. (1988). "Physiological Heterogeneity: Fractals Link Determinism and Randomness in Structures and Functions." News Physiol Sci **3**(1): 5-10.

Bassingthwaighte, J. B., R. B. King, et al. (1989). "Fractal nature of regional myocardial blood flow heterogeneity." Circulation Research **65**(3): 578-590.

Bassingthwaighte, J. B., L. S. Liebovitch, et al. (1994). Fractal Measures of Heterogeneity and Correlation. Fractal physiology. New York, Oxford University Press**:** 63-107.

Bassingthwaighte, J. B., L. S. Liebowitch, et al. (1994). Fractal Physiology, Oxford University Press.

Biswal, B., F. Z. Yetkin, et al. (1995). "Functional connectivity in the motor cortex of resting human brain using echo-planar MRI." Magnetic Resonance in Medicine **34**(4): 537-541.

Bradley, K. M., G. M. Bydder, et al. (2002). "Serial brain MRI at 3-6 month intervals as a surrogate marker for Alzheimer's disease." Br J Radiol **75**(894): 506-513.

Brewer, J. B., S. Magda, et al. (2009). "Fully-Automated Quantification of Regional Brain Volumes for Improved Detection of Focal Atrophy in Alzheimer Disease." AJNR. American Journal of Neuroradiology **30**(3): 578-580.

Broyd, S. J., C. Demanuele, et al. (2009). "Default-mode brain dysfunction in mental disorders: a systematic review." Neurosci Biobehav Rev **33**(3): 279-296.

Bullmore, E., M. Brammer, et al. (1996). "Statistical methods of estimation and inference for functional MR image analysis." Magnetic Resonance in Medicine **35**(2): 261-277.

Bullmore, E., C. Long, et al. (2001). "Colored noise and computational inference in neurophysiological (fMRI) time series analysis: resampling methods in time and wavelet domains." Human Brain Mapping **12**(2): 61-78.

Bullmore, E. and O. Sporns (2009). "Complex brain networks: graph theoretical analysis of structural and functional systems." Nat Rev Neurosci **10**(3): 186-198.

Bullmore, E. T., M. J. Brammer, et al. (1994). "Fractal analysis of electroencephalographic signals intracerebrally recorded during 35 epileptic seizures: evaluation of a new method for synoptic visualisation of ictal events." Electroencephalography and Clinical Neurophysiology **91**(5): 337-345.

Calhoun, V. D., T. Adali, et al. (2001). "A method for making group inferences from functional MRI data using independent component analysis." Human brain mapping **14**(3): 140-151.

Churilla, A. M., W. A. Gottschalke, et al. (1996). "Membrane potential fluctuations of human T-lymphocytes have fractal characteristics of fractional Brownian motion." Annals of Biomedical Engineering **24**(1): 99-108.

Clark, D. D. and L. Sokoloff (1999). Basic Neurochemistry: Molecular, Cellular, and Medical Aspects. Philadelphia, Lippincott.

Cole, D. M., S. M. Smith, et al. (2010). "Advances and pitfalls in the analysis and interpretation of resting-state FMRI data." Frontiers in systems neuroscience **4**: 8.

Costantini, L. C., L. J. Barr, et al. (2008). "Hypometabolism as a therapeutic target in Alzheimer's disease." BMC Neurosci **9 Suppl 2**: S16.

Craciunescu, O. I., S. K. Das, et al. (1999). "Dynamic contrast-enhanced MRI and fractal characteristics of percolation clusters in two-dimensional tumor blood perfusion." Journal of Biomechanical Engineering **121**(5): 480-486.

D'Addio, G., G. Corbi, et al. (2009). "Fractal behaviour of heart rate variability reflects severity in stroke patients." Studies in Health Technology and Informatics **150**: 794-798.

de Graaf, R. A. (2007). Magnetic Resonance Imaging. In Vivo NMR Spectroscopy, John Wiley & Sons, Ltd**:** 191-231.

de Jong, L. W., K. van der Hiele, et al. (2008). "Strongly reduced volumes of putamen and thalamus in Alzheimer's disease: an MRI study." Brain **131**(Pt 12): 3277-3285.

de Leon, M. J., A. E. George, et al. (1989). "Early marker for Alzheimer's disease: the atrophic hippocampus." Lancet **2**(8664): 672-673.

De Weerd, A. W. and P. Clarenbach (1999). "Recording sleep and wake. The International Federation of Clinical Neurophysiology." Electroencephalography and Clinical Neurophysiology. Supplement **52**: 159-170.

Dubois, B., H. H. Feldman, et al. (2007). "Research criteria for the diagnosis of Alzheimer's disease: revising the NINCDS-ADRDA criteria." Lancet Neurol **6**(8): 734-746.

Eke, A., P. Hermán, et al. (2000). "Physiological time series: distinguishing fractal noises from motions." Pflügers Archiv : European journal of physiology **439**(4): 403-415.

Eke, A., P. Herman, et al. (2002). "Fractal characterization of complexity in temporal physiological signals." Physiol Meas **23**(1): R1-38.

Elzibak, A. H., A. D. Davis, et al. (2011). Fractal-like signals from non-physiological sources. Proceedings of the 28th Annual Scientific Meeting, European Society of Magnetic Resonance in Medicine and Biology (ESMRMB) Leipzig, Germany.

Ernst, T. and J. Hennig (1994). "Observation of a fast response in functional MR." Magnetic Resonance in Medicine **32**(1): 146-149.

Fadili, M. J. and E. T. Bullmore (2002). "Wavelet-generalized least squares: a new BLU estimator of linear regression models with 1/f errors." NeuroImage **15**(1): 217--232.

Fleisher, A. S., A. Sherzai, et al. (2009). "Resting-state BOLD networks versus task-associated functional MRI for distinguishing Alzheimer's disease risk groups." Neuroimage **47**(4): 1678-1690.

Frahm, J., G. Kruger, et al. (1996). "Dynamic uncoupling and recoupling of perfusion and oxidative metabolism during focal brain activation in man." Magnetic Resonance in Medicine **35**(2): 143-148.

Glover, G. H. (2011). "Overview of functional magnetic resonance imaging." Neurosurgery clinics of North America **22**(2): 133-139, vii.

Glover, G. H. (2012). "Spiral imaging in fMRI." Neuroimage **62**(2): 706-712.

Gómez, C., A. Mediavilla, et al. (2009). "Use of the Higuchi's fractal dimension for the analysis of MEG recordings from Alzheimer's disease patients." Med Eng Phys **31**(3): 306-313.

Greicius, M. D., G. Srivastava, et al. (2004). "Default-mode network activity distinguishes Alzheimer's disease from healthy aging: evidence from functional MRI." Proc Natl Acad Sci USA **101**(13): 4637-4642.

Haacke, E. M. (2010). "SPIN (signal processing in NMR) Software." 2012, from http://www.mrimaging.com/category.88.html.

Haacke, E. M., Y. Miao, et al. (2010). "Correlation of putative iron content as represented by changes in R2* and phase with age in deep gray matter of healthy adults." Journal of magnetic resonance imaging : JMRI **32**(3): 561-576.

Hampel, H., K. Bürger, et al. (2008). "Core candidate neurochemical and imaging biomarkers of Alzheimer's disease." Alzheimer's & dementia : the journal of the Alzheimer's Association **4**(1): 38-48.

Han, S. D., K. J. Bangen, et al. (2009). "Functional magnetic resonance imaging of compensatory neural recruitment in aging and risk for Alzheimer's disease: review and recommendations." Dement Geriatr Cogn Disord **27**(1): 1-10.

Hasey, G. M. (1999). "Transcranial magnetic stimulation: using a law of physics to treat psychopathology." Journal of Psychiatry and Neuroscience **24**(2): 97-101.

He, Y., L. Wang, et al. (2007). "Regional coherence changes in the early stages of Alzheimer's disease: a combined structural and resting-state functional MRI study." Neuroimage **35**(2): 488-500.

Herman, P., L. Kocsis, et al. (2009). "Fractal characterization of complexity in dynamic signals: application to cerebral hemodynamics." Methods Mol Biol **489**: 23-40.

Hillman, E. M. (2007). "Optical brain imaging in vivo: techniques and applications from animal to man." J Biomed Opt **12**(5): 051402.
Hoop, B., H. Kazemi, et al. (1993). "Rescaled range analysis of resting respiration." Chaos **3**(1): 27-29.
Hsu, Y.-Y., N. Schuff, et al. (2002). "Comparison of automated and manual MRI volumetry of hippocampus in normal aging and dementia." J Magn Reson Imaging **16**(3): 305-310.
Hu, J., S. Yang, et al. (2007). "Simultaneous detection of resolved glutamate, glutamine, and gamma-aminobutyric acid at 4 T." J Magn Reson **185**(2): 204-213.
Hurst, H. E. (1951). "Long-Term Storage Capacity of Reservoirs." Transactions of the American Society of Civil Engineers **116**: 770-799.
Jakovcevic, D. and D. R. Harder (2007). "Role of astrocytes in matching blood flow to neuronal activity." Current Topics in Developmental Biology **79**: 75-97.
Jobsis, F. F. (1977). "Noninvasive, infrared monitoring of cerebral and myocardial oxygen sufficiency and circulatory parameters." Science **198**(4323): 1264-1267.
Kandel, E. R., J. H. Schwartz, et al. (2000). Principles of neural science. New York, McGraw-Hill, Health Professions Division.
Kannathal, N., S. K. Puthusserypady, et al. (2004). "Complex dynamics of epileptic EEG." Conf Proc IEEE Eng Med Biol Soc **1**: 604-607.
Kelley, R. E. and A. Minagar (2009). "Memory complaints and dementia." Med Clin North Am **93**(2): 389-406, ix.
Kennedy, S. H., P. Giacobbe, et al. (2011). "Deep brain stimulation for treatment-resistant depression: follow-up after 3 to 6 years." American Journal of Psychiatry **168**(5): 502-510.
Keyserling, H. and S. Mukundan, Jr. (2005). "The role of conventional MR and CT in the work-up of dementia patients." Neuroimaging Clin N Am **15**(4): 789-802, x.
Kirsch, W., G. McAuley, et al. (2009). "Serial susceptibility weighted MRI measures brain iron and microbleeds in dementia." J Alzheimers Dis **17**(3): 599-609.
Kitzbichler, M. G., M. L. Smith, et al. (2009). "Broadband criticality of human brain network synchronization." PLoS Computational Biology **5**(3): e1000314.
Kiviniemi, V. (2008). "Endogenous brain fluctuations and diagnostic imaging." Human brain mapping **29**(7): 810-817.
Lai, M.-C., M. V. Lombardo, et al. (2010). "A shift to randomness of brain oscillations in people with autism." Biol Psychiatry **68**(12): 1092--1099.
Lerch, J. P., J. Pruessner, et al. (2008). "Automated cortical thickness measurements from MRI can accurately separate Alzheimer's patients from normal elderly controls." Neurobiol Aging **29**(1): 23-30.
Li, S.-J., Z. Li, et al. (2002). "Alzheimer Disease: evaluation of a functional MR imaging index as a marker." Radiology **225**(1): 253-259.
Li, X., J. Polygiannakis, et al. (2005). "Fractal spectral analysis of pre-epileptic seizures in terms of criticality." J Neural Eng **2**(2): 11-16.
Liu, Y., K. Wang, et al. (2008). "Regional homogeneity, functional connectivity and imaging markers of Alzheimer's disease: a review of resting-state fMRI studies." Neuropsychologia **46**(6): 1648-1656.

Logothetis, N. K. (2008). "What we can do and what we cannot do with fMRI." Nature **453**(7197): 869-878.
Lynall, M. E., D. S. Bassett, et al. (2010). "Functional connectivity and brain networks in schizophrenia." Journal of Neuroscience **30**(28): 9477-9487.
Mandal, P. K. (2012). "In vivo proton magnetic resonance spectroscopic signal processing for the absolute quantitation of brain metabolites." European Journal of Radiology **81**(4): e653-664.
Mandelbrot, B. B. (1977). Fractals : form, chance and dimension. San Francisco, Freeman.
Mandelbrot, B. B. (1982). The fractal geometry of nature. San Francisco, W.H. Freeman.
Manova, E. S., C. A. Habib, et al. (2009). "Characterizing the mesencephalon using susceptibility-weighted imaging." AJNR Am J Neuroradiol **30**(3): 569-574.
Mansfield, P. and A. A. Maudsley (1977). "Medical imaging by NMR." British Journal of Radiology **50**(591): 188-194.
Maxim, V., L. Sendur, et al. (2005). "Fractional Gaussian noise, functional MRI and Alzheimer's disease." Neuroimage **25**(1): 141-158.
MedicalNews (2010). "Rising prevalence of dementia will cripple Canadian families the health care system and economy." The Medical News(1): 1-3.
Minati, L., M. Grisoli, et al. (2007). "MR spectroscopy, functional MRI, and diffusion-tensor imaging in the aging brain: a conceptual review." J Geriatr Psychiatry Neurol **20**(1): 3-21.
Mosso, A. (1881). Ueber den Kreislauf des Blutes im menschlichen Gehirn, etc, pp. vi. 222. pl. IX. Leipzig.
Nair, D. G. (2005). "About being BOLD." Brain Research. Brain Research Reviews **50**(2): 229-243.
Ogawa, S., T. M. Lee, et al. (1990). "Brain magnetic resonance imaging with contrast dependent on blood oxygenation." Proc Natl Acad Sci USA **87**(24): 9868-9872.
Patterson, C. J., S. Gauthier, et al. (1999). "The recognition, assessment and management of dementing disorders: conclusions from the Canadian Consensus Conference on Dementia." CMAJ **160**(12 Suppl): S1-15.
Pauling, L. and C. D. Coryell (1936). "The Magnetic Properties and Structure of Hemoglobin, Oxyhemoglobin and Carbonmonoxyhemoglobin." Proceedings of the National Academy of Sciences of the United States of America **22**(4): 210-216.
Perrin, R. J., A. M. Fagan, et al. (2009). "Multimodal techniques for diagnosis and prognosis of Alzheimer's disease." Nature **461**(7266): 916-922.
Pinero, D. J. and J. R. Connor (2000). "Iron in the Brain: An Important Contributor in Normal and Diseased States." The Neuroscientist **6**(6): 435-453.
Prince, M. and J. Jackson (2009). "World Alzheimer Report 2009." World Alzheimer Report: 1-96.
Pritchard, W. S. (1992). "The brain in fractal time: 1/f-like power spectrum scaling of the human electroencephalogram." Int J Neurosci **66**(1-2): 119-129.
Provencher, S. W. (1993). "Estimation of metabolite concentrations from localized in vivo proton NMR spectra." Magn Reson Med **30**(6): 672-679.

Raichle, M. E. (1998). "Behind the scenes of functional brain imaging: a historical and physiological perspective." Proceedings of the National Academy of Sciences of the United States of America **95**(3): 765-772.

Raichle, M. E. and D. A. Gusnard (2002). "Appraising the brain's energy budget." Proceedings of the National Academy of Sciences of the United States of America **99**(16): 10237-10239.

Raichle, M. E., A. M. MacLeod, et al. (2001). "A default mode of brain function." Proceedings of the National Academy of Sciences of the United States of America **98**(2): 676-682.

Raichle, M. E. and M. A. Mintun (2006). "Brain work and brain imaging." Annual Review of Neuroscience **29**: 449-476.

Raz, N., K. M. Rodrigue, et al. (2007). "Brain aging and its modifiers: insights from in vivo neuromorphometry and susceptibility weighted imaging." Ann N Y Acad Sci **1097**: 84-93.

Richards, T. L., G. A. Gates, et al. (1997). "Functional MR spectroscopy of the auditory cortex in healthy subjects and patients with sudden hearing loss." AJNR. American Journal of Neuroradiology **18**(4): 611-620.

Rodrigue, K. M., A. M. Daugherty, et al. (2012). "The Role of Hippocampal Iron Concentration and Hippocampal Volume in Age-Related Differences in Memory." Cerebral Cortex.

Rosazza, C. and L. Minati (2011). "Resting-state brain networks: literature review and clinical applications." Neurological sciences : official journal of the Italian Neurological Society and of the Italian Society of Clinical Neurophysiology **32**(5): 773-785.

Roy, C. S. and C. S. Sherrington (1890). "On the Regulation of the Blood-supply of the Brain." J Physiol **11**(1-2): 85-158 117.

Schepers, H. S., J. H. G. M. van Beek, et al. (1992). "Four Methods to Estimate the Fractal Dimension from Self-Affine Signals." IEEE Engineering in Medicine and Biology **11**(2): 57-64.

Schlaepfer, T. E., M. S. George, et al. (2010). "WFSBP Guidelines on Brain Stimulation Treatments in Psychiatry." World J Biol Psychiatry **11**(1): 2-18.

Schmidt, R., D. Havas, et al. (2009). "MRI in dementia." Neurol Clin **27**(1): 221-236, ix.

Schmidt, R., S. Ropele, et al. (2008). "Longitudinal multimodal imaging in mild to moderate Alzheimer disease: a pilot study with memantine." J Neurol Neurosurg Psychiatry **79**(12): 1312-1317.

Schrag, M., G. McAuley, et al. (2009). "Correlation of hypointensities in susceptibility-weighted images to tissue histology in dementia patients with cerebral amyloid angiopathy: a postmortem MRI study." Acta Neuropathol.

Schuff, N., A. A. Capizzano, et al. (2002). "Selective reduction of N-acetylaspartate in medial temporal and parietal lobes in AD." Neurology **58**(6): 928-935.

Sehgal, V., Z. Delproposto, et al. (2005). "Clinical applications of neuroimaging with susceptibility-weighted imaging." J Magn Reson Imaging **22**(4): 439-450.

Sharma, V. (2009). "Deterministic chaos and fractal complexity in the dynamics of cardiovascular behavior: perspectives on a new frontier." Open Cardiovasc Med J **3**: 110-123.

Sheffield, P. and M. D. Noseworthy (2010). Simultaneously assessed GABA/Glutamate/Glutamine concentration gender differences at 3.0T. Proceedings of the 17th scientific meeting, International Society for Magnetic Resonance in Medicine, Honolulu.

Small, B. J., E. Gagnon, et al. (2007). "Early identification of cognitive deficits: preclinical Alzheimer's disease and mild cognitive impairment." Geriatrics **62**(4): 19-23.

Small, G. W., S. Y. Bookheimer, et al. (2008). "Current and future uses of neuroimaging for cognitively impaired patients." Lancet Neurol **7**(2): 161-172.

Soares, D. P. and M. Law (2009). "Magnetic resonance spectroscopy of the brain: review of metabolites and clinical applications." Clin Radiol **64**(1): 12-21.

Song, I.-H., S.-M. Lee, et al. (2005). "Multifractal Analysis of Electroencephalogram Time Series in Humans." Lecture Notes in Computer Science **3512**: 921-926.

Sorg, C., V. Riedl, et al. (2007). "Selective changes of resting-state networks in individuals at risk for Alzheimer's disease." Proceedings of the National Academy of Sciences of the United States of America **104**(47): 18760-18765.

Sperling, R. A., J. F. Bates, et al. (2003). "fMRI studies of associative encoding in young and elderly controls and mild Alzheimer's disease." J Neurol Neurosurg Psychiatry **74**(1): 44-50.

Tank, D. W., M. Sugimori, et al. (1988). "Spatially resolved calcium dynamics of mammalian Purkinje cells in cerebellar slice." Science **242**(4879): 773-777.

Tapanainen, J. M., P. E. Thomsen, et al. (2002). "Fractal analysis of heart rate variability and mortality after an acute myocardial infarction." American Journal of Cardiology **90**(4): 347-352.

Teipel, S. J., C. Born, et al. (2007). "Multivariate deformation-based analysis of brain atrophy to predict Alzheimer's disease in mild cognitive impairment." Neuroimage **38**(1): 13-24.

Thulborn, K. R., J. C. Waterton, et al. (1982). "Oxygenation dependence of the transverse relaxation time of water protons in whole blood at high field." Biochimica et biophysica acta **714**(2): 265-270.

Valenzuela, M. J. and P. Sachdev (2001). "Magnetic resonance spectroscopy in AD." Neurology **56**(5): 592-598.

Van Dijk, K. R. A., T. Hedden, et al. (2010). "Intrinsic functional connectivity as a tool for human connectomics: theory, properties, and optimization." Journal of neurophysiology **103**(1): 297-321.

Vitali, P., R. Migliaccio, et al. (2008). "Neuroimaging in dementia." Semin Neurol **28**(4): 467-483.

Wagshul, M. E., P. K. Eide, et al. (2011). "The pulsating brain: A review of experimental and clinical studies of intracranial pulsatility." Fluids and barriers of the CNS **8**(1): 5.

Wang, K., M. Liang, et al. (2007). "Altered functional connectivity in early Alzheimer's disease: a resting-state fMRI study." Hum Brain Mapp **28**(10): 967-978.

Wardlaw, G., R. Wong, et al. (2008). "Identification of intratumour low frequency microvascular components via BOLD signal fractal dimension mapping." Phys Med **24**(2): 87-91.

Warsi, M., W. Molloy, et al. (2012). "Correlating brain blood oxygenation level dependent (BOLD) fractal dimension mapping with magnetic resonance spectroscopy (MRS) in Alzheimer's disease." Magnetic Resonance Materials in Physics, Biology and Medicine: 1-10.

Warsi, M. A., G. Hasey, et al. (2012). Fractal Dimension Compared to Resting State Network Analysis of BOLD MRI in Alzheimer's Disease. Proceedings of the Scientific Sessions of the Society of Biological Psychiatry, Philladelphia, USA.

Weitkunat, R. (1991). Digital biosignal processing. Amsterdam ; New York, Elsevier.

Werring, D. J., S. M. Gregoire, et al. (2010). "Cerebral microbleeds and vascular cognitive impairment." Journal of the Neurological Sciences **299**(1-2): 131-135.

West, G. B. (2012). "The importance of quantitative systemic thinking in medicine." Lancet **379**(9825): 1551-1559.

Wilson, M., G. Reynolds, et al. (2011). "A constrained least-squares approach to the automated quantitation of in vivo (1)H magnetic resonance spectroscopy data." Magnetic Resonance in Medicine **65**(1): 1-12.

Wink, A. M., F. Bernard, et al. (2006). "Age and cholinergic effects on hemodynamics and functional coherence of human hippocampus." Neurobiol Aging **27**(10): 1395-1404.

Wintermark, M., M. Sesay, et al. (2005). "Comparative overview of brain perfusion imaging techniques." J Neuroradiology **32**(5): 294-314.

Worsley, K. J., C. H. Liao, et al. (2002). "A general statistical analysis for fMRI data." Neuroimage **15**(1): 1-15.

Xu, N. and J. H. Xu (1988). "The fractal dimension of EEG as a physical measure of conscious human brain activities." Bulletin of Mathematical Biology **50**(5): 559-565.

Yacoub, E., T. H. Le, et al. (1999). "Further evaluation of the initial negative response in functional magnetic resonance imaging." Magnetic Resonance in Medicine **41**(3): 436-441.

Yavuz, Standish, et al. (2009). "Yavuz 2009 Antibiotics in Dementia- What's Next? The DARAD Trial." Academic Geriatrics Journal of Turkey: 67-72.

Yoshikawa, T., K. Murase, et al. (2003). "Quantification of the heterogeneity of cerebral blood flow in vascular dementia." Journal of Neurology **250**(2): 194-200.

Zarahn, E., G. K. Aguirre, et al. (1997). "Empirical analyses of BOLD fMRI statistics. I. Spatially unsmoothed data collected under null-hypothesis conditions." Neuroimage **5**(3): 179-197.